Replies to Referee Comments (RC1, RC2) and Short Comment (SC1)

We thank both referees No.1 and No.2 for their detailed and insightful comments which helped to further improve the manuscript. Below we address all referee comments as well as the contributed short comment (in italics). Revised text, keyed to the ACPD online version, is shown in blue, and is included in the final manuscript we are submitting to ACP. Updated figures and tables as well as material for a supplement are attached at the end of our reply.

RC1: *Source assignment of proxies is a basic prerequisite for interpreting climate archives in terms of past climate as well as climate change. Concerning polar ice cores, ionic impurities originate primarily from aerosol deposition. Amongst them, interpretation of sea salt aerosol deposition archived in ice cores is especially challenging and contro- versial because the contribution of two different and competing sources - viz. open water versus sea ice - is up for debate. In addition it became apparent that sea salt aerosol production over ice-covered oceans may contribute significantly to the global sea salt aerosol budget. The manuscript at hand addresses this pivotal subject and provides thorough and direct observational evidence of sea salt aerosol production from blowing snow above sea ice. The important conclusions drawn are based on comprehensive state of the art ship-borne aerosol and snow measurements during winter / early springtime in the Weddell Sea region. Although the main conclusions are primarily restricted to the chosen site, there are certainly strong implications for climate research in the Southern Ocean realm and climate related interpretation of sea salt profiles from ice cores in general. The authors have accomplished a clear, well-organised and concise paper. The methodology is sound and assumptions are identified clearly and conscientiously. From my point of view, all parts, including figures, are essential. The manuscript certainly addresses the scientific scope of ACP and I recommend a final publication after some minor revisions I specified below.*

Reply: We thank the reviewer for the positive assessment of this work.

RC1: *1. Abstract, page 1, line 13 and Conclusions, page 24, line19: The authors state that bromine enrichment was typical at 29 m height, but from Chapter 3.4.2 and Fig. 15, bromine depletion is evident. Please clarify.*

Reply: In both cases it should read "depleted", which is now corrected.

RC1: *2. Chapter 2.3, Aerosol chemical composition: Could you assess the impact of pollution on chemical aerosol composition? Was the bulk aerosol sampling contamination controlled?*

Reply: The setup of this study did not include any contamination control of the bulk aerosol filter sampling such as pump control based on wind speed and direction. As described aerosol number concentrations at the crows nest showed significant spikes, when air came from the direction of the ship stack, whereas no evidence of pollution was detected in aerosol number concentrations observed on the sea ice. We clarified text in section 2.2 including also the fraction of CLASP data filtered out:

Raw aerosol number concentrations at the crow's nest showed significant spikes, when air came from the direction of the ship's engine stack, whereas no evidence of pollution was detected in the observations on the sea ice. Pollution spikes were effectively filtered out prior to averaging by excluding all data when relative wind direction was in the 135–225° sector encompassing the ship's engine stack. A total of 21% of the available 1-second data was removed from the crow's nest data.

We now include an assessment of the potential impact of pollution on bulk aerosol chemistry from filters and added the following text to section 2.3:

In order to assess the impact of potential pollution on bulk aerosol chemistry from filters collected at the crow's nest we calculated for each filter sample the fraction of the total filter run time during which relative wind direction was within the 135–225° sector encompassing the ship's engine stack. Considering all filters sampled from June to September 2013 (N=141) the fraction of total filter run time with winds from the polluted sector was on average 9.5%. Polluted time fraction and atmospheric concentrations of Na^+, Cl^-, SO_4^{2-} and Br^- did not show any correlation ($R^2<0.05$), suggesting that the impact of pollution on the respective ion concentrations is small. A weak, but significant negative correlation was found between polluted time fraction and depletion factors $DF_{SO_4^{2-}}$ ($R^2=0.19$, $p<0.01$)

and DF_{Br^-} (R^2=0.13, p<0.01) suggesting that enrichment in sulphate (and bromide) may be more likely during polluted conditions. The bulk aerosol chemistry observations on the sea ice showed no evidence of pollution. Thus, in the case of sulfate we cannot rule out that some of the sulfate enrichment in atmospheric aerosol observed at the crow's nest may be due to ship exhaust rather than presence of mirabilite. It follows that estimates of sea ice contributions to total SSA derived from depletion factors discussed in section 3.4.4 have to be considered as lower bounds of true values.

RC1: *3. Chapter 3.2: Impact of snow precipitation on blowing/drifting snow: Did you access the regular weather reports from the ships meteorological office in this case?*
Reply: The available 3-hourly weather reports from the ship provided only limited information, but confirmed for the case of precipitation shown in Fig.10 (3-4 July 2013) overcast skies, variable visibility from 0.5 (fog) to 10 km, and occasional ice needles. As stated in the text we inferred occurrence of precipitation qualitatively from direct observation supported by webcam images, if usable, and presence of clouds (p9-l14). The still images of a webcam installed at the crows nest (p8-l16) allowed to see at times, including 4 July, large airborne snow crystals during night time in the beam of the ships search lights. We added a sentence in section 3.3.2 to further clarify.
For the early morning of 4 July 2013 webcam images from the crow's nest confirmed the presence of large airborne snow crystals visible during darkness in the beam of the ship's search lights, whereas the ship's 3-hourly weather report noted the presence of airborne ice needles.

RC1: *4. Pages 12/13 and Fig.7: Regarding the salinity (S_p) of blowing snow, corresponding S_p-values of the uppermost surface snow layer are decisive. Did you take samples from surface snow; say <1 cm deepness below surface? Figure 7: The reader cannot get an idea about the salinity of the surface snow layer from this graph. It would be informative as well to specify the total depth of the snow layer shown here, not just the snow height above sea ice.*
Reply: Typically snow pit profiles were measured at 2 cm depth resolution (see methods section 2.4); except at ice station S6 some profiles include a surface snow sample from a layer of ~0.5-1.0 cm thickness. As discussed, S_p in blowing snow is consistent with the local surface snow measurements (section 3.2.2). In Figure 7 depth information is readily available since data points at the top of each profile, i.e. with the largest snow height above ice, represent the surface snow layer. We updated Figure 7 and caption accordingly (Fig. 1).

RC1: *5. Chapter 3.3.2, Snow particle size distribution: Is it possible to rate the impact of the ships profile on the local wind field and eventually on the measured snow particle size distribution?*
Reply: We did not attempt to quantify the distortion of the local wind field by the ship and its impact on measured snow particles, and had therefore included a respective caveat in the method description (p4 line 30): "It should be borne in mind that the distortion of flow caused by the ship may mean both that speed at 39 m is not representative of flow in the far field at that height, and further, the turbulent field strength, which governs the gradient of the logarithmic profile, may be a residual from a different, likely lower, height. Thus, we suggest care when interpreting the data, and estimate that the conversion from particle counts to number density be seen as an estimate suitable for comparison, rather than quantitative with a well behaved uncertainty."

RC1: *6. Chapter 3.4.1, page 19, lines 28-30: As for Antarctic winter, acid induced Cl^- loss is rather extraordinary because production of acidic sulphur compounds usually cease at the end of summer / fall. Are there any indications for alternative HNO_3 induced Cl^- loss in your data?*
Reply: We agree. Sea salt reaction with atmospheric HNO_3 is a plausible alternative chloride loss process in winter; e.g. at Halley on the nearby Antarctic coast observations in winter show low but non-zero levels of atmospheric HNO_3 of 1-2 pptv (Jones et al., 2011). Unfortunately, no usable filter data of aerosol nitrate are available from this study to test the suggested process due to a very high lab procedure blanc. However, we include the point in section 3.4.1 as follows.
Snow on sea ice follows closely the theoretical mirabilite fractionation line, whereas aerosol shows large scatter and a tendency to apparent Na^+ enrichment with respect to Cl^- of up to 20 %, equivalent

to Cl^- depletion with respect to Na^+ of 17 % (Fig. 14). Dechlorination of sea salt aerosol observed in Antarctica has a maximum in spring/summer, when gaseous acidic species (nitric, sulfuric and methanesulfonic acid) are available to replace chloride on sea-salt aerosol (Wagenbach et al., 1998; Rankin and Wolff, 2003; Legrand et al., 2017). Acidic sulphur species are close to zero during winter in coastal Antarctica e.g. at Neumayer (Weller et al., 2011), whereas nitric acid is low but non-zero, e.g. 1-2 pptv at Halley (Jones et al., 2011). Thus nitric acid induced Cl^- loss from sea salt is a plausible explanation for the observed Cl^- depletion either in airborne SSA or as a sampling artefact from sea salt already accumulated on the filter surface as suggested previously (Wagenbach et al., 1998; Legrand et al., 2017). Unfortunately no usable filter data of aerosol nitrate are available from this study to further test the association between nitrate and sea salt due to a very high lab procedure blank.

RC1: *7. Chapter 3.4.2, Chemical fractionation of* Br^-*, lines 28-33 and Fig. 15: There is strong bromine depletion during polar night in July when global radiation was about zero (Fig. 15b). This peculiarity deserves some discussion.*

Reply: We did mention (p21-line16) that bromide escape from aerosol was detected previously year-round at DDU in coastal Antarctica, including during winter months, except in June (Legrand et al., 2016). As suggested, we expand the discussion in section 3.4.2:

Contrary to expectation bromide depletion of aerosol was significant even during winter darkness from mid June to mid July (Fig. 15b), whereas previous observations at DDU showed a similar trend but less bromide depletion and none in June (Legrand et al., 2016). At DDU DF_{Br^-} in bulk aerosol increased gradually from a minimum in June (0.04), intermediate values in July to Sep (0.22-0.39) to a maximum in October (0.42) (Legrand et al., 2016). Light conditions are unlikely a cause of differences in bromide depletion, since DDU is located at a similar latitude (66° 40'S) as the area covered by this study. However, one of a number of processes identified leading to bromide loss from snow or aerosol involves HOBr oxidation of bromide, which leads to its autocatalytic release (Abbatt et al., 2012). The early laboratory study by Oum et al. (1998) has shown that the required HOBr can be chemically produced in darkness through the reaction of ozone with bromide. Another study during the ANT-XXIX/6 expedition reports significant bromoform (CH_3Br) production in sea ice during winter darkness (Abrahamsson et al., 2018), which requires HOBr (and organic matter) as precursors, and therefore indicates that bromine loss processes were active in the sea ice in the absence of sunlight. It therefore appears plausible that the same reactions may have caused significant bromide depletion observed here in sea salt aerosol, provided the aerosol pH was low enough.

RC1: *8. Figure 5 and page 12, lines 8-9: By the way: During late afternoon of the 11 July, there is an outstanding* Na^+ *peak associated with corresponding sulphate depletion, while the wind speed seemed just close to the threshold value (well below 10 m/s throughout the whole day). Any ideas?*

Reply: From midnight to the early morning of 11 July 2013 wind speed was indeed at or slightly above the snow drift threshold (= 7.1 m/s) (Fig.5a) suggesting that drifting snow near the surface was present and after sublimation contributed to the observed sodium peak. The increase in SSA number densities and atmospheric sodium occurred in the afternoon a few hours after wind speed had dropped again below the threshold, consistent with a similar phasing observed during the blowing snow event on 14-16 July and discussed in section 3.2.2. To better illustrate episodes of snow drift we include in Figures 4-6 of the revised manuscript a horizontal line marking the estimated threshold wind speed U_t.

RC2: *Frey et al present an observational study of sea salt aerosol (SSA) production from blowing snow above sea ice, through measurements during winter 2013 in the Weddell Sea, Antarctica. Since the modelling hypothesis presented by Yang et al (2008, GRL), the mechanism of SSA production from blowing snow has been implemented in numerous modelling studies, unfortunately without observational evidence of the mechanism itself. This work provides a detailed study of the proposed mechanism through measurements of size distributions and inorganic chemical composition of aerosols and blowing snow, and comparisons to modelled parameters of blowing snow SSA production. Given the prevalence of the use of the blowing snow SSA production parameterisation, this is a very valuable study.*
Reply: We thank the reviewer for the positive assessment.

RC2: *My comments mainly focus on clarification of the manuscript and assessment of statistical significance throughout. Given the significant length and many figures and tables, the authors are encouraged to consider moving some material to a supplementary information file if appropriate.*
Reply: We consider tables and figures all essential, in agreement with reviewer 1. However, additional material as suggested is now included and presented in a supplement (see below).

RC2: *One overarching and major comment that needs to be addressed throughout the manuscript is for uncertainties (or standard deviations) to be listed with average values. This is important for assessing data variability, as well as for assessment of statistical significance. Indeed, statistical tests of significance should be applied to inform whether 'trends' and 'differences' are indeed statistically significant, which would greatly strengthen the findings presented in the manuscript. This is important because trends sometimes seem to be overstated in the text when compared to large scatter shown in the figures. Routine statements of statistical significance would significantly strengthen the conclusions throughout.*
Reply: We added standard deviations for all averages reported in the tables (Tables 1, 2) and include in the final manuscript significance of trends and differences, where appropriate. As an example below updated text in section 3.4.4.
During storms median atmospheric sea salt concentrations from both estimates showed increases above background values (Fig. 17a) that were statistically significant based on the Wilcoxon rank-sum test ($p<0.01$).

RC2: *I highly recommend reorganising the manuscript to improve readability. Section 3.2 relies significantly on depletion factors. Therefore, I recommend reorganising to move Sections 3.4.1-3.4.3 to be before Section 3.2. Also, the current Section 3.4.3 would be best after Section 3.3.*
Reply: We are considering this suggestion for the final manuscript.

RC2: *Major Comments: Page 1, Line 21 & Page 25, Lines 14-15: These sentences state generally that 'similar processes take place in the Arctic', yet no supporting discussion is provided. Since the current work focuses on the specific conditions of the Antarctic work and no data are provided to evaluate this statement, these sentences should be removed.*
Reply: Agreed. We removed the sentence referring to the Arctic from abstract and conclusions, and added text in the conclusions as follows:
Similar in situ measurements are needed to corroborate the importance of sea salt aerosol production from blowing snow also in the Arctic to validate atmospheric and ice core models (e.g. Rhodes et al., 2017; Huang and Jaeglé, 2017).

RC2: *Page 1, Lines 2-3 and Page 3, Lines 5-7: The statement 'validating a model hypothesis to account for winter time SSA maxima in polar regions not explained otherwise' generalises beyond the Antarctic, which is not appropriate, and it also not consider other factors, such as lower boundary layer height and lead-based SSA production. This statement should be rephrased to focus on validating wintertime SSA production from blowing snow (which is excellent), as a comprehensive discussion of wintertime SSA maxima causes in both the Arctic and Antarctic is not presented in*

this work. Further, the work of Huang and Jaegle (2017) did not consider the observed influence of lead-based SSA production in the Arctic (May et al. 2016, JGR). I suggest focusing on the Antarctic, as this is the strength of this work.
Reply: We agree and rephrased in abstract (1.) and introduction (2.) accordingly.
1. Two consecutive cruises in the Weddell Sea, Antarctica, in winter 2013 provided the first direct observations of sea salt aerosol (SSA) production from blowing snow above sea ice, thereby validating a model hypothesis to account for winter time SSA maxima in the Antarctic. 2. Indeed, model agreement with SSA winter maxima observed at a number of locations in the polar regions is much improved when a SSA source from blowing snow based on the parameterisation of (Yang et al., 2008) is included in the model (Huang and Jaeglé, 2017; Yang et al., 2019).

RC2: *Figure 1; Page 3, Lines 30-33; Page 13, Lines 22-23: Please provide a legend for sea ice concentration. It appears that stations S2, S3, and S9 were in areas of reduced sea ice concentration. While there is significant evidence for blowing snow SSA production based on chemical analyses, a discussion of the distance to open leads, in addition to open water (Page 3, Line 32), needs to be included, since there is measurement evidence of wind-dependent lead-based SSA production (e.g., Nilsson et al. 2001, JGR).*
Reply: A legend is now included in Fig. 1 and we added the following text in section 2 (1.) and in the discussion p13 - after line26 (2.).
1. Sea ice concentrations in mid July 2013 derived from Nimbus-7 satellite microwave radiometer measurements (Comiso, 2018) show areas with 85-95 % ice cover near ice stations S2-3 and S7-9 indicating that open leads may be present (Figure 1). 2. Open leads, which may have been present in areas of reduced sea ice concentration e.g. near ice stations S2-3 and S7-9 (Figure 1) are another potential wind-dependent source of SSA from open water as observed in the Arctic (Nilsson et al., 2001; May et al., 2016), albeit with a much smaller flux contribution per surface area compared to the open ocean due to reduced fetch and low fraction of surface coverage (<15 %).

RC2: *Page 7, Lines 3-5: Please clarify whether these time periods of ship exhaust influence were also removed from the aerosol size distribution data, as they should be.*
Reply: Ship exhaust influence on measurements of aerosol size and concentration was removed by using a wind-sector filter (section 2.2). We clarified text in section 2.2 including also the fraction of CLASP data filtered out as follows (see corresponding reply to RC1):
Raw aerosol number concentrations at the crow's nest showed significant spikes, when air came from the direction of the ship's engine stack, whereas no evidence of pollution was detected in the observations on the sea ice. Pollution spikes were effectively filtered out prior to averaging by excluding all data when relative wind direction was in the 135–225° sector encompassing the ship's engine stack. A total of 21% of the available 1-second data was removed from the crow's nest data.

RC2: *Page 7, Line 9 and Table 3: LODs are normally defined as 3*sigma, rather than 2*sigma. What is the authors justification here? Also, LODs should be reported with one significant figure (too many shown in Table 3, which can be misleading).*
Reply: Here we follow Wagenbach et al. (1998) who employed a similar aerosol filter method and defined the mean detection limits as 2*sigma. Two figures for LOD were reported in Table 3 to account for increased LOD at the shorter run times of filters deployed on the sea ice. However, we removed that line to report only one figure for LOD and clarified the footnote of Table 3 as follows.
[c] based on crow's nest mean air sample STP-volume (6.4 m^3); mean air sample STP-volume for filters deployed on the sea ice was 3.3 m^3 increasing respective LODs by a factor 1.6

RC2: *Tables 4-5: Data below the LOD should be labeled as such, as exact values below LOQs are not meaningful.*
Reply: Agreed. Snow concentrations (Tab. 2) were typically 2 orders of magnitude above the LOD of $\sim 2\,\mathrm{ng\,g^{-1}}$, whereas some aerosol concentrations (Tab. 1) where below the estimated LOD. In the final manuscript a corresponding footnote is added to those values in Table 4:

[c]below the estimated LOD (see Table 3)

RC2: *Page 8, Lines 3-5: Instead of reporting depletion factors, I highly encourage the authors to consider reporting 'enrichment factors' (e.g. Krvanek et al. 2012, Atmos. Environ.), which are more intuitive to understand in my opinion (i.e. enrichments are >1, depletion corresponds to <1).*
Reply: Deviations from bulk sea water ion rations are reported in the literature in both ways, either as enrichment or as depletion factors (e.g. Sander et al., 2003). Since the focus here is on depletion processes we choose to report depletion rather than enrichment factors, also to be consistent with some of the previous related work (Yang et al., 2008). To help interpretation we added a sentence to section 2.4:
For example, DF_x =-1.5 or 150 % enrichment means the respective ion concentration is 2.5 times that in reference sea water.

RC2: *Page 8, Lines 8-11: I am quite concerned that data were selectively removed from the datasets presented. I can understand if certain samples are not used for externally identified reasons, but if, for example, sulfate concentration is removed for a given sample, I'm concerned about continuing to use other ions from that sample, as appears to have been done based on the numbers shown in Tables 4 and 5. I worry that the presented datasets are skewed based on the removal of these data points. What fraction of the time did ship emissions impact the dataset? It needs to be clarified what fraction of the data were removed. This data treatment is very important for later statements about the distribution of depletion factors (e.g., statements on Page 10, Lines 7-9).*
Reply: No snow data were removed whereas the fraction of aerosol filter data removed was relatively small, and is now mentioned in the revised text. Filter samples suspected of contamination based on anomalous sulfate enrichment (total of 6 samples) are not anymore used in the statistics. The pollution impact on filter chemistry is now discussed (see reply to RC1 above). Bromide depletion factors below a threshold of -7 are considered outliers and removed. The corresponding statistics in Table 4 are updated. Follow up statements are not affected by any of these changes.
A total of 6 (= 6% of all crow's nest samples) $DF_{\mathrm{SO_4^{2-}}}$ values were below that of pure mirabilite (= -7.3) and are attributed either to sulfate contamination from the ship's engine emissions discussed below or measurement error. We therefore removed all ion concentrations of the corresponding filter samples from the dataset. $DF_{\mathrm{Br^-}}$ only below -7 were considered outliers due to measurement error and removed: a total of 4 (= 3% of all samples) from the crow's nest data, and a total of 6 (= 14% of all samples) from the sea ice data.

RC2: *Page 9, Lines 28-30; Page 10, Lines 1-3: Please reference where these data are presented, or please add them as supplementary information.*
Reply: Agreed. In a supplement we include now a Figure S1 (Fig. 2) with an overview of the available observations during ANT-XXIX/7, and Table S1 and Table S2 (Table 3, 4) with the statistics of particle concentration and size. The text has been amended as follows:
1. At 29 m mean total number densities N_{46-478} were 8.7×10^3 $\mathrm{m^{-3}}$ during ANT-XXIX/6 and very similar 7.2×10^3 $\mathrm{m^{-3}}$ during ANT-XXIX/7 (Table S1, Figure S1c).
2. At 29 m mean total number densities $N_{0.4-12}$ were 2.1×10^6 $\mathrm{m^{-3}}$ during ANT-XXIX/6 (Table S2, Figure 2d). $N_{0.4-12}$ mean values at 2.0 and 0.2 m during ice stations were 1.4×10^6 and 1.7×10^6 $\mathrm{m^{-3}}$, respectively, about the same as the number densities observed during the same time at 29 m (Table S2). The median aerosol particle diameters $\overline{d_p}$ at the measurement heights 0.2, 2.0m and 29 m ranged between 0.60 and 0.66 µm (Table S2) showing dominance of sub-micron sized particles in atmospheric aerosol below the instrument particle size cut-off (>11 µm).
3. Median $DF_{SO_4^{2-}}$ values at 29 m were very similar during ANT-XXIX/6 (=0.34) and ANT-XXIX/7 (=0.30), but larger near the sea ice surface (=0.49), suggesting throughout a significant contribution to the total SSA burden from a fractionated sea ice source (Table 4, Figure S1e).

RC2: *Section 3.4.2 and associated text in Conclusions: The authors should be mindful that only aerosol and snow bromine were measured and that no measurements of reactive bromine are pre-*

sented. Therefore, the strength of the implications for reactive bromine production should be weakened to account for this uncertainty and other factors that contribution to reactive bromine production and abundance.

Reply: Indeed, we do not infer any details on speciation of reactive bromine chemistry. We added a sentence in section 3.4.2 (1.) and amended a sentence in conclusions (2.):

1. Detailed measurements of participating bromine species in air, snow and aerosol are needed to further understand relevant processes and constrain the mass budget.

2. It is found that SSA produced by blowing snow is depleted in bromide suggesting it is a source of reactive bromine to the atmosphere, which then can contribute to ozone depletion events.

RC2: *Page 21, Lines 9-10: Depletion factors examine the degree of depletion, but they do not provide information on the mass present. Therefore, the data here cannot assess contribution to the fraction of net bromine release, as currently presented, especially without reactive bromine measurements.*

Reply: Agreed, we don't discuss detail of the bromine mass budget. We amended the corresponding sentence in section 3.4.2, conclusions and abstract (1.), as well added a note (2.) (see reply to previous comment):

1. On average snow on sea ice and blowing snow showed no or small depletion of bromide relative to sodium with respect to sea water, whereas aerosol at 29 m was depleted suggesting that significant bromine loss takes place in the aerosol phase between 2 and 29 m above the sea ice surface.

2. Detailed measurements of participating bromine species in air, snow and aerosol are needed to further understand relevant processes and constrain the mass budget.

RC2: *Page 19, Lines 22-25: This analysis is only valid if you assume there is no precipitation of NaCl.2H2O. Please verify that based on temperature, and perhaps take out the very low temperature points.*

Reply: A complete model of freezing seawater is beyond the scope of this study. Thus we acknowledge that precipitation of NaCl.2H2O introduces some uncertainty to this analysis by adding the sentence below.

Further Na^+ depletion may arise from the precipitation of hydrohalite ($NaCl{\cdot}2\,H_2O$) once ambient temperature drops below the threshold of -22.9 °C (e.g. Butler et al., 2016), which occurred here during some periods of time (Fig.2b). In the analysis below however we consider only the precipitation of mirabilite.

RC2: *Page 19, Lines 127-28: Does this also mean that the aerosols collected were a mixture of sea salt emitted from the ocean and sublimation of blowing snow?*

Reply: Mixing with a pool of non-fractionated sea salt aerosol from the open ocean (DF_{Na^+}, $DF_{SO_4^{2-}}=0$) would move data points towards the origin in Figure 14, but would not explain apparent Na^+ enrichment or Cl^- loss in aerosol at a given SO_4^{2-} depletion. We believe a plausible explanation for the deviation of aerosol observations from the mirabilite precipitation model is HNO_3 induced Cl^- loss from sea salt either in airborne SSA or as an artefact on filters, as stated in the reply to reviewer 1. Below we repeat the amended text.

Snow on sea ice follows closely the theoretical mirabilite fractionation line, whereas aerosol shows large scatter and a tendency to apparent Na^+ enrichment with respect to Cl^- of up to 20 %, equivalent to Cl^- depletion with respect to Na^+ of 17 % (Fig. 14). Dechlorination of sea salt aerosol observed in Antarctica has a maximum in spring/summer, when gaseous acidic species (nitric, sulfuric and methanesulfonic acid) are available to replace chloride on sea-salt aerosol (Wagenbach et al., 1998; Rankin and Wolff, 2003; Legrand et al., 2017). Acidic sulphur species are close to zero during winter in coastal Antarctica e.g. at Neumayer (Weller et al., 2011), whereas nitric acid is low but non-zero, e.g. 1-2 pptv at Halley (Jones et al., 2011). Thus nitric acid induced Cl^- loss from sea salt is a plausible explanation for the observed Cl^- depletion either in airborne SSA or as a sampling artefact from sea salt already accumulated on the filter surface as suggested previously (Wagenbach et al., 1998; Legrand et al., 2017). Unfortunately no usable filter data of aerosol nitrate are available from this study to further test the association between nitrate and sea salt due to a very high lab procedure blank.

RC2: *Page 22, Lines 32-33: A conversion factor is used to calculate [SSA] based on Na+ and using seawater composition, but this seems to undermine and not take into account the sulfate-depletion observed.*

Reply: It does not. The impact of the depletion due to mirabilite precipitation on our calculation is indeed very small, and is therefore neglected. We added the text below to clarify:

As shown in section 3.4.1 depletion of SO_4^{2-} due to the precipitation of mirabilite decreases Na^+ by up to 12 %. Reduction in both ions decreases the mass fraction of Na^+ in the depleted sea salt aerosol by a maximum of ~0.7 % compared to reference seawater. Thus, by not considering the depletion effect conversion factor and calculated SSA mass are underestimated by up to ~0.7 %, which is negligible given all other uncertainties.

RC2: *Page 21, Lines 30-31 and elsewhere: Is this U10m and the associated data in Fig 16 an average, or threshold? It isn't clear how the data were binned. Please clarify calm and stormy conditions. Does calm represents U10m<5 m/s? How about stormy?*

Reply: We used a relatively narrow wind speed range for calm and windy conditions. We amended this to include more data, particularly for the open ocean case when only a few days of measurements were available. Aerosol data are now selected based on a wind speed threshold: calm conditions when U_{10m} <4 m s^{-1} and windy conditions when U_{10m} >9 m s^{-1}. We updated Figure 16, including also the standard deviation of the mean, to show statistical significance of differences in size distributions, as suggested further below (Fig. 3). And the text in section 3.4.3 is clarified as follows:

Average aerosol number density and volume distributions observed in the Weddell sea show that during calm conditions (U_{10m}<4 m s^{-1}) concentrations across most of the size spectrum were smaller above sea ice than above the open ocean (Fig. 16a). Depending on particle size the variability was relatively large as illustrated by the standard deviation of the mean values (Fig. 16a). Thus differences in mean size distributions were statistically significant only for d_p <2 μm in the case of aerosol number density, and d_p 1-8 μm in the case of aerosol volume distributions (Fig. 16b). The wind speed threshold chosen for calm conditions is well below the mean snowdrift threshold wind speed U_t of 7.1 m s^{-1} observed during this study and within the range when breaking of waves commences (3-4 m s^{-1}; O'Dowd et al., 1997). ... During stormy conditions (U_{10m}>9 m s^{-1}) average aerosol number densities above sea ice increased significantly for particle diameters d_p<2 μm, reaching at the lower end of the size spectrum levels similar to those observed above the open ocean (Fig. 16a). Average aerosol volume concentrations above sea ice also showed an increase during storms, significant for particle sizes d_p 0.8 to 9 μm (Fig. 16b).

RC2: *Page 22, Lines 16-19: It seems "not all water is lost" could represent a large uncertainty of blowing snow sublimation. This is important for reactions that depend on the surface area of aerosols. It could be highlighted in the abstract or conclusion. Also, please justify how to get 10^{-3} μm. Using snow salinity of 0.06 psu from Table 5, median snow particle of 100 um from Table 6, yields d(dry) of 1 um.*

Reply: We agree the degree to which water ice is lost on particles during sublimation has implications for heterogeneous chemistry, something future experiments will need to address; text below has been added to the conclusions.

The degree of water ice loss from particles has implications for particle surface area and heterogeneous chemistry, which future experiments will need to address.

Reply: We disagree regarding the calculation of d_{dry}: to convert S_p from psu (equivalent to g of dissolved salt per kg of sea water as defined in Section 2.4) into units of kg per kg in order to be consistent with units of density (kg of salt per m^3 of salt) requires division by one thousand as the equation states (Page 22, Line 16), correctly yielding d_{dry} of ~1 nm.

RC2: *Page 23, Lines 1-3: Please show this comparison and data in a supplementary file.*

Reply: We included Figure S3 in the supplement to show the comparison (Fig. 4), and amended the sentence as follows:

The sea salt mass estimates show that most filter-based values have a low bias compared to median sea salt concentrations derived from $N_{0.4-12}$ during filter sampling intervals (Fig. S3), on average of $\sim$26 %. The bias shows also a weak but significant positive correlation wind speed (R=0.4, p<0.01) (Fig. S3). A low bias of the filter samples especially during high wind speeds is expected because the smaller cut-off diameter (<6 μm) compared to the optical particle counter (>11 μm) limits capture of coarse sea salt aerosol, where much of the particle mass is located (Fig. 16b).

RC2: *Page 25, Lines 5-10: This is not a new finding and has been presented in other work. Therefore, either these sentences should be removed here or other work should be referenced to further support these findings.*

Reply: Presenting the links between snow salinity, differences in sea ice age and SSA source strength of blowing snow together with direct observations is of course new. However, we reference relevant work on sea ice and snow on sea ice as follows:

- at a given salt migration distance from the sea ice surface it is total snowpack depth, that determines the salinity probability distribution of snow on sea ice consistent with previous studies (Domine et al., 2004; Massom et al., 2001). FYI can therefore be distinguished from MYI based on snow salinity, because snow on FYI is in general more shallow than on MYI. Secondary factors potentially increasing the difference in salinity between FYI and MYI and identified previously (e.g. Massom et al., 2001) are more frequent flooding of FYI with seawater due to negative freeboard and MYI desalination due to brine drainage.

RC2: *Data Availability: Since the current work is expect to be very valuable for informing future modelling work and other studies, I highly encourage the authors to put these data in a public archive.*

Reply: All data from this study used are stored in the UK Polar Data Centre. The DOI is provided in the final manuscript.

All data are stored in the UK Polar Data Centre, Natural Environment Research Council, UK Research and Innovation (https://doi.org/10.5285/853dd176-bc7a-48d4-a6be-33bcc0f17eeb, Frey et al., 2019).

RC2: *Figure 7: Please add a legend to give meaning to the colors presented. Also, it is stated throughout the manuscript that the surface snow is typically significantly sulfate depleted (justifying the sea ice source for sulfate-depleted aerosol), but here the surface is more often near 0. Please clarify.*

Reply: Figure 7 now includes a legend (Fig. 1). There is significant spatial heterogeneity in the sampled local snowpack profiles, whereas blowing snow integrates over a wider area of sea ice. We clarified the discussion of the snow pit observations (Page 13 - Lines 9-14) as follows:

$DF_{SO_4^{2-}}$ profiles exhibited large scatter: except at one location surface-near snow showed no or small depletion, whereas most profiles showed significant depletion in deeper layers within 5-10 cm of the sea ice surface (Fig. 7c). ... However, the $DF_{SO_4^{2-}}$ values of blowing snow were at the top end of the range observed only in the deeper and more saline local snowpack (Fig. 6c). A plausible explanation for this observation during the storm on 15 July is that blowing snow integrates snow contributions from a wider area. And given the spatial heterogeneity of local snowpack thickness and composition blowing snow contributions must have dominated from areas where fractionated snow was at or near the surface such as seen in one of the profiles sampled on 12 July (Fig. 7c).

RC2: *The highly relevant work of Giordano et al. (2018, ACP) 'The importance of blowing snow to halogen-containing aerosol in coastal Antarctica: influence of source region versus wind speed' should be considered in this manuscript.*

Reply: We agree and correct the oversight by referring to this work in the introduction:

A recent observational study in the Ross Sea sector of coastal Antarctica also shows a significant association between increased SSA and high wind speed suggesting a link to blowing snow above sea ice as a source (Giordano et al., 2018).

RC2: *Minor/Technical Comments: Throughout the manuscript, watch for 'paragraphs' that are only 1-2 sentences, as this disrupts the flow and limits discussion. Consider reorganization to prevent this.*
Reply: We reorganised, where appropriate.

RC2: *Page 1, Line 9: Please state the size of the sulphate-depleted aerosol.*
Reply: Done.
Similar depletion in bulk aerosol observed in the 1-6 μm range suggests that most sea salt originated from snow on sea ice and not the open ocean or leads, e.g. on average ~93% during the 8 June and 12 August 2013 period.

RC2: *Page 1, Line 13: Based on the data presented later, 'enriched' is likely a typo and should be 'depleted' here with respect to aerosol at 29 m.*
Reply: This is now corrected (see reply to reviewer 1 above).

RC2: *Page 2, Line 20: Provide a reference to a SSA review here.*
Reply: The reference below is now included.
de Leeuw et al. (2011)

RC2: *Page 4, Lines 27-28: I think it is dividing kappa instead of multiplying. Please check. Also, please provide the value for the von Karman constant in parentheses.*
Reply: Corrected as follows:
To do this a logarithmic wind profile $U(z)$ is assumed given by $U(z) = u_*/\kappa \ln(z/z_0)$ (e.g. Li and Pomeroy, 1997), with measurement height z, the von Karman constant κ (= 0.4), friction velocity u_* and the surface roughness length of momentum z_0 set to 5.6×10^{-5} m as measured very consistently above snow at Halley (King and Anderson, 1994).

RC2: *Page 5, Lines 12-14: Please provide a greater description of the inlet. Also, please clarify whether the data presented where corrected for these particle loss estimates ('we adopt' is confusing phrasing).*
Reply: Clarified as follows.
Particle losses to inlet walls are minimised by using a short and straight inlet tube of 0.3 m length similar to the original configuration (Hill et al., 2008, Figure 9). We assume as an upper limit of particle losses those estimated previously for a similar inlet configuration (Norris et al., 2012), which amount to 43% at d_p = 11.32 μm, 19% at d_p = 6.06 μm and 0.1% at d_p = 0.44 μm, respectively.

RC2: *Page 5, Lines 22 and 27: Please clarify the size range of aerosol collected.*
Reply: Clarified as follows.
Filters were estimated to collect aerosol in the diameter range ~0.3 μm to less than 6 μm. The lower end of the range is based on previous measurements of collection efficiencies of PTFE filters as a function of particle size (Soo et al., 2016), whereas the upper end is based on the estimated cut-off diameter described below.

RC2: *Page 9, Line 8: I assume the authors are discussion temperature in degrees Celsius, but this needs to be stated.*
Reply: Added.
Near-zero or positive ambient temperatures T_a in degrees Celsius ...

RC2: *Page 9, Line 14: Where is the timing of the snowfall presented/shown?*
Reply: Only the timing of airborne snow particles is shown. Occurrence of precipitation is based on 3-hourly ship's weather reports and occasional webcam images. We rephrased accordingly.
Winter storms occurred frequently with wind speeds ranging between 10 and 20 m/s, occasionally exceeding 20 m/s, and coincided often with snowfall based on the ship's 3-hourly weather report, occasional webcam images and presence of clouds (data not shown).

RC2: *Page 9, Line 22-23: Please provide a reference that connects the friction velocity with the boundary layer conditions. Also, reference where these data are shown, or add to a SI.*

Reply: We included Jacobson (2005) and Nishimura and Nemoto (2005) as references, as well as a figure (Fig. 5) in the supplement showing the correlation between friction velocity u_* and horizontal wind speed U.

RC2: *Page 10, Line 16: Please clarify 'two 7-10 day long periods'. I'd suggest wording such as 'two periods, one lasting 7 days and another 10 days', or similar.*

Reply: Added as follows.

Two periods, one lasting 7 days and another 10 days, were chosen based on data coverage to discuss key features of observed blowing snow and associated SSA increases.

RC2: *Page 11, Lines 3-4: Please provide concentrations in parentheses for context.*

Reply: Clarified as follows.

Near the surface spectral number densities $N_{0.4-12}$ for particles with $d_p<2\,\mu$m during the storm on 24 June remained with 10^5 m^{-3} below those seen at 29 m (10^6 m^{-3}) likely due to scavenging of aerosol by snow particles (Fig. 4d-e).

RC2: *Page 13, Lines 16-17: The direct comparison of $N_{0.4-12}$ to $d_pp<2\mu$m here is confusing since these are different size ranges.*

Reply: Clarified as follows.

Aerosol size spectra show that number densities of particles with size $d_p<2\,\mu$m increased during individual storms by 2-3 orders of magnitude above background levels.

RC2: *Page 14, Line 15: Please define SWE (snow water equivalent?) and the 'saltation layer' (what height?).*

Reply: Amended as follows.

1. (mm day^{-1} snow water equivalent) 2. The saltation layer is a layer just above the snow surface usually several centimetres thick (e.g. Déry and Yau, 1999).

RC2: *Page 15, Line 3: What does '(0.001)' correspond to here? Please clarify.*

Reply: Amended as follows.

... when snow drift density μ right above the snow surface exceeds a critical value μ_c (= 0.005 kg m^{-3}). For comparison a lower value of μ_c (= 0.001 kg m^{-3}) is also considered.

RC2: *Page 15, Lines 6 and 11: Please clarify that Ut and u*t are calculated, not observed.*

Reply: U_t and u^* are not calculated. Windspeed and snow particle number densities are both measured quantities; thus drift threshold wind speed is an observed quantity based on the combination of two measurements (symbols in Figure 8) as opposed to modelled values (Eq 4). Similar for friction velocity u^*. We added a sentence to clarify.

The observed threshold wind speed U_t and friction velocity u^*_t are the respective measurements at the onset of drifting or blowing snow.

RC2: *Page 15, Line 15: Please show how u*t values were calculated.*

Reply: u^* is not calculated. See reply above.

RC2: *Page 15, Line 32: Please define what you mean by 'minor' here. Please quantify.*

Reply: We did not run the model but the model bias in absolute values will cancel out because ratios are used (see Eq.2). Clarified as follows.

The model bias in q_{bsalt} is expected to cancel out in estimates of bulk sublimation rate Q_s (Eq. 2) and therefore also of SSA production Q_{SSA} (Eq. 1) because the calculation uses not absolute values but ratios of actual q_{bsalt} and its maximum q_{b0}.

RC2: *Page 17, Line 13: Please delete 'have' typo.*
Reply: done

RC2: *Page 17, Line 3: Didn't mean d_p increase?*
Reply: Decrease is correct. Expected is a decrease of d_p with height above the surface snow particle source in the absence of snowfall due to gravitational settling.

RC2: *Page 19, Line 32: Do you mean 0.1204 here?*
Reply: This has been corrected.

RC2: *Page 20, Lines 8-10: The wording 'well established' should be removed, as the Yang et al papers are models based on a hypothesis rather than measurement based and this associated uncertainty should be noted.*
Reply: Agreed and clarified as follows.
Modelling studies suggest that sea salt may be an important source of atmospheric bromine species in the mid to high southern latitudes, and that SSA from blowing snow releases bromine (Yang et al., 2008, 2010) driving ozone depletion events observed during or after snow storms (Jones et al., 2009).

RC2: *Page 20, Line 27: Data in Table 5 are presented in $\mu g\, g^{-1}$. Please fix or clarify.*
Reply: Corrected as follows.
Median bromide concentrations in snow ranged between 0.07 and 0.18 μg g^{-1} (Table 5).

RC2: *Page 21, Line 11: Change "due a" to "due to a".*
Reply: Corrected.

RC2: *Page 21, Line 14: No data are presented examining the acidity of the surface snowpack.*
Reply: Agreed, pH of aerosol and snow was not measured. We therefore removed reference to acidity.
The bromine release from SSA produced by blowing snow may be more efficient because it has a large fraction of sub-micron sized particles (see section 3.4.3), and resides at the well ventilated top of the blowing snow layer.

RC2: *Page 23, Line 22: Delete extra "the".*
Reply: Corrected.

RC2: *Page 23, Lines 29-30: Remove "always" and replace with "often" to more appropriately reflect the data shown.*
Reply: Agreed and amended.

RC2: *Page 25, Line 27: "LL & MM"?*
Reply: Mentors who prefer to remain anonymous

RC2: *Figure 16: The variations in these distributions (e.g. standard deviations) should be shown.*
Reply: Agreed, we updated Figure 16 including the standard deviation of the mean values, and corrected the caption (Fig. 3).

RC2: *Figure 17: This figure is difficult to understand currently.*
Reply: We updated Figure 17 and clarified the caption (Fig. 6).

SC1: *This manuscript describes an interesting set of measurements and detailed analysis confirming the blowing snow as a significant source for sea salt aerosol in the vicinity of sea ice in coastal Antarctica. We agree that this is an important result with significant implications for polar tropospheric aerosol loadings and heterogeneous halogen chemistry. However, it would be helpful to both the authors and readers of this article to refer to prior work also published in ACP showing similar results from measurements taken on sea ice in the Ross Sea. Giordano et al., 2018 also clearly identifies blowing snow on sea ice as a significant source of chlorine rich sea salt aerosol from online Aerosol Mass Spectrometer measurements of aerosol composition, optical measurements of blowing snow and interstitial aerosol concentrations and offline measurements of surface and blowing snow composition. The consistency between the results from observations using different techniques and on opposite sides of the Antarctic continent further indicates the importance of this mechanism to the overall Antarctic aerosol budget.*

Lars Kalnajs and Peter DeCarlo

Reference: Giordano, M. R., Kalnajs, L. E., Goetz, J. D., Avery, A. M., Katz, E., May, N. W., Leemon, A., Mattson, C., Pratt, K. A., and DeCarlo, P. F.: The importance of blowing snow to halogen-containing aerosol in coastal Antarctica: influence of source region versus wind speed, Atmos. Chem. Phys., 18, 16689-16711, https://doi.org/10.5194/acp-18- 16689-2018, 201

Reply: We agree and apologise for the oversight of this interesting study (see also reply to RC2 above). We now refer to this work in the introduction:

A recent observational study in the Ross Sea sector of coastal Antarctica also shows a significant association between increased SSA and high wind speed suggesting a link to blowing snow above sea ice as a source (Giordano et al., 2018).

References

Abbatt, J. P. D., Thomas, J. L., Abrahamsson, K., Boxe, C., Granfors, A., Jones, A. E., King, M. D., Saiz-Lopez, A., Shepson, P. B., Sodeau, J., Toohey, D. W., Toubin, C., von Glasow, R., Wren, S. N., and Yang, X.: Halogen activation via interactions with environmental ice and snow in the polar lower troposphere and other regions, Atmos. Chem. Phys., 12, 6237–6271, doi:10.5194/acp-12-6237-2012, 2012.

Abrahamsson, K., Granfors, A., Ahnoff, M., Cuevas, C. A., and Saiz-Lopez, A.: Organic bromine compounds produced in sea ice in Antarctic winter, Nature Communications, 9, 5291, doi:10.1038/s41467-018-07062-8, 2018.

Abram, N. J., Wolff, E. W., and Curran, M. A.: A review of sea ice proxy information from polar ice cores, Quaternary Science Reviews, 79, 168–183, doi:10.1016/j.quascirev.2013.01.011, 2013.

Butler, B. M., Papadimitriou, S., Santoro, A., and Kennedy, H.: Mirabilite solubility in equilibrium sea ice brines, Geochimica et Cosmochimica Acta, 182, 40 – 54, doi:10.1016/j.gca.2016.03.008, 2016.

Comiso, J. C. 2017. Bootstrap Sea Ice Concentrations from Nimbus-7 SMMR and DMSP SSM/I-SSMIS, Version 3, Boulder, Colorado USA. NASA National Snow and Ice Data Center Distributed Active Archive Center, doi:10.5067/7Q8HCCWS4I0R, accessed on 22 February 2018.

de Leeuw, G., Andreas, E. L., Anguelova, M. D., Fairall, C. W., Lewis, E. R., O'Dowd, C., Schulz, M., and Schwartz, S. E.: Production flux of sea spray aerosol, Rev. Geophys., 49, doi:10.1029/2010RG000349, 2011.

Déry, S. J. and Yau, M.: A Bulk Blowing Snow Model, Bound.-Lay. Meteorol., 93, 237–251, doi:10.1023/A:1002065615856,1999.

Dominé, F., Sparapani, R., Ianniello, A., and Beine, H. J.: The origin of sea salt in snow on Arctic sea ice and in coastal regions, Atmos. Chem. Phys., 4, 2259–2271, doi:10.5194/acp-4-2259-2004, 2004.

Hill, M. K., Brooks, B. J., Norris, S. J., Smith, M. H., Brooks, I. M., and de Leeuw, G.: A Compact Lightweight Aerosol Spectrometer Probe (CLASP), J. Atmos. Ocean Tech., 25, 1996–2006, doi:10.1175/2008JTECHA1051.1, 2008.

Huang, J. and Jaeglé, L.: Wintertime enhancements of sea salt aerosol in polar regions consistent with a sea ice source from blowing snow, Atmos. Chem. Phys., 17, 3699–3712, doi:10.5194/acp-17-3699-2017, 2017.

Jacobson, M. Z.: Fundamentals of Atmospheric Modeling, Cambridge University Press, Cambridge, United Kingdom, 2005.

Jones, A. E., Wolff, E. W., Ames, D., Bauguitte, S. J.-B., Clemitshaw, K. C., Fleming, Z., Mills, G. P., Saiz-Lopez, A., Salmon, R. A., Sturges, W. T., and Worton, D. R.: The multi-seasonal NO_y budget in coastal Antarctica and its link with surface snow and ice core nitrate: results from the CHABLIS campaign, Atmos. Chem. Phys., 11(17), 9271–9285, doi:10.5194/acp-11-9271-2011, 2011.

Jones, A. E., Anderson, P. S., Begoin, M., Brough, N., Hutterli, M. A., Marshall, G. J., Richter, A., Roscoe, H. K., and Wolff, E. W.: BrO, blizzards, and drivers of polar tropospheric ozone depletion events, Atmos. Chem. Phys., 9, 4639–4652, 2009.

King, J. C. and Anderson, P. S.: Heat and water vapor fluxes and scalar roughness lengths over an Antarctic ice shelf, Bound.-Lay. Meteorol., 69, 101–121, 1994.

Legrand, M., Preunkert, S., Wolff, E., Weller, R., Jourdain, B., and Wagenbach, D.: Year-round records of bulk and size-segregated aerosol composition in central Antarctica (Concordia site) – Part 1: Fractionation of sea-salt particles, Atmos. Chem. Phys., 17, 14 039–14 054, doi:10.5194/acp-17-14039-2017, 2017.

Legrand, M., Yang, X., Preunkert, S., and Theys, N.: Year-round records of sea salt, gaseous, and particulate inorganic bromine in the atmospheric boundary layer at coastal (Dumont d'Urville) and central (Concordia) East Antarctic sites, J. Geophys. Res., doi:10.1002/2015JD024066, 2016.

Li, L. and Pomeroy, J. W.: Estimates of Threshold Wind Speeds for Snow Transport Using Meteorological Data, J. Appl. Meteorol., 36, 205–213, doi:10.1175/1520-0450(1997)036<0205:EOTWSF>2.0.CO;2, 1997.

Massom, R. A., Eicken, H., Hass, C., Jeffries, M. O., Drinkwater, M. R., Sturm, M., Worby, A. P., Wu, X., Lytle, V. I., Ushio, S., Morris, K., Reid, P. A., Warren, S. G., and Allison, I.: Snow on Antarctic Sea Ice, Rev. Geophys., 39, 413–445, doi:10.1029/2000RG000085, 2001.

May, N. W., Quinn, P. K., McNamara, S. M., and Pratt, K. A.: Multiyear study of the dependence of sea salt aerosol on wind speed and sea ice conditions in the coastal Arctic, J. Geophys. Res., 121, 9208–9219, doi:10.1002/2016JD025273, 2016JD025273, 2016.

Nilsson, E. D., Rannik, Ü., Swietlicki, E., Leck, C., Aalto, P. P., Zhou, J., and Norman, M.: Turbulent aerosol fluxes over the Arctic Ocean: 2. Wind-driven sources from the sea, J. Geophys. Res., 106, 32 139–32 154, doi:10.1029/2000JD900747, 2001.

Nishimura, K. and Nemoto, M.: Blowing snow at Mizuho station, Antarctica, Phil. Trans. R. Soc. A, 363, 1647–1662, doi:10.1098/rsta.2005.1599, 2005.

Norris, S. J., Brooks, I. M., Hill, M. K., Brooks, B. J., Smith, M. H., and Sproson, D. A. J.: Eddy covariance measurements of the sea spray aerosol flux over the open ocean, J. Geophys. Res., 117, doi:10.1029/2011JD016549, 2012.

O'Dowd, C. D., Smith, M. H., Consterdine, I. E., and Lowe, J. A.: Marine aerosol, sea-salt, and the marine sulphur cycle: a short review, Atmos. Environ., 31, 73 – 80, doi:10.1016/S1352-2310(96)00106-9, 1997.

Oum, K. W., Lakin, M. J., and Finlayson-Pitts, B. J.: Bromine activation in the troposphere by the dark reaction of O3 with seawater ice, Geophys. Res. Lett., 25, 3923–3926, doi:10.1029/1998GL900078, 1998.

Rankin, A. M. and Wolff, E. W.: A year-long record of size-segregated aerosol composition at Halley, Antartica, J. Geophys. Res., 108, doi:10.1029/2003JD003993, 2003.

Sander, R., Keene, W. C., Pszenny, A. A. P., Arimoto, R., Ayers, G. P., Baboukas, E., Cainey, J. M., Crutzen, P. J., Duce, R. A., Hönninger, G., Huebert, B. J., Maenhaut, W., Mihalopoulos, N., Turekian, V. C., and Van Dingenen, R.: Inorganic bromine in the marine boundary layer: a critical review, Atmos. Chem. Phys., 3, 1301–1336, doi:10.5194/acp-3-1301-2003, 2003.

Rhodes, R. H., Yang, X., Wolff, E. W., McConnell, J. R., and Frey, M. M.: Sea ice as a source of sea salt aerosol to Greenland ice cores: a model-based study, Atmos. Chem. Phys., 17, 9417–9433, doi:10.5194/acp-17-9417-2017, 2017.

Soo, J.-C., Monaghan, K., Lee, T., Kashon, M., and Harper, M.: Air sampling filtration media: Collection efficiency for respirable size-selective sampling, Aerosol Sci. Technol., 50, 76–87, 2016.

Wagenbach, D., Ducroz, F., Mulvaney, R., Keck, L., Minikin, A., Legrand, M., Hall, J. S., and Wolff, E. W.: Sea-salt aerosol in coastal Antarctic regions, J. Geophys. Res., 103, 10 961–10 974, doi:10.1029/97JD01804, 1998.

Weller, R., Wagenbach, D., Legrand, M., Elsässer, C., Tian-Kunze, X., and König-Langlo, G.: Continuous 25-yr aerosol records at coastal Antarctica – I: inter-annual variability of ionic compounds and links to climate indices, Tellus B, 63, 901–919, doi:10.1111/j.1600-0889.2011.00542.x, 2011.

Yang, X., Frey, M. M., Rhodes, R. H., Norris, S. J., Brooks, I. M., Anderson, P. S., Nishimura, K., Jones, A. E., and Wolff, E. W.: Sea salt aerosol production via sublimating wind-blown saline snow particles over sea ice: parameterizations and relevant microphysical mechanisms, Atmos. Chem. Phys., 19, 8407–8424, doi:10.5194/acp-19-8407-2019, 2019.

Yang, X., Pyle, J. A., Cox, R. A., Theys, N., and Van Roozendael, M.: Snow-sourced bromine and its implications for polar tropospheric ozone, Atmos. Chem. Phys., 10, 7763–7773, doi:10.5194/acp-10-7763-2010, 2010.

Yang, X., Pyle, J. A., and Cox, R. A.: Sea salt aerosol production and bromine release: Role of snow on sea ice,, Geophys. Res. Lett.,, 35, doi:10.1029/2008GL034536, 2008.

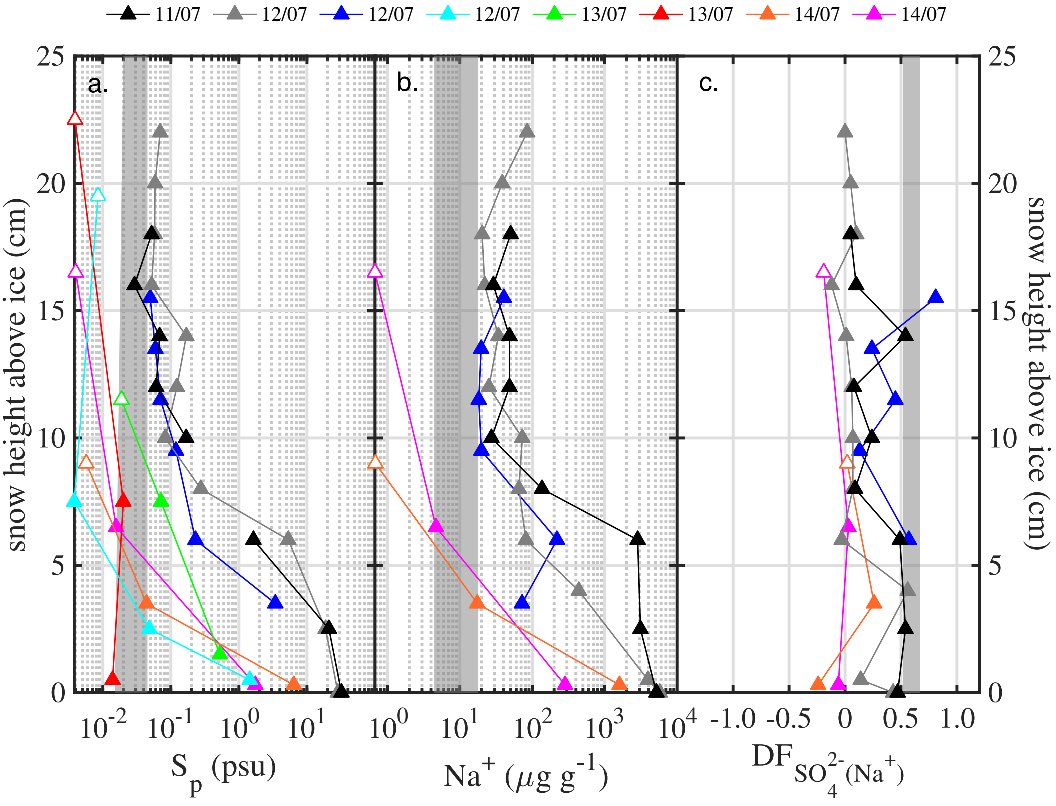

Figure 1: manuscript Figure 7 - Vertical snowpack profiles sampled at various locations on the ice floe of ice station S6 during the 11–14 July 2013 period (color indicates day of sampling): (a) salinity S_p, (b) Na^+ concentrations and (c) sulfate depletion factor $DF_{SO_4^{2-}}$ with respect to Na^+ as a function of snow height above the sea ice surface. Symbols illustrate averages for snow layers of 2 cm thickness, except those with white face color indicating 0.5-1.0 cm layer thickness. Data points at the top of each profile represent the surface snow layer, thus adding half the snow layer thickness to snow height yields total snowpack depth. Shaded areas illustrate the range of the respective parameter measured in blowing snow on 15 July 2013 (Fig. 6e-f).

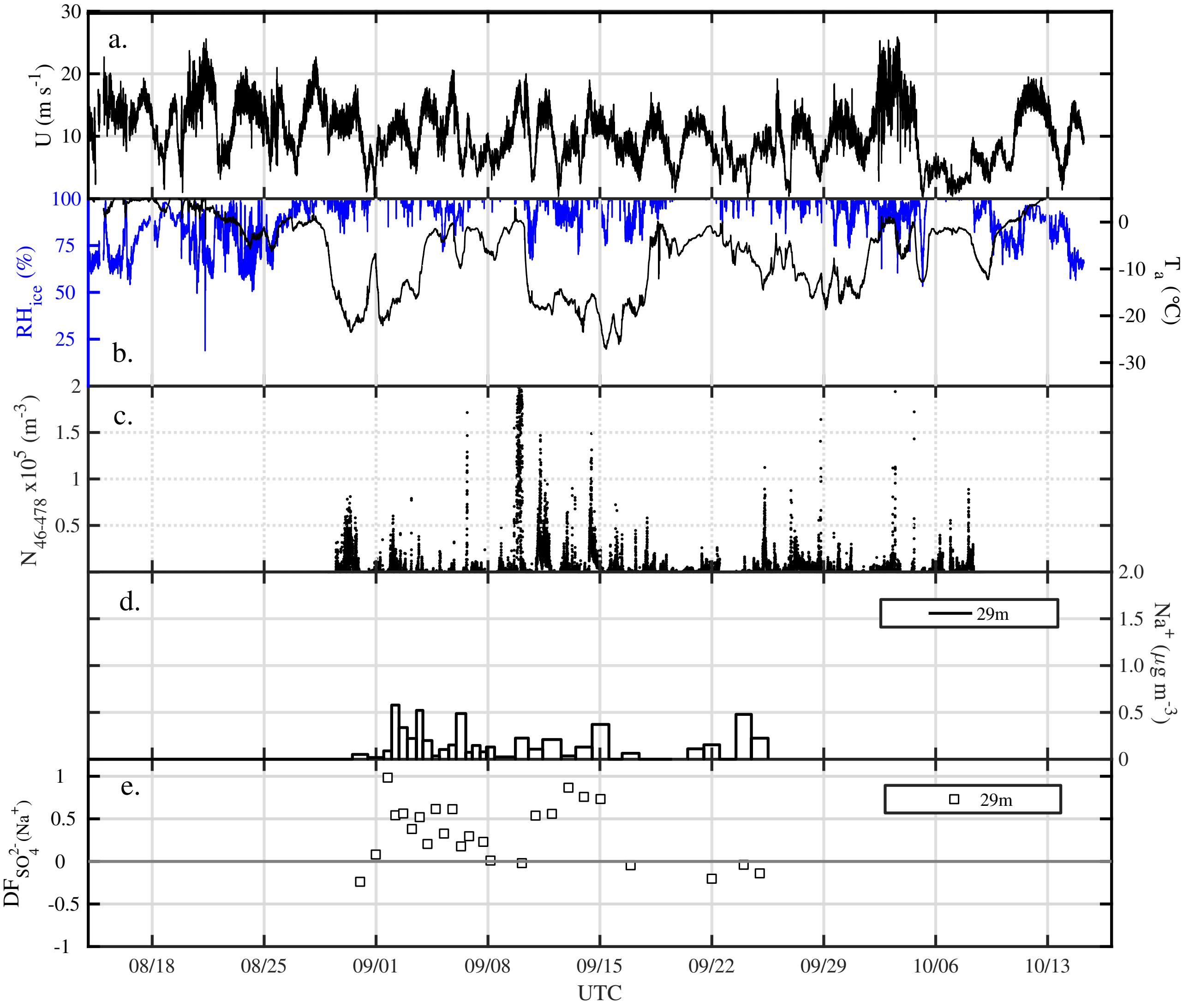

Figure 2: manuscript Figure S1 - Overview of atmospheric observations in the Weddell Sea from 14 August to 17 October 2013 (ANT-XXIX/7): (a) horizontal wind speed U at 39 m. (b) ambient temperature T_a and relative humidity with respect to ice RH_{ice} at 29 m. (c) total number densities N_{46-478} of airborne snow particles at 29 m. (d) aerosol Na^+ concentrations and (e) sulphate depletion factor $DF_{\mathrm{SO}_4^{2-}}$, both at 29 m.

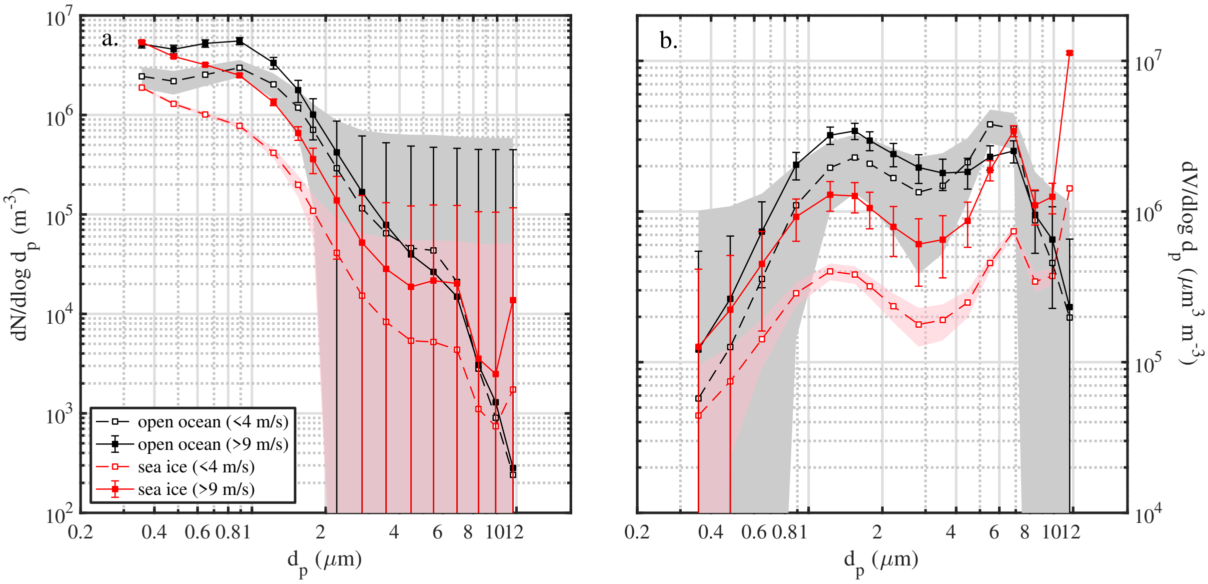

Figure 3: manuscript Figure 16 - Comparison of mean number distributions (panel a) and volume distributions (panel b) of aerosol above the open ocean (13 to 16 June 2013) and sea ice in the Weddell Sea (18 June to 21 July 2013) during calm (U_{10m}<4 m s^{-1}) and windy (U_{10m}>9 m s^{-1}) conditions. Shaded areas and error bars show the standard deviation of the mean during calm and windy conditions, respectively. Data included are observations from 29 m above the sea surface at ambient RH.

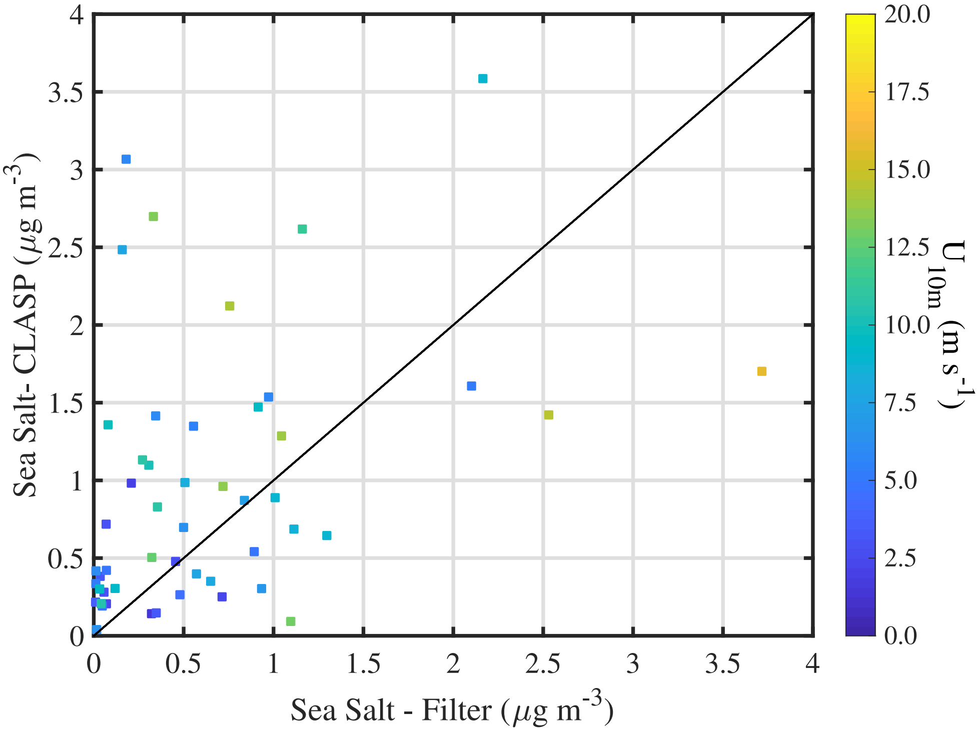

Figure 4: manuscript Figure S3 - Comparison of atmospheric sea salt concentrations during the 8 June to 26 July 2013 period derived from filter measurements and from median number densities $N_{0.4-12}$ measured with the CLASP during filter sampling intervals. Data included are observations from 29 m above the sea surface. Symbols are color coded based on wind speed U_{10m}.

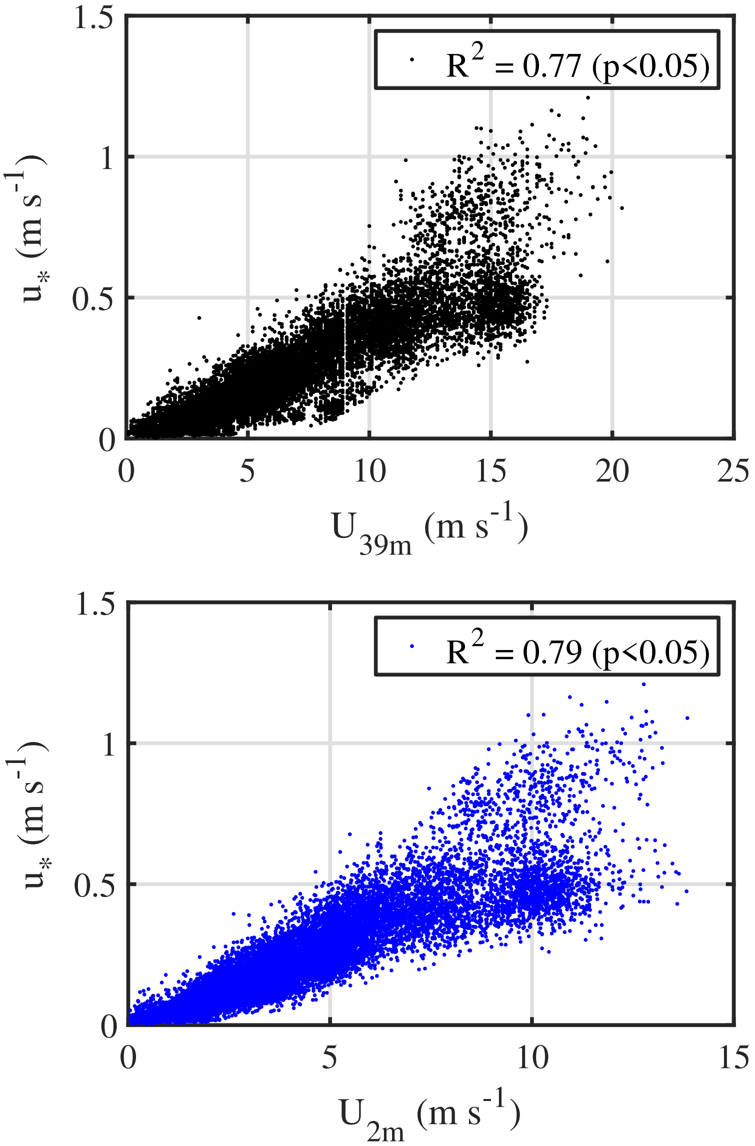

Figure 5: manuscript Figure S2 - Comparison between friction velocity u_* and horizontal wind speed U at 2 and 39 m above the sea ice surface. The legends shows respective coefficients of determination of the linear regression. Note that U_{2m} has been derived from the 3-D wind measurements of the sonic anemometer.

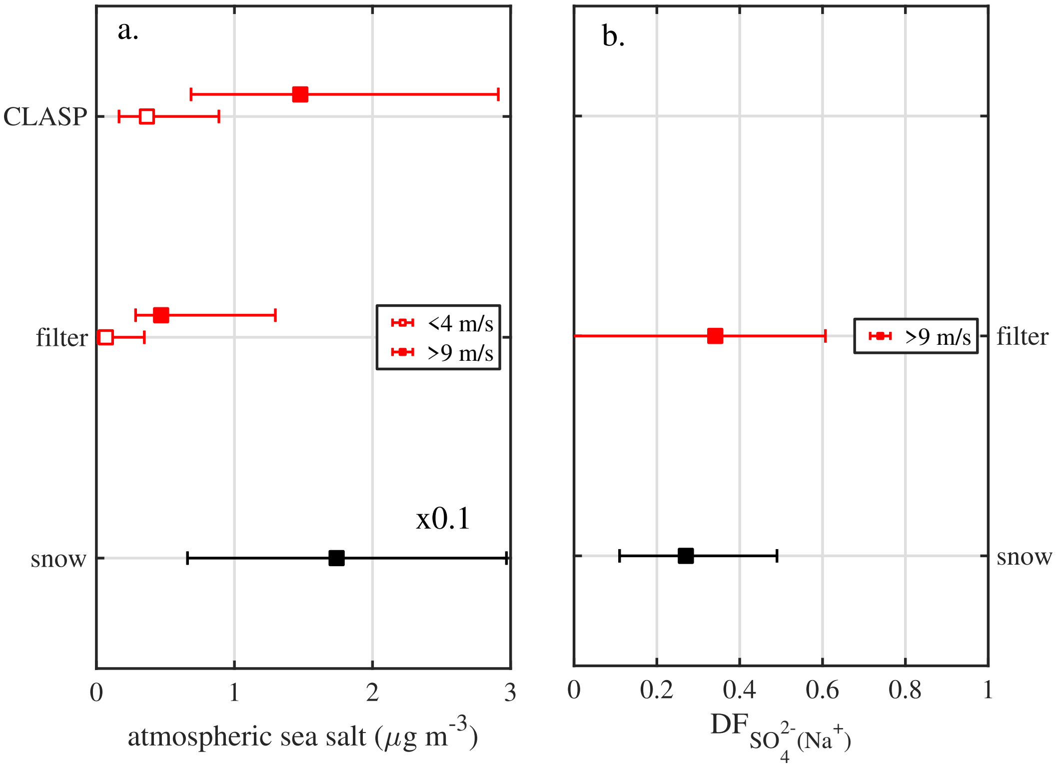

Figure 6: manuscript Figure 17 - The partitioning of sea salt between atmosphere and snow, and sulfate depletion above first year sea ice from 18 June to 21 July 2013. Panel (a) shows median atmospheric sea salt concentrations during calm (U_{10m} <4 $\mathrm{m\,s^{-1}}$) and windy (U_{10m} >9 $\mathrm{m\,s^{-1}}$) conditions derived from aerosol filter measurements (filter) and spectral particle number densities $N_{0.4-12}$ (CLASP) (see text). For comparison, a potential atmospheric concentration is calculated assuming that all sea salt observed in the top 0.1 mm of snow on sea ice was released by sublimation and mixed into a 100 m thick boundary layer (for better comparison multiplied here by 0.1). Panel (b) shows for the same time period median sulfate depletion factors $DF_{SO_4^{2-}}$ (with respect to $\mathrm{Na^+}$) in in surface snow and in aerosol during windy (U_{10m} >9 $\mathrm{m\,s^{-1}}$) conditions. Symbols and errorbars represent median and lower and upper quartiles, respectively.

Table 1: manuscript Table 4 - Descriptive statistics of the aerosol chemistry during ANT-XXIX/6 (ANT6) and ANT-XXIX/7 (ANT7) with mean and median values weighted by the filter sampling interval. Ion and sea salt concentrations are in units of ng m^{-3}. See section 2.4 for definition of depletion factors DF.

Parameter	ANT6						ANT7		
	at 2 m			at 29 m			at 29 m		
	mean $\pm\sigma$	median	N^a	mean $\pm\sigma$	median	N^a	mean $\pm\sigma$	median	N^a
sea-salt^b	707 ±1500	336	43	1253 ±2319	639	106	559 ±486	425	28
Na$^+$	217 ±460	103	43	384 ±711	196	106	171 ±149	130	28
Cl$^-$	379 ±765	179	43	656 ±1225	302	106	311 ±282	232	27
SO$_4^{2-}$	28^c ±61	19^c	38	75 ±152	45	84	33 ±30	23^c	28
Br$^-$	2.0 ±1.0	1.9	42	1.5^c ±3.0	0.7^c	98	0.5^c ±0.6	0.5^c	23
$DF_{SO_4^{2-}}$	0.29 ±0.57	0.48	38	0.07 ±0.94	0.29	74	0.12 ±0.60	0.21	27
DF_{Na^+}	-0.08 ±0.29	-0.03	43	-0.46 ±2.29	-0.04	97	-0.02 ±0.19	-0.01	27
DF_{Br^-}	-1.66 ±1.86	-1.86	36	0.04 ±0.96	0.37	89	0.05 ±1.26	0.49	23

[a] sample size [b] sea salt concentration is derived by multiplying the Na$^+$ concentration by 3.262 based on the Na$^+$ mass fraction in reference seawater after Millero et al., 2008 [c] below the estimated LOD (Table 3)

Table 2: manuscript Table 5 - Descriptive statistics of the volume-integrated snow chemistry during ANT-XXIX/6 on first-year sea ice (FYI) at ice stations S1-S6, on multi-year sea ice (MYI) at ice stations S7-9, and for snow layers within 10 cm of the snow surface (TOP10). Ion and sea salt concentrations are in units of μg g^{-1}. See section 2.4 for definition of depletion factors DF.

Parameter	FYI			MYI			TOP10		
	mean $\pm\sigma$	median	N^a	mean $\pm\sigma$	median	N^a	mean $\pm\sigma$	median	N^a
snow depth (cm)	20.9 ±8.3	19.0	17	50.0 ±32.2	33.0	7	-	-	-
S_p (psu)	1.40 ±3.99	0.11	110	0.82 ±4.31	0.02	104	0.31 ±0.90	0.06	96
sea salt^b	1176 ±3518	83	86	590 ±3157	22	95	249 ±729	58	80
Na^+	361 ±1079	26	86	181 ±968	7	95	76 ±223	18	80
Cl^-	680 ±2035	48	87	305 ±1842	13	98	141 ±415	34	81
SO_4^{2-}	61 ±182	6	87	30 ±166	1	98	17 ±62	3	81
Br^-	4.28 ±12.23	0.18	85	1.76 ±10.92	0.07	90	1.01 ±3.72	0.12	78
$DF_{SO_4^{2-}}$	0.19 ±0.41	0.24	86	0.33 ±0.44	0.35	94	0.27 ±0.39	0.27	80
DF_{Na^+}	0.01 ±0.38	0.06	86	-1.09 ±8.88	0.07	94	-0.11 ±0.99	0.06	80
DF_{Br^-}	-0.25 ±0.98	0.05	83	-0.28 ±1.16	-0.01	86	-0.21 ±0.99	0.04	76

[a] sample size [b] sea salt concentration is derived by multiplying the Na^+ concentration by 3.262 based on the Na^+ mass fraction in reference seawater after Millero et al., 2008

Table 3: manuscript Table S1 - Descriptive statistics of airborne snow particles observed for 8 June to 12 August 2013 (ANT6) and for 14 August to 16 October 2013 (ANT7): total number densities N_{46-478} and particle diameter d_p. Statistics refer to periods when airborne snow particles were present, i.e. times with no snow particles observed were removed prior to averaging.

Parameter	ANT6 at 0.2 m	at 29 m[a]	at 29 m	ANT7 at 29 m
N_{46-478} (m^{-3})				
mean	2.6×10^5	4.0×10^3	8.7×10^3	7.2×10^3
σ	7.4×10^3	9.5×10^3	2.7×10^4	2.2×10^4
median	4.7×10^3	7.7×10^2	9.9×10^2	1.3×10^3
d_p (µm)				
mean	138	132	133	143
σ	59	59	53	53
median	132	117	124	136
N[b]	8608	11766	42959	37123
sampling time (days)[c]	6	8	30	26

[a] for direct comparison of vertical differences statistics of the 29 m measurements only for times when sea ice observations at 0.2 m were available [b]sample size [c]total aggregated time during which airborne snow particles were detected

Table 4: manuscript Table S2 - Descriptive statistics of aerosol observed during 8 June - 26 July 2013 (ANT6): total number densities $N_{0.4-12}$ and particle diameter d_p.

Parameter	at 0.2 m	at 2 m	at 29 m[a]	at 29 m
$N_{0.4-12}$ (m^{-3})				
mean	1.7×10^6	1.4×10^6	1.4×10^6	2.1×10^6
σ	2.5×10^6	1.9×10^6	1.6×10^6	6.4×10^6
median	8.6×10^5	5.6×10^5	8.0×10^5	1.1×10^6
d_p (µm)				
mean	0.67	0.60	0.67	0.69
σ	0.11	0.06	0.11	0.14
median	0.66	0.60	0.65	0.66
N[b]	13077	14907	9963	48892
sampling time (days)[c]	9	10	7	34

[a] for direct comparison of vertical differences statistics of the 29 m measurements only for times when sea ice observations at 2 m were available [b]sample size [c]total aggregated sampling time

First direct observation of sea salt aerosol production from blowing snow above sea ice

Markus M. Frey[1], Sarah J. Norris[2], Ian M. Brooks[2], Philip S. Anderson[3], Kouichi Nishimura[4], Xin Yang[1], Anna. E. Jones[1], Michelle G. Nerentorp Mastromonaco[5], David H. Jones[1,6], and Eric W. Wolff[7]

[1]Natural Environment Research Council, British Antarctic Survey, Cambridge, UK
[2]University of Leeds, Leeds, UK
[3]Scottish Association for Marine Science, Oban, UK
[4]Nagoya University, Nagoya, Japan
[5]IVL Swedish Environmental Institute, Stockholm, Sweden
[6]now at: Neptec, UK LtD., Oxford, UK
[7]University of Cambridge, Cambridge, UK

Correspondence: M. M. Frey (maey@bas.ac.uk)

Abstract. Two consecutive cruises in the Weddell Sea, Antarctica, in winter 2013 provided the first direct observations of sea salt aerosol (SSA) production from blowing snow above sea ice, thereby validating a model hypothesis to account for winter time SSA maxima in ~~polar regions not explained otherwise~~the Antarctic. Blowing or drifting snow ~~always~~ often lead to increases in SSA during and after storms. Observed aerosol gradients suggest that net production of SSA takes place near the top of the blowing or drifting snow layer. The observed relative increase of SSA concentrations with wind speed suggests that on average the corresponding aerosol mass flux during storms was equal or larger above sea ice than above the open ocean, demonstrating the importance of the blowing snow source for SSA in winter and early spring. For the first time it is shown that snow on sea ice is depleted in ~~sulphate~~ sulfate relative to sodium with respect to sea water. Similar depletion in bulk aerosol observed in the ~~aerosol~~ ∼0.3-6 µm range suggests that most sea salt originated from snow on sea ice and not the open ocean or leads, e.g. ~~on average ∼93~~based on median values >90 % during the 8 June and 12 August 2013 period. A mass budget calculation shows that sublimation of snow even with low salinity (<1 psu) can account for observed increases of atmospheric sea salt from blowing snow. Furthermore, snow on sea ice and blowing snow showed no or small depletion of bromide relative to sodium with respect to sea water, whereas aerosol ~~at~~ was enriched at 2 m and depleted at 29 m ~~was enriched suggesting that~~ suggesting that significant bromine loss takes place in the aerosol phase further aloft and that SSA from blowing snow is a source of atmospheric reactive bromine, an important ozone sink, ~~with bromine loss taking place preferentially in the aerosol phase between 2 and 29 above the sea ice surface~~even in winter. Evaluation of the current model for SSA production from blowing snow showed that the parameterisations used can generally be applied to snow on sea ice. Snow salinity, a sensitive model parameter, depends to a first order on snowpack depth and therefore is higher above first-year (FYI) than above multi-year sea ice (MYI). Shifts in the ratio of FYI and MYI over time are therefore expected to change the seasonal SSA source flux and contribute to the variability of

SSA in ice cores, which both represents an opportunity and a challenge for the quantitative interpretation of the sea salt sea ice proxy. ~~It is expected that similar processes take place above Arctic sea ice.~~

1 Introduction

Atmospheric aerosol represents the largest source of uncertainty in global climate predictions (Boucher et al., 2013), and includes sea salt aerosol (SSA), which is the main background aerosol above the oceans. In general global climate and aerosol models strongly under-predict Aitken and accumulation mode particle concentrations compared to observations (Mann et al., 2014) and do not capture the winter maximum of SSA observed at several locations in the Arctic and Antarctica (e.g. Huang and Jaeglé, 2017). A quantitative understanding of SSA sources is critical since SSA influences radiative forcing and therefore climate both directly by absorbing and scattering sunlight and indirectly by modifying the reflectivity, lifetime, and extent of clouds (O'Dowd et al., 1997; DeMott et al., 2016). Uncertainties in cloud properties explain much of the spread in the modelled climate sensitivity (Flato et al., 2013) and are due in large part to lacking knowledge about aerosol sources. SSA plays also an important role in polar tropospheric ozone and halogen chemistry through the release of active bromine in polar spring contributing to ozone depletion events (ODEs) (e.g. Yang et al., 2010; Kalnajs et al., 2013; Choi et al., 2018). Furthermore, SSA is easily measured in polar ice cores but its use as a quantitative proxy of past sea ice conditions is complicated by uncertainties related to SSA source contributions and processes as well as transport meteorology (Abram et al., 2013; Levine et al., 2014; Rhodes et al., 2017), and more recently in the case of bromide Br^- (e.g. Spolaor et al., 2013) also to post-depositional processing associated with the bromine explosion chemistry of ODEs (Simpson et al., 2005; Pratt et al., 2013).

Globally most SSA originates from the open ocean, where sea spray is produced by wave breaking and bubble bursting generating film and jet drops (de Leeuw et al., 2011). However, previous observations in Antarctica provide two-fold evidence of the existence of a significant SSA source associated with sea ice. First, SSA exhibits maxima during winter/spring in the atmosphere (Rankin and Wolff, 2003; Jourdain et al., 2008; Legrand et al., 2017) and in seasonally resolved ice core records (e.g. Frey et al., 2006); in deep ice cores highest values are seen during glacial periods (Wolff et al., 2003). Thus the highest values are observed when sea ice is at its seasonal or long-term maximum. And second, SSA in the lower atmosphere above coastal Antarctica is strongly depleted in ~~sulphate~~ sulfate (SO_4^{2-}) compared to seawater (Wagenbach et al., 1998) as are also brine and frost flowers in the sea ice nearby (Rankin et al., 2000). Fractionation of SO_4^{2-} and to much lesser extent of sodium (Na^+) in sea ice occurs during the cooling of sea ice brine down to its eutectic point due to precipitation of the mineral mirabilite ($Na_2SO_4 \cdot 10\,H_2O$) at temperatures below -6.4 °C resulting in ion ratios in liquid and solid phase that are different compared to sea water (Butler et al., 2016). At first it had been thought that observed fractionated SSA originates mostly from highly saline frost flowers, which exhibit a similar ~~sulphate~~ sulfate depletion (Rankin et al., 2000). However, recent laboratory (Roscoe et al., 2011; Yang et al., 2017) and model (Huang and Jaeglé, 2017) studies indicate that frost flowers likely play only a minor role in producing SSA because they do not get easily airborne and do not occur widely enough in space and time to produce large enough SSA quantities.

A more recent hypothesis based on a numerical model suggests that salty blowing snow that undergoes sublimation may be a significant source of SSA with a production per unit area equal or larger than that above the open ocean (Yang et al., 2008). Indeed, model agreement with SSA winter maxima observed at a number of locations in the polar regions ~~can only be explained if the~~ is much improved when a SSA source from blowing snow based on the parameterisation of ~~Yang et al. (2008)~~ (Yang et al., 2008) is included in the model ~~(Huang and Jaeglé, 2017).~~ (Huang and Jaeglé, 2017; Yang et al., 2019). A recent observational study in the Ross Sea sector of coastal Antarctica also shows a significant association between increased SSA and high wind speed suggesting a link to blowing snow above sea ice as a source (Giordano et al., 2018).

However, the blowing snow hypothesis and mechanism lack validation by direct observation. In particular, the applicability of the scheme used by all model studies to date ~~(Huang and Jaeglé, 2017; Rhodes et al., 2017; ?)~~ (Huang and Jaeglé, 2017; Rhodes et al., 2017; Yang et al., 2019) for sea ice is not known, because model parameterisations are based on blowing snow measurements above ice sheets (Budd, 1966; Mann et al., 2000; Nishimura and Nemoto, 2005) and the Canadian prairies (Déry and Yau, 2001, and ref. therein).

In this study we report the first direct observations of sea salt aerosol from within the Antarctic sea ice zone during winter, when the blowing snow source is expected to be most active. We discuss ~~SSA variability~~ the chemical fractionation in aerosol and snow as well as SSA variability and origin during and after blowing snow events supported by a unique set of measurements of physical and chemical properties of atmospheric aerosol, snow particles and the snowpack on sea ice. We then critically evaluate the current model parameterisation of sea salt aerosol production from blowing snow based on the *in situ* observations and discuss ~~chemical fractionation of sulphate and bromide, aerosol size distribution and~~ the mass budget of sea salt aerosol above sea ice. A comparison between our observations and a global chemistry transport model is described in a companion study ~~(?)~~(Yang et al., 2019).

2 Methods

Two consecutive Antarctic expeditions were carried out in the Weddell Sea aboard the German icebreaker *RV Polarstern* in 2013, the ~~*Antarctic Winter Ecosystem Climate Study (AWECS)*~~ *Antarctic Winter Ecosystem Climate St* ANT-XXIX/6 between 8 June and 12 August (Lemke, 2014), and the spring expedition ANT-XXIX/7 between 14 August and 16 October (Meyer, 2014) (Fig. 1). We report mainly on results from ANT-XXIX/6, which provided a significantly more extensive dataset. Atmospheric measurements and sampling were carried out continuously from the crow's nest of *RV Polarstern*, and on the sea ice during nine 3–104 hr long ice stations (Table 1). Ice station S3 was occupied for 3 hr (Table 1) allowing only for collection of snow samples. Instruments were set up on the sea ice typically at 0.8 to 1.5 km distance from the ship. Sea ice thickness measurements during ANT-XXIX/6 (Arndt and Paul, 2018) showed that ice stations S1-6 in the eastern sector of the Weddell Sea were on first-year sea ice, whereas ice stations S7-S9 near the Antarctic Peninsula were on multi-year sea ice (Fig. 1). This is in agreement with the observation that persistent multi-year sea ice in the Weddell sea occurs only east of the Antarctic peninsula due to a circulating ocean current. The distance to the nearest open water was ∼600–1000 km for ice stations S1-6 and ∼200–400 km for ice stations S7-9 (Fig. 1, Table 1). Sea ice concentrations in mid July 2013 derived from Nimbus-7 satellite microwave radiometer measurements (Comiso, 2018) show areas with 85-95 % ice cover near ice stations S2-3 and S7-9 indicating that open leads may be present (Fig. 1). As *RV Polarstern* travelled south day lengths decreased until the sun remained entirely below the horizon between 23 June and 7 July providing only a few hours of twilight per day. All times are in UTC. A summary of instrumentation and temporal coverage is given in Table 2 and experimental details for each measurement are described below.

2.1 Airborne snow particles

Size resolved number densities of airborne snow particles in the diameter range 36–490 µm were measured at a mean height of ∼0.16 m (range 0.07-0.37 m) on the sea ice, and at 29 m from the crow's nest of *RV Polarstern* using an open-path snow particle counter (SPC-95, Niigata Electric Co., Ltd) described previously (Nishimura and Nemoto, 2005; Nishimura et al., 2014). In brief, the SPC is a ~~single slit~~ single-slit sensor with a laser diode and measures diameter and number of drifting snow particles by detecting their shadows. The SPC is mounted on a self-steering wind vane, and hence, the sampling area A (2×10^{-3}m × 25×10^{-3}m) and volume ($A\times0.5\times10^{-3}$m) are maintained perpendicular to the prevailing wind direction. Electric pulse signals resulting from snow particles passing through the sampling volume are sent to a transducer and an analysing data logging system. Assuming that the detected particle size is the equivalent diameter d_p of a sphere each signal is classified into one of 64 mean particle diameter classes between 36 and 490 µm. The SPCs were calibrated by the manufacturer in Japan at -10 and -30 °C for particle diameters 137, 229, 314, 399 and 449 µm, respectively. The instrument output at the calibration temperature of -10 °C, close to the ANT-XXIX/6 median of -11.8 °C, showed very good agreement with the expected representative particle diameter. Therefore no temperature corrections were applied. Particle counts from the smallest diameter class (d_p=36 µm) have large uncertainties due to the instrument's detection limit, whereas particle counts from the largest diameter class (d_p=490 µm) showed frequent spikes due to detection of precipitating snow. Particle counts from the smallest and largest diameter class were therefore discarded.

Particle counts h measured at a sampling rate SR of 1 Hz are integrated to 1-minute values and divided by sampling area A to obtain particle number flux F in units of m^{-2} minute^{-1}. Snow particle number densities for the diameter range 46–478 µm, N_{46-478}, are then computed using $N_{46-478} = FU^{-1}$ with horizontal wind speed U and are reported at ambient temperature, pressure and relative humidity in units of m^{-3}. Wind speeds measured near the crow's nest at 39 m by the ship's meteorology observatory (see section 2.5) and on the sea ice at 2 m by a sonic anemometer (see section 2.5) were extrapolated to the respective instrument heights. To do this a logarithmic wind profile $U(z)$ is assumed given by $U(z) =$ ~~k~~ $u_*/\kappa \ln(z/z_0)$ (e.g. Li and Pomeroy, 1997), with measurement height z, the von Karman constant κ $(= 0.4)$, friction velocity u_* and the surface roughness length of momentum z_0 set to 5.6×10~~-5~~$^{-5}$ m as measured very consistently above snow at Halley (King and Anderson, 1994). Wind speed at instrument level is then derived using $U(z_2) = U(z_1)\ \ln(z_2/z_0) / \ln(z_1/z_0)$. It should be borne in mind that the distortion of flow caused by the ship may mean both that speed at 39 m is not representative of flow in the far field at that height, and further, the turbulent field strength, which governs the gradient of the logarithmic profile, may be a residual from a different, likely lower, height. Thus, we suggest care when interpreting the data, and estimate that the conversion from particle counts to number density be seen as an estimate suitable for comparison, rather than quantitative with a well behaved uncertainty.

2.2 Sea salt aerosol

Size-resolved number densities of SSA sized particles were measured at mean heights of 0.19 m (range 0.13-0.25 m) and 2.16 m (range 1.98-2.2 m) on the sea ice, and at 29 m from the crow's nest of *RV Polarstern* using a Compact Lightweight Aerosol Spectrometer Probe (CLASP) (Hill et al., 2008; Norris et al., 2008). The CLASP is a closed-path optical particle spectrometer, which aspirates sample air at a nominal flow rate Q of ∼3 STP-L min^{-1}, which is actively controlled by onboard electronics, and recorded to allow subsequent correction of the particle spectra for any minor flow variations. An improved version of the CLASP instrument as used by Norris et al. (2012) was deployed, which measures a 16–channel size spectrum covering particle diameters d_p in the range of 0.36–11.62 µm at ambient humidity at a sampling rate SR of 1 Hz. CLASP pump and scatter cell were calibrated in the lab before and after the cruise. Particle losses to inlet walls are ~~minimized by use of a short inlet of <~~minimised by using a short and straight inlet tube of 0.3~~. As~~ m length similar to the original configuration (Hill et al., 2008, Figure 9). We assume as an upper limit ~~for particle losses we adopt the estimates by Norris et al. (2012) for a different inlet configuration~~ of particle losses those estimated previously for a similar inlet configuration (Norris et al., 2012), which amount to 43 % at ~~d_p~~ $\mathrm{d}_p = 11.32\,\mu\mathrm{m}$, 19 % at ~~$d_p$~~ $\mathrm{d}_p = 6.06\,\mu\mathrm{m}$ and 0.1 % at ~~d_p~~ $\mathrm{d}_p = 0.44\,\mu\mathrm{m}$, respectively. With an estimated cut-off diameter of >11 µm all but the coarsest SSA particles are expected to be detected. Number densities $N_{0.4-12}$ are computed from particle counts h with $N_{0.4-12} = h\,SR\,Q^{-1}$ at IUPAC standard temperature (273.15 K) and pressure (1 bar) and then averaged to 1-minute means. ~~Engine pollution was effectively removed from the~~ Due to pump failure of the CLASP unit in the crow's nest ~~data~~ usable data at the 29 m level are only available from 8 June to 26 July 2013. Raw aerosol number concentrations at the crow's nest showed significant spikes, when air came from the direction of the ship's engine stack, whereas no evidence of pollution was detected in the observations on the sea ice. Pollution spikes were effectively filtered out prior to averaging by excluding all data when relative wind direction was in the 135–225° sector encompassing the ship's engine stack. ~~Due to pump failure of~~ A total of 21 % of the available 1-second data was removed from the ~~CLASP unit in the~~ crow's nest ~~usable dataat the 29 level are only available from 8 June to 26 July 2013.~~ data.

2.3 Aerosol chemical composition

Aerosol was collected on filters via continuous low-volume sampling using open-face filter holders protected by a wind shield ~~. The method described below follows~~ following the approach from a previous study in coastal Antarctica (Wolff et al., 1998). One sampling unit was deployed on the sea ice for the duration of each ice station, and another one was operated continuously from the crow's nest of *RV Polarstern*.

Aerosol filters were polytetrafluoroethylene (PTFE) 1.0–µm pore membrane filters of 37 mm diameter (Zefluor~~®~~® P5PL037 Pall Lab.) with an aerosol retention of >99.99 % as stated by the manufacturer. Filters were pre-mounted prior to the expedition in 3-piece styrene acrylonitrile (SAN) filter holders onto porous cellulose support pads (Pall International Sarl). At the head of each sampling unit, the filter holder was mounted, open-face downward, inside an upturned polyethylene jar intended to prevent blowing snow blocking the filter. On the sea ice the jar was attached to a metal mast at ~2 m above the snowpack and on the crow's nest to a horizontal metal arm at ~29 m above the sea ice surface, and was free to swing in the wind, aiding the removal of snow and rime. An air pump was attached with PFA tubing ~10 m downstream of the sampling head to pull ambient air through the filters. The sea ice unit had a 12 VDC diaphragm vacuum pump (22 W, N815-KNDC, KNF Neuenberger) powered by a rechargeable lead-acid battery (12-5000X, Sunlyte) with an average flow rate of 9.8 STP-L min^{-1}, whereas the crow's nest unit had a 220 VAC diaphragm vacuum pump (420 W, Mod-No. DOA-P725-BN, GAST, Michigan, USA) with a mean flow rate of 8.8 STP-L min^{-1}.

Total sample air volume was measured upstream of the pump using a diaphragm gas meter (KG-2-G1.6, BES), which was not temperature compensated. However, gas meter temperature continuously recorded with a TinyTag logger (RS, Gemini) and atmospheric pressure available from the ship's meteorology observatory (see section 2.5) allowed to determine the total air sample volume at IUPAC standard temperature and pressure. Rotameters with glass float (ColeParmer) installed upstream of the gas meter were used to manually check flow rates 1-2 times daily. Post-season lab tests confirmed accuracy of the crow's nest gas meter, whereas the sea ice gas meter showed a negative bias of 30 %, which is accounted for in the computation of final atmospheric concentrations. Filter sampling intervals were on average 6 hr (range 1.5-8.6 hr) at 2 m and 12 hr (range 3.5-31 hr) at 29 m, with more frequent filter changes applied during storms. The resulting sample air ~~volumes~~ STP-volumes were 3.3 (range 0.8-5.1) m^3 at 2 m and 6.4 (range 1.8-17.3) m^3 at 29 m.

~~Since isokinetic sampling could not be applied, sea salt aerosol concentrations are expected to be generally underestimated, especially during high wind speeds. The~~ Filters were estimated to collect aerosol in the diameter range ~0.3 µm to less than 6 µm. The lower end of the range is based on previous measurements of collection efficiencies of PTFE filters as a function of particle size (Soo et al., 2016). The upper end, the cut-off diameter of the air intake system, which critically controls the observed aerosol load, ~~had not been quantified. However, previously~~ is estimated as follows. Previously a cut-off diameter of 6 µm was empirically estimated for a similar sampling set up with filter face velocities of 1.1 $\mathrm{m\,s}^{-1}$ (Wagenbach et al., 1998). In this study average filter face velocities were

~~$\sim$~~$0.15\,\mathrm{m\,s^{-1}}$ implying a cut-off diameter smaller than 6 µm. Since isokinetic sampling could not be applied, sea salt aerosol concentrations are expected to be generally underestimated, especially during high wind speeds. The filter low-bias for sea salt is found to ~~be on average ∼40~~depend weakly on wind speed and is on average 26 % compared to ~~the~~ median values during filter sampling intervals derived from CLASP measurements as discussed in section 3.5.

Filter units, consisting of filters, support pads and filter holders were cleaned and assembled prior to shipping to Antarctica in a Class 100 clean laboratory in Cambridge (United Kingdom). Filters and support pads were soaked over-night in methanol (ACS >99.9 %, Fisher Scientific) in batches of 25, rinsed 4 times with ultra-high purity water (UHP, electric resistivity 18.2 MΩcm), micro-waved for 3 minutes then rinsed once more with UHP. Filters were dried on their support pads under vacuum in a clean dessiccator. Filter holders were UHP-rinsed, placed for 10 minutes into an ultra-sonic bath, UHP-rinsed 3 times and micro-waved for 5 minutes, then soaked over-night in UHP, followed by 4 UHP rinses and 5 minute microwaving. Filter holders were then dried in the incoming, filtered airflow of the Class 100 laboratory. Filter units were assembled in the Class 100 laboratory, sealed air-tight with plugs and then bagged in 2 layers of polyethylene bags.

In Antarctica, filter units were removed from the bags, mounted onto the sampling head by removing one plug, then opened to give open-face sampling. Field blanks were collected at regular intervals by placing a filter onto the head and leaving it for a few minutes without pumping. After sampling the procedure was reversed, and filter units were shipped in a freezer (-20 °C) back to the United Kingdom and kept frozen until prior to extraction. Filters were transferred in the Class 100 laboratory into 10 ml pre-cleaned ~~polysterene~~ polystyrene sample vials (Dionex AS-AP Autosampler vial). Pre-cleaning of vial, lid and septum involved UHP-rinsing followed by 3-minute micro-waving repeated 5 times, soaking over-night in UHP, repeating the same set of UHP-rinse and microwaving before drying and double-bagging. Filters were then extracted in 8 ml of UHP by repeated shaking and immersion into an ultra-sonic bath for >30 min. Samples were analysed using ion chromatography (IC) as described in the following section. ~~About 7 % (10 out of 151) of all filters were visibly grey from exposure to ship exhaust and therefore not analysed in order to protect the IC columns.~~

The field blank, mostly due to the filter itself with contributions from field and extraction procedures, was significant for all ions (Table 3). A mean value has been subtracted from all concentrations leading in some cases to negative values. The combination of small air sample volumes and high field blanks led to relatively high limits of detection (LOD) defined here as 2 times the standard deviation of the field blank (Table 3).

Chemical fractionation of ion x (=$\mathrm{SO_4^{2-}}$, $\mathrm{Br^-}$, $\mathrm{Na^+}$) relative to ion y (=$\mathrm{Na^+}$ or $\mathrm{Cl^-}$) in aerosol and snow with respect to sea water is evaluated based on the depletion factor DF_x = 1-R_{spl}/R_{RSW}, with R being the x:y mass ratio in sample (spl) and reference sea water (RSW) after Millero et al. (2008), respectively. Throughout $DF_{\mathrm{SO_4^{2-}(Na^+)}}$ and $DF_{\mathrm{Br^-(Na^+)}}$ refer to sulfate and bromide depletion relative to $\mathrm{Na^+}$, and $DF_{\mathrm{Na^+(Cl^-)}}$ refers to sodium depletion relative to $\mathrm{Cl^-}$. DF_x between 0 and 1 indicates 0-100 % depletion, whereas DF_x<0 indicates enrichment. For example, DF_x =-1.5 or 150 % enrichment means the respective ion concentration is 2.5 times that in reference sea water. A total of 6 (= ∼6% of all crow's nest samples) $DF_{\mathrm{SO_4^{2-}}}$ values were below that of pure mirabilite (= -7.3) and are attributed either to sulfate contamination from the ship's engine emissions discussed below or measurement error. We therefore removed all ion concentrations of the corresponding filter samples from the dataset. DF_{Br^-} smaller than -7 were considered outliers due to measurement error and also removed: a total of 4 (= 3 % of all samples) from the crow's nest data, and a total of 6 (= 14 % of all samples) from the sea ice data. Propagation of the analytical error yields mean uncertainties in DF_x of 0.03–0.04.

About 7 % (10 out of 151) of all filters collected at the crow's nest during June to September 2013 were visibly grey from exposure to ship exhaust and therefore not analysed in order to protect the IC columns. In order to assess the impact of potential pollution on reported bulk aerosol chemistry from filters collected at the crow's nest we calculated for each filter sample the fraction of the total filter run time during which relative wind direction was within the 135–225° sector encompassing the ship's engine stack. Considering all filters sampled from June to September 2013 (N=141) the fraction of total filter run time with winds from the polluted sector was on average 9.5 %. Polluted time fraction and atmospheric concentrations of Na^+ and Cl^- were uncorrelated ($R<0.05$, $p>0.1$) not suggesting any impact of pollution on the respective ion concentration. A weak, but significant negative correlation was found between polluted time fraction and $\mathrm{SO_4^{2-}}$ (R=-0.21, $p<0.05$), $\mathrm{DF}_{\mathrm{SO_4^{2-}}}$ (R=-0.44, $p<0.01$), Br^- (R=-0.17, $p<0.06$) and $\mathrm{DF}_{\mathrm{Br}^-}$ (R=-0.37, $p<0.01$) suggesting that enrichment in sulfate (and bromide) may be more likely during polluted conditions. The bulk aerosol chemistry observations on the sea ice showed no evidence of pollution. Thus, in the case of sulfate we cannot rule out that some of the sulfate enrichment in atmospheric aerosol observed at the crow's nest may be due to ship exhaust rather than presence of mirabilite. It follows that estimates of sea ice contributions to total SSA inferred from depletion factors in this study have to be considered as lower bounds of true values.

2.4 Snow chemical composition

In order to determine the snow chemical composition a total of 24 snow pits was sampled at 9 ice stations during ANT-XXIX/6, between 1–2 snow pits at shorter ice stations and up to 8 at the multi-day ice stations S6 and S8 (Table 1). Snow pit profiles were sampled at 2 cm depth resolution with a custom-built, cylindrical, stainless-steel sampling tool yielding ~~samples~~ a sample volume of $\sim$60 cm^3. Blowing or drifting snow was collected at approximately 0.3, 0.9 and 1.6 m above the snow surface using modified Mellor ~~gages~~ gauges with a clear thermoplastic body (Schmidt et al., 1984) referred to as rocket traps. ~~All~~ Snow samples were transferred into 50 ml polypropylene tubes with screw-caps (Corning CentriStar), which prior to field deployment had been UHP-rinsed and dried in a Class 100 clean laboratory in Cambridge. One set of snow samples was melted onboard *RV Polarstern* to measure aqueous conductivity using a conductivity meter (SensIon 5, Hach) with a measurement range of 0-200 mS cm^{-1} and a maximum resolution of 0.1 μS cm^{-1} at low conductivities (0-199.9 μS cm^{-1}). The conductivity meter has an automatic non-linear temperature compensation based on a NaCl solution and reference temperature of 25 °C and was calibrated with a standard salt solution (12.880 mS cm^{-1} at 25.1 °C), certified and traceable to NIST (REAGECON Prod. No. CSKC12880, Lot No. CS1288012K1). Conductivity values were converted into practical salinity S_p using the Gibbs-SeaWater (GSW) Oceanographic Toolbox (McDougall and Barker, 2011), which applies the algorithm of the Practical Salinity Scale of 1978 (PSS–78) (Unesco, 1981, 1983) with an extension to salinities $S_p < 2$ psu (Hill and Woods, 1986). S_p is reported in psu (practical salinity unit), approximately equivalent to the weight of dissolved inorganic matter in grams per kilogram of seawater, and has an accuracy as stated by the manufacturer of ±0.001 psu at low salinities (<1 psu).

The other snow samples were shipped frozen back to Cambridge and only melted prior to analysis in spring 2014 and December 2016. Elevated salinities required dilution of samples with UHP water, typically by a factor 100 for most snow samples and a factor 10000 for sea ice and frost flower samples. Samples were analysed for major ions using Dionex ICS2000 ion chromatography systems with reagent free eluent generation. Cation analysis was performed with a CS12A separator column with isocratic methylsulfonic acid elution and a 250 µl sample loop. Anion analysis was performed using an AS17 separator column, gradient elution with potassium hydroxide and a 250 µl sample loop. Measurement accuracies were evaluated using European reference materials ERM–CA408 (simulated rain water) and CA616 (groundwater) and were all within 5 % and respective LODs ∼2 ng g^{-1}. Here we only report and discuss concentrations of ions relevant to this study: Na^+, Cl^-, SO_4^{2-} and Br^-.

~~Chemical fractionation of ion x (=, ,) with respect to ion y (=or) in aerosol and snow compared to sea water is evaluated based on the depletion factor $DF_x = (R_{RSW}$-$R_{spl})/R_{RSW}$, with R being the x:y mass ratio in reference sea water (RSW) after Millero et al. (2008) and sample, respectively. Throughout $DF$and DFrefer to sulphate and bromide depletion with respect to , and DFrefers to sodium depletion with respect to . DF_x between 0 and 1 indicates depletion, whereas DF_x<0 indicates enrichment. DFvalues below that of pure mirabilite (= -7.3) are attributed either due to measurement error or sulphate contamination from the ship's engine emissions, and were therefore removed. $DF$and DFsmaller than -3 were also considered outliers and removed. Propagation of the analytical error yields mean uncertainties in DF_x of 0.03–0.04.~~

2.5 Ancillary measurements

General meteorology measurements were taken from *RV Polarstern* onboard sensors described in detail at https://spaces.awi.de/confluence/display/PSdevices/Bordwetterwarte, and include ambient temperature T_a and relative humidity with respect to water RH_{aq} at 29 m (HMT337, Vaisala, Finland), wind speed U and direction at 39 m (Sonic 2D a, Thies, Germany) and global radiation (Pyranometer CM11, Kipp&Zonen, Netherlands). Still images recorded every ~~5~~ minute by a webcam in the ~~crows nest provided on occasion when light conditions were adequate~~ crow's nest provided further qualitative information on the presence of airborne snow particles, when light conditions were adequate. During ice stations the three-dimensional wind components (u, v, w) were measured above the sea ice at 25 Hz with an unheated sonic anemometer (Metek USA-1) that was mounted on a mast at ∼2 m. Processing of raw sonic data in 1-min blocks included temperature cross-wind correction and a double coordinate rotation to force mean w to zero (Kaimal and Finnigan, 1994; Van Dijk et al., 2006), followed by computation of friction velocity u_*. T_a and RH_{aq} were also measured above the sea ice on a 2-m mast at approximately 0.6, 1.2 and 2.0 m, respectively, using temperature-humidity probes (HMP45, VAISALA). RH_{aq} was converted to relative humidity with respect to ice RH_{ice}. RH_{ice} from the HMP45 was further corrected after Anderson (1994) to extend the calibrated temperature range to T_a<-20 °C. Based on the available data the calibration of RH_{ice} is most accurate for the -40 to -20 °C range, and has greater uncertainty in RH_{ice} in near freezing conditions. Accurate correction of the HMT337 output was not possible since available RH_{aq} values are biased as they had been post-processed by accepting only values up to 105 % and setting any values >100 % to 100 %. In general, measuring RH_{ice} during blizzards is very difficult and its estimated non-systematic error of ∼5 % limits its use for blowing snow calculations. We therefore discuss below only RH_{ice} trends.

3 Results and discussion

The presentation and discussion of results in the sections below are organised as follows. An overview of observed meteorology ~~, particle concentrations and aerosol chemistry~~ and particle concentrations (section 3.1) is followed by the ~~description of blowing snow events~~ discussion of chemical fractionation of aerosol and snow and size spectra of sea salt aerosol above sea ice (section 3.2). Blowing snow events are then described in detail during two time periods (section 3.3). We then evaluate the current model mechanism proposed by ~~Yang et al. (2008); ?~~ Yang et al. (2008, 2019) for SSA production from blowing snow (section 3.4) and finally discuss ~~chemical composition, aerosol size spectra and~~ the air-snow budget of sea salt aerosol above sea ice (section ~~3.2~~3.5).

3.1 Overview of atmospheric observations

Near-zero or positive ambient temperatures T_a in degrees Celsius occurred when *RV Polarstern* was in the open ocean at the start and end of ANT-XXIX/6, as well as from the 22 July 2013 onwards, when the ship had moved into the marginal sea ice zone (MIZ) closer to open water (marker B in Fig. 1,2b). After entry into the sea ice zone on 17 June 2013 (marker A in Fig. 1) T_a decreased to below -20 °C but showed thereafter frequent increases associated with storms (Fig. 1,2a-b). The correlation between T_a and U_{39m} is weak but significant (R = 0.37, p<0.05).

Winter storms occurred frequently with wind speeds ranging between 10 and 20 $\mathrm{m\,s^{-1}}$, occasionally exceeding 20 $\mathrm{m\,s^{-1}}$ (Fig. 2a), and coincided ~~almost always with snowfall inferred from direct observation~~ often with snowfall based on the ship's 3-hourly weather report, occasional webcam images and presence of clouds (data not shown). Bearing in mind that wind direction and origin of air mass depend on the ship's position relative to the path of a low or high pressure system the following is observed: winds were most of the time from W to SSW advecting cold (-15 to -30 °C) air of a low water load with specific humidities $q_v < 3\,\mathrm{g\,kg^{-1}}$ (Fig. 3). Second most frequent were winds from SSE to SE advecting relatively warm air often between -5 and 0 °C with higher q_v values often between 3–5 $\mathrm{g\,kg^{-1}}$ (Fig. 3) indicating origin from lower latitudes. And third most frequent were winds from the N coinciding with the highest wind speeds (Fig. 3). The air was (super)saturated with respect to ice most of the time (RH_{ice}>100 %), with increased frequency of subsaturation (RH_{ice}<100 %) when the winds were from

SE (Fig. 3d). Horizontal wind speed at 2 and 39 m correlated well with friction velocity u_* (R=~~0.89~~0.9, $p<0.05$) (Fig. S1) indicating a well-mixed near-neutral turbulent boundary layer above the sea ice during blowing snow (Nishimura and Nemoto, 2005; Jacobson, 2005).

Airborne snow particle concentrations at 29 m showed strong variability and a weak but significant correlation with wind speed (R=~~0.24~~0.27, p<~~0.05~~0.01) (Fig. 2a,c). During most storms measured snow particle concentrations have contributions from both blowing snow from the sea ice and precipitation from above as further discussed in section 3.4.2. At 29 m mean total number densities N_{46-478} were 8.7×10^3 m^{-3} during ANT-XXIX/6 and very similar 7.2×10^3 m^{-3} during ANT-XXIX/~~7.~~7 (Table S1, Fig. S2c). Near the sea ice surface snow particles were measured for a total sampling time of 6 days and showed a mean N_{46-478} of 2.6×10^5 m^{-3}, on average ∼60 times the number density observed during the same time at 29 m.

Aerosol concentrations at 29 m showed strong variability with many but not all increases associated with storms and blowing snow (Fig. 2d), illustrated by a weak but significant correlation with wind speed (R=0.18, $p<0.01$). At 29 m mean total number densities $N_{0.4-12}$ were 2.1×10^6 m^{-3} during ANT-XXIX/6 (Table S2, Fig. 2d). $N_{0.4-12}$ mean values at 2.0 and 0.2 m during ice stations were 1.4×10^6 and 1.7×10^6 m^{-3}, respectively, about the same as the number densities observed during the same time at 29 m (Table S2). The median aerosol particle diameters $\overline{d_p}$ at the measurement heights 0.2, 2.0m and 29 m ranged between 0.60 and 0.66 µm (Table S2) showing dominance of sub-micron sized particles in atmospheric aerosol below the instrument particle size cut-off (>11 µm).

Descriptive statistics of the aerosol chemistry are summarised in Table 4. The Na^+ concentrations of bulk aerosol showed strong variability with most increases coinciding with storms and aerosol number density $N_{0.4-12}$ peaks (Fig. 2e). Na^+ and sea salt concentrations were in general higher at 29 m than at 2 m (Table 4) except during S8 (Fig. 2e). $DF_{SO_4^{2-}}$ values of aerosol at 29 and 2 m ~~varied~~ showed strong variability ranging most of the time between values near 0 (small depletion) and close to 1 (strong depletion), with occasional $DF_{SO_4^{2-}}<0$ indicating enrichment (Fig. 2e).

Median $DF_{SO_4^{2-}}$ values at 29 m were ~~very~~ similar during ANT-XXIX/6 (=~~0.34~~0.29) and ANT-XXIX/7 (=~~0.30~~0.21), but larger near the sea ice surface (=~~0.49), suggesting~~ 0.48), although vertical differences were not statistically significant based on the Wilcoxon rank-sum test ($p<0.01$). Non-zero $DF_{SO_4^{2-}}$ values suggest throughout a significant contribution to the total SSA burden from a fractionated sea ice source (Table 4, Fig. S1e). Conversely, when in open water at the beginning and end of ANT-XXIX/6 Na^+ concentrations of bulk aerosol were relatively large but with small or no ~~sulphate~~ sulfate depletion consistent with the open ocean as the main SSA source, except for the very first and last sample (Fig. 2e).

3.2 ~~Blowing snow events~~ The sea ice source of sea salt aerosol

~~Drifting and blowing snow events were frequently observed during ANTXXIX-6 (~~Below we discuss sea salt aerosol properties characteristic for the blowing sea ice source, including the chemical fractionation of SO_4^{2-} and Br^- as well as aerosol size distributions observed above sea ice.

3.2.1 Chemical fractionation of $\mathbf{SO_4^{2-}}$

In non-summer months when biogenic non-ss SO_4^{2-} is at a minimum Antarctic aerosol was observed to be depleted in SO_4^{2-} (relative to Na^+) and in Na^+ (relative to Cl^-) (Wagenbach et al., 1998; Legrand et al., 2017). Similar fractionation in brine and frost flowers in the sea ice nearby attributed to precipitation of the mineral mirabilite ($Na_2SO_4 \cdot 10\,H_2O$) suggested that the observed SSA must originate from the sea ice and not from the open ocean (Wagenbach et al., 1998; Rankin et al., 2000). Here we show for the first time that snow on sea ice is depleted in sulfate (Fig. ~~2c) ,~~ 4a). $DF_{SO_4^{2-}}$ of most snow samples was positive, showing large scatter and no particular dependence on snowpack depth or sea ice age (Fig. 4a). Negative $DF_{SO_4^{2-}}$ suggests presence of mirabilite precipitated during freezing. The median volume-integrated $DF_{SO_4^{2-}}$ in snow ranged between 0.24 and 0.35 (Table 5) overlapping with the sulfate depletion found in aerosol during the period the snow was sampled (ANT6) with median $DF_{SO_4^{2-}}$ ranging between 0.29 and 0.48 (Table 4). Considering all $DF_{SO_4^{2-}}$ values no statistical difference is detected between snow and aerosol based on the Wilcoxon rank-sum test ($p<0.01$). The similarity of sulfate depletion in both snow and aerosol strongly suggests that snow sea ice in the Weddell Sea is the dominant source of regional sea salt aerosol.

The sulfate depletion observed in aerosol and snow (Figs. 2f, 4a) is consistent with mirabilite precipitation. Mean temperatures during all ice stations except S3 were below the -6.4 °C threshold of mirabilite precipitation (Table 1). And a recent lab study found that mirabilite precipitation results in $DF_{SO_4^{2-}}$ of ~~which seven occurred during the 14 days of total time spent at ice stations. Based on data coverage two 7-10 day long periods were chosen~~ 0.93 in sea water brine cooled down to -20.6 °C (Butler et al., 2016). Conversely, $DF_{SO_4^{2-}}<0$ in snow or aerosol suggests contributions from non-sea salt SO_4^{2-} or crystallized mirabilite, which has a $DF_{SO_4^{2-}}$ of -7.3. The latter is supported by the observation that most $DF_{SO_4^{2-}}<0$ occur in or near the sea ice surface, where most of the partitioning between brine and mineral is expected to have occurred during freezing (Fig. 4a). If the partitioning of crystallized $Na_2SO_4 \cdot 10\,H_2O$ between brine and the snow-ice matrix is the dominating SO_4^{2-} fractionation process then Na^+ should be depleted as well in the brine. Further Na^+ depletion may arise from the precipitation of hydrohalite ($NaCl \cdot 2\,H_2O$) once ambient temperature drops below the threshold of -22.9 °C (e.g. Butler et al., 2016) , which occurred here during some periods of time (Fig. 2b, Table 1). In the analysis below however we consider only the precipitation of mirabilite. Following the approach of Wagenbach et al. (1998) we take Cl^- as the reference species for bulk sea water and find from a mass balance calculation that the Cl^- to Na^+ mass ratio would then be linearly related to the SO_4^{2-} to Na^+ ratio with a slope of -0.98 and an intercept of 2.04. From that a theoretical relationship between DF_{Na^+} (with respect to Cl^-) and $DF_{SO_4^{2-}}$ (with respect to Na^+) is derived and compared to observations (Fig. 5). The observed fractionation is largely in agreement with the model prediction. Snow on sea ice follows closely the theoretical mirabilite fractionation line, whereas aerosol shows large scatter and a tendency to apparent Na^+ enrichment with respect to Cl^- of up to 20 %, equivalent to Cl^- depletion with respect to Na^+ of 17 % (Fig. 5). Dechlorination of sea salt aerosol observed in Antarctica has a maximum in spring/summer, when gaseous acidic species (nitric, sulfuric and methanesulfonic acid) are available to replace chloride on sea-salt aerosol

(Wagenbach et al., 1998; Rankin and Wolff, 2003; Legrand et al., 2017). Acidic sulfur species are close to zero during winter in coastal Antarctica e.g. at Neumayer (Weller et al., 2011), whereas nitric acid is low but non-zero, e.g. 1-2 pptv at Halley (Jones et al., 2011). Thus nitric acid induced Cl^- loss from sea salt is a plausible explanation for the observed Cl^- depletion either in airborne SSA or as a sampling artefact from sea salt already accumulated on the filter surface as suggested previously (Wagenbach et al., 1998; Legrand et al., 2017). Unfortunately no usable filter data of aerosol nitrate are available from this study to further test the association between nitrate and sea salt due to a very high lab procedure blank. It is noted that if all sulfate is removed by mirabilite precipitation ($DF_{SO_4^{2-}}$=1) then sodium depletion reaches a theoretical maximum of ~12 % (DF_{Na^+}= 0.1204) (Fig. 5).

The median $DF_{SO_4^{2-}}$ values of bulk aerosol observed during this study were smaller than previous winter observations at coastal Antarctic sites, where the sea-ice surface was shown to be the dominant source of sea-salt aerosol. Wagenbach et al. (1998) reported sulfate depletion in aerosol corresponding to $DF_{SO_4^{2-}}$ of 0.72 at Halley (75°S, 26°W), of 0.76 at Neumayer (70°S, 85°W), and of 0.62 at Dumont d'Urville (66°S, 140°E). The main cause of smaller $DF_{SO_4^{2-}}$ observed in aerosol above the Weddell Sea in winter 2013 appears to be the snow source being less depleted in sulfate during that particular year. In summary, $DF_{SO_4^{2-}}$ in Antarctic winter aerosol can be used as a tracer to estimate sea ice SSA fractions of the total aerosol burden at a specific location (e.g. Legrand et al., 2017) , however temporal and spatial variability in $DF_{SO_4^{2-}}$ of the sea ice source introduce additional uncertainty if not accounted for.

3.2.2 Chemical fractionation of $\mathbf{Br^-}$

Modelling studies suggest that sea salt may be an important source of atmospheric bromine species in the mid to high southern latitudes, and that SSA from blowing snow releases bromine (Yang et al., 2008, 2010) driving ozone depletion events observed during or after snow storms (Jones et al., 2009). One of a number of processes identified to cause halogen release from aerosol or ice surfaces involves the reaction of HOBr with halides (Br^- and Cl^-) on acidic ice surfaces forming BrCl and Br_2 that are subsequently photolyzed to form reactive halogen atoms (Abbatt et al., 2012, and references therein). This is a multiphase process which, depending upon the substrate, may or may not proceed faster under acidic conditions (Abbatt et al., 2012), and associated uncertainties are currently still significantly limiting the modelling of impacts on tropospheric halogen chemistry (Sander et al., 2003; Long et al., 2014). Multi-phase bromine chemistry models use observed sea salt aerosol depletion of bromide relative to sodium (or chloride) with respect to seawater composition, i.e. bromide depletion factors DF_{Br^-}, to estimate the bromine flux from sea-salt aerosol (e.g. Yang et al., 2008; Long et al., 2014) . However, to date observations of bromide aerosol depletion are only available from north of 55°S (Sander et al., 2003, and references therein), with the exception of two recent pioneering studies in Antarctica (Legrand et al., 2016; Hara et al., 2018). Below we discuss bromine chemistry observations above the Weddell Sea during this study.

Bulk aerosol concentrations of bromide ranged between <1 and 19 $\mathrm{ng\,m^{-3}}$ (Fig. 6a), showing occasional large increases to levels seen elsewhere in coastal Antarctica only during summer (Legrand et al., 2016). However, median bulk aerosol concentrations of $\mathrm{Br^-}$ (Table 4) were similar to coastal observations at Dumont d'Urville during winter (Legrand et al., 2016). It should be borne in mind that the bromide aerosol concentrations were often below the estimated LOD due to the short filter exposure times employed (Fig. 6a). Median bromide concentrations in snow ranged between 0.07 and 0.18 $\mathrm{\mu g\,g^{-1}}$ (Table 5). It is found that aerosol at 29 m was on average strongly depleted in bromide relative to sodium with respect to seawater, whereas aerosol near the sea ice surface at 2 m showed mostly strong enrichment (Table 4, Fig. 6b). Median $DF_{\mathrm{Br^-}}$ in the snowpack ranged between -0.01 and 0.05 suggesting overall no or small depletion in bromide (Table 5). However, examination of individual snow layers as well as blowing snow samples shows large scatter with both positive and negative $DF_{\mathrm{Br^-}}$, suggesting both bromide depletion and enrichment (Fig. 4b). The sea ice surface below the snow was with the exception of one sample always enriched in bromide (Fig. 4b). During the storm on 14-15 July (see section 3.3.2) it is found that the median $DF_{\mathrm{Br^-}}$ in blowing snow collected on 15 July at <1 m was close to zero but 0.39 in aerosol at 29 m sampled over the same time interval. These observations are in agreement with previous studies in coastal Antarctica: Legrand et al. (2016) were the first to report year-round bromide depletion in aerosol at Dumont D'Urville (DDU) including during winter months except June. And Hara et al. (2018) observed at Syowa Station bromide depletion in aerosol also year-round, but not in blowing snow, which was enriched, and concluded that heterogeneous chemistry driving bromine activation occurs on sea salt aerosol and not on blowing snow. Lieb-Lappen and Obbard (2015) observed bromide depletion in blowing snow near McMurdo station, but only at >5 m above the surface.

From this study it is concluded that air-ice recycling of bromine occurs on surface snow, airborne snow and aerosol particles. However, the vertical gradient in $DF_{\mathrm{Br^-(Na^+)}}$ observed in aerosol suggests that significant net bromine release must take place in the aerosol phase between 2 and 29 m above the sea ice surface. The bromine net release from large snow particles is expected to be reduced compared to aerosol due to a combination of shorter atmospheric lifetime and smaller specific surface area limiting diffusional outgassing. The bromine release from SSA produced by blowing snow may be more efficient because it has a large fraction of sub-micron sized particles (see section 3.2.3), and resides at the well ventilated top of the blowing snow layer. Thus sea salt aerosol from blowing snow provides an additional bromine reservoir, which is readily depleted. Detailed measurements of participating bromine species in air, snow and aerosol are needed to further understand relevant processes and constrain the mass budget.

Models assume a dependence of $DF_{\mathrm{Br^-}}$ on season and aerosol diameter (Yang et al., 2008; Sander et al., 2003) . The observed $DF_{\mathrm{Br^-}}$ of aerosol showed a weak but significant trend (R=0.19, $p<0.05$) from winter into spring largely due to less frequent negative values during August and September (Fig. 6b, Table 4). This becomes more evident considering monthly median $DF_{\mathrm{Br^-}}$ values of aerosol at 29 m, which increased from June (0.25), July (0.43), August (0.50) into September (0.59). $DF_{\mathrm{Br^-}}$ values would be even higher had they been referenced to a sea water ratio adjusted for the maximum possible removal of sodium due to precipitation of mirabilite as done by Legrand et al. (2016). For comparison, at DDU $DF_{\mathrm{Br^-}}$ in bulk aerosol increased gradually from a minimum in

June (0.04), intermediate values in July to Sep (0.22-0.39) to a maximum in October (0.42) (Legrand et al., 2016). Increasing DF_{Br^-} is consistent with enhanced bromine loss from aerosol as incident radiation increases concurrent with activation of the reactive bromine ($\mathrm{BrO_x}$) cycle (Fig. 6b). Assuming that observed DF_{Br^-} is representative of SSA with median particle diameters d_p of ~0.60-0.66 µm (Table S2), it is also found that the observed bromide depletion is larger than that reported by Sander et al. (2003) who state a maximum of 0.4 for a d_p of 1.3 µm, dropping to 0.1 at 10 µm.

Contrary to expectation bromide depletion of aerosol was significant even during winter darkness from mid June to mid July (Fig. 6b), whereas previous observations at DDU showed a similar trend but less bromide depletion and none in June (Legrand et al., 2016). Light conditions are unlikely a cause of differences in bromide depletion, since DDU is located at a similar latitude (66° 40'S) as the area covered by this study. However, the early laboratory study by Oum et al. (1998) has shown that HOBr required for Br^- oxidation can be chemically produced in darkness through the reaction of ozone with bromide. Another study during the ANT-XXIX/6 expedition reports significant bromoform ($\mathrm{CH_3Br}$) production in sea ice during winter darkness (Abrahamsson et al., 2018), which requires HOBr (and organic matter) as precursors, and therefore indicates that bromine loss processes were active in the sea ice in the absence of sunlight. It therefore appears plausible that the same reactions may have caused significant bromide depletion observed here in sea salt aerosol, provided the pH was low enough.

3.2.3 Aerosol size distribution

Average aerosol number density and volume distributions observed in the Weddell sea show that during calm conditions (U_{10m}<4 $\mathrm{m\,s^{-1}}$) concentrations across most of the size spectrum were smaller above sea ice than above the open ocean (Fig. 7). Depending on particle size the variability was relatively large as illustrated by the standard deviation of the mean values (Fig. 7). Thus differences in mean size distributions were statistically significant only for d_p<2 µm in the case of aerosol number density, and d_p 1-8 µm in the case of aerosol volume distributions (Fig. 7). The wind speed threshold chosen for calm conditions is well below the mean snowdrift threshold wind speed U_t of 7.1 $\mathrm{m\,s^{-1}}$ observed during this study (section 3.4.1) and within the range when breaking of waves commences (3-4 $\mathrm{m\,s^{-1}}$; O'Dowd et al., 1997). A low sea salt aerosol background above compact sea ice during calm conditions is consistent with the absence of any active local sources and the long distance to the nearest open ocean (Table 1). The average aerosol volume distribution shows two modes, one at 1-2 µm and the other at 5-9 µm (Fig. 7b), indicating that most of the aerosol particle mass resides in the super-micron range as expected for sea salt aerosol. During stormy conditions (U_{10m}>9 $\mathrm{m\,s^{-1}}$) average aerosol number densities above sea ice increased significantly for particle diameters d_p<2 µm, reaching at the lower end of the size spectrum levels similar to those observed above the open ocean (Fig. 7a). Average aerosol volume concentrations above sea ice also showed an increase during storms, significant for particle sizes d_p 0.8 to 9 µm (Fig. 7b). It is striking that above the sea ice the relative increase of aerosol number and volume concentrations during storms above background levels was equal or larger than above the open ocean (Fig. 7). This implies that corresponding aerosol number and mass fluxes during storms were also equal or larger above sea ice than above the open ocean consistent with Yang et al. (2008) and underlining the importance of a winter sea ice source for atmospheric sea salt aerosol.

The main observational constraint for the origin of the observed sea salt aerosol comes from its chemical source signature as discussed above. In addition, the relatively larger increase of small particle number densities provides further support for the blowing snow SSA source based on physical arguments: snow particles of low salinity as observed during this study will generate very small sea salt particles after complete loss of water ice by sublimation. Taking the dry particle diameter $d_{dry} = d_p(S_p/1000\,\rho_{ice}/\rho_{\mathrm{NaCl}})^{1/3}$, where ρ_{ice} and ρ_{NaCl} are densities of ice and NaCl, respectively, we would expect based on observed snow salinity and snow particle size (Table 5, 6) potential d_{dry} on the order of 10^{-3} µm, or larger if not all water is lost. Instruments with a lower size detection limit than available in this study are needed to further investigate very small particle formation from blowing snow.

It is important to note that the use of sea salt measured in ice cores as a proxy of past sea ice conditions requires that average emissions above sea ice exceed those above an equivalent area of open ocean and consequently lead to a comparatively larger burden of atmospheric SSA. Observations from this study support the former requirement, but not the latter. The low SSA background concentrations observed above sea ice may have been due to a combination of low storm frequency and low snow salinities in the area. Indeed, model calculations suggest that size distribution and associated flux of SSA originating from blowing snow are very sensitive to snow salinity S_p, e.g. decreasing S_p from 0.92 to 0.06 psu causes SSA spectral number densities to decrease by about one order of magnitude (Yang et al., 2019). Further atmospheric modelling is needed to address this issue and will be subject of future research.

3.3 Blowing snow events

Below we discuss key features of ~~observed blowing snow~~ blowing snow events and associated SSA increases ~~.~~ that were frequently observed during ANTXXIX-6 (Fig. 2c). A total of seven events occurred during the 14 days of total time spent at ice stations. Two periods, one lasting 7 days and another 10 days, were chosen based on data coverage.

3.3.1 Period 23 June to 3 July 2013

The period 23 June to 3 July featured a major storm with 4 wind speed maxima between 15 and 25 m s^{-1} centred around midnight of the 24, 25, 27 and 28 June (Fig. 8a). Temperature T_a increased during that time from -20 °C on 23 June to -3 °C on 26 June before dropping again to -20 °C on 30 June (Fig. 2b).

~~Wind speed U_{39}~~ Wind speed U extrapolated to 10 m increased from <5 m s^{-1} in the late evening of 23 June over a 24 hr period to >20 m s^{-1} (Fig. 8a). First snow particles were detected at 29 m once ~~U_{39}~~ U exceeded a threshold of ~9 m s^{-1} with spectral number densities N_{46-478} reaching values on the order of 10^4 m^{-3} including large snow particles with d_p>300 µm (Fig. 8b). Near-surface N_{46-478} measured at ice station S2 on 24 June (Table 1) showed very large number densities on the order of 10^6 m^{-3} across the entire particle size spectrum confirming blowing snow from the sea ice surface as the main particle source (Fig. 8c). A decrease in wind speed U always concurred with a drop in snow particle number densities at 29 m and often also in RH_{ice} (25 June, 26 and 28 June) indicative of air being ~~subsaturated~~ sub-saturated with respect to ice (Fig. 8a-b).

Aerosol at 29 m showed background spectral number densities $N_{0.4-12}$ of 10^5 m^{-3} for particles with d_p<2 µm during the calm periods on 23 June, 30 June and 2 July (U_{39m}<5 m $^{-1}$), when no blowing snow or precipitation was present (Fig. 8d). During or after the 4 wind speed maxima on 24, 25, 27 and 28 June large increases of aerosol spectral number densities were observed especially of sub-micron sized particles reaching up to 10^7 m^{-3}, often at RH_{ice}<100 % consistent with a source from sublimating snow particles (Fig. 8a,d). Near the surface spectral number densities ~~$N_{0.4-12}$~~ $\mathrm{N}_{0.4-12}$ for particles with ~~d_p~~ d_p<2 μm during the storm on 24 June remained with ~~10^5~~ 10^5 m^{-3} below those seen at 29 m (~~Fig. 8e~~10^6 m^{-3}) likely due to scavenging of aerosol by snow particles ~~.~~

(Fig. 8d-e). Na^+ concentrations in aerosol at 29 m show strong increases from background values of ∼0.1 µg m^{-3} to 1.4 µg m^{-3} on 25 June and to 1.1–1.7 µg m^{-3} during 28–29 June coinciding with wind speed maxima and increased number densities of aerosol and snow particles (Fig. 8). Na^+ concentrations returned to background values after the storm on 30 June coinciding with low wind speeds U_{39m}<5 m s^{-1}, reduction in aerosol number concentrations and absence of any airborne snow particles (Fig. 8). Na^+ concentrations also dropped to background values during the storm on 26-27 June, consistent with the absence of blowing snow particles due to wind speed falling below the drift threshold (~~discussed in~~ section 3.4.1) and a concurrent slight decrease in aerosol concentrations (Fig. 8).

During the calm periods on 24 June, 26–27 June and 29 June $DF_{\mathrm{SO}_4^{2-}}$ of aerosol was negative or near 0, while during the storm episodes aerosol became increasingly more depleted in ~~sulphate~~ sulfate with $DF_{\mathrm{SO}_4^{2-}}$ maxima of 0.53-0.59 coinciding with peaks in aerosol Na^+ concentration (Fig. 8f). In order to constrain the origin of the observed aerosol three snow pit profiles were sampled at ice station S2 on 24 June. The mean snow depth was 33 cm, and bulk mean Na^+ concentrations were 50, 6 and 17 µg g^{-1} and bulk median $DF_{\mathrm{SO}_4^{2-}}$ values were 0.30, 0.24 and 0.48, respectively. Assuming a linear mixing model and that measured snow chemistry at S2 is representative of the regional snowpack the $DF_{\mathrm{SO}_4^{2-}}$ in aerosol and snow suggest that up to 80-90 % of the sea salt aerosol observed during the storm originates from snow on sea ice. Negative $DF_{\mathrm{SO}_4^{2-}}$ in aerosol during calm periods may arise either from contamination by ship's engine exhaust or contributions of non-local nss-SO_4^{2-}. The local snowpack near ice station S2 was less likely a contributing source as only one snow pit showed some snow layers with $DF_{\mathrm{SO}_4^{2-}}$<0.

3.3.2 Period 10 to 16 July 2013

From 10 to 16 July 2013, prior and during ice station S6 (Table 1), three snow drift episodes on 11, 12 and 14 July 2013, and a major blowing snow event from 14 to 16 July 2013 concurrent with strong warming were observed (Fig. 9). Starting on 14 July ambient temperature T_a rapidly increased over a 12-hr period from ∼-22 to -1 °C (Fig. 2b).

During the snow drift episodes wind speed ~~at 39~~extrapolated to 10 m~~U_{39m} peaked at 7–10~~, U_{10m}, peaked at 6–9 m s^{-1} (Fig. 9a) near or above the estimated snowdrift threshold (section 3.4.1), snow particle spectral number densities N_{46-478} reached up to 10^6 m^{-3} near the surface, but remained relatively low at 29 m with 10^2–10^3 m^{-3}

with $d_p<100$ µm except on 11 July (Fig. 9b-c). During the blowing snow event 14-16 July ~~U_{39m} ranged between 15 and 20~~U_{10m} ranged between 13 and 18 m s^{-1} (Fig. 9a). Spectral number densities N_{46-478} reached again up to 10^6 m^{-3} near the surface but 10^4 m^{-3} at 29 m for particle diameters d_p 50-200 µm (Fig. 9b-c). The air within 2 m of the surface was supersaturated with respect to ice during drifting or blowing snow, but then became undersaturated towards the end of the snow drift episodes on 11 and 12 July as wind speed and snow particle concentrations decreased (Fig. 9a-c).

Aerosol at 29 and 2 m above the sea ice showed during the calm periods on 10, 12 and 14 July background spectral $N_{0.4-12}$ of 10^4 to 10^5 m^{-3} for particle sizes $d_p<2$ µm (Fig. 9d-e). During ~~the~~ or a few hours after snow drift episodes aerosol number densities increased significantly especially of sub-micron sized particles at both measurement heights showing more particles near the surface, with spectral $N_{0.4-12}$ of up to 10^7 m^{-3} for $d_p<2$ µm (Fig. 9d-e). During blowing snow spectral number densities $N_{0.4-12}$ showed similar increases as during drifting snow, however at 29 m concentrations were higher and particles were larger ($d_p>9$ µm) than at 2 m (Fig. 9d-e). Similar to the observations from 24 June this is consistent with net production of SSA taking place near the top of the layer containing suspended snow particles at $RH_{ice}<100\,\%$. Within the blowing snow layer SSA net production is suppressed due to saturated conditions and scavenging by snow particles which is efficient at warmer temperatures.

Na$^+$ concentrations in aerosol at 29 m showed strong increases from a background of 0.1 µg m^{-3} to 1.8 µg m^{-3} ~~during~~ a few hours after the drift episode on 11 July, and to 1.2 µg m^{-3} during the blowing snow event on 14-16 July (Fig. 9f). During the same times Na$^+$ concentrations in aerosol at 2 m showed only small increases by 0.1 µg m^{-3} (Fig. 9f). $DF_{\mathrm{SO}_4^{2-}}$ of aerosol showed large scatter and mostly positive values, with the exception of 2 samples (15-16 July), varying between 0.1 and 1 (Fig. 9f, 10d). Median $DF_{\mathrm{SO}_4^{2-}}$ values from 11 to 16 July were 0.61 at 29 m and 0.48 at 2 m confirming that SSA originates from a fractionated sea ice source.

A more detailed view of the blowing snow event from 14 to 16 July reveals trends and phasing of particle number densities and chemical composition, which are consistent with the hypothesised sequence of processes from the onset of blowing snow to the release of sea salt aerosol due to snow sublimation (Fig. 10). Onset of snow drift at 0.1 m above the snow surface occurred once wind speed ~~U_{39m} exceeded a drift threshold of 12.1~~ U_{10m} exceeded 11 m s^{-1} followed about 1 hr later by detection of blowing snow at 29 m (Fig. 10b). Total snow particle number densities N_{46-478} near the surface and at 29 m decreased again a few hours later despite constant wind speeds of ~~15~~13.5 m s^{-1} (Fig. 10b) due to strong warming during the storm causing an increase in drift threshold wind speed and therefore less uplift of particles, as shown in section 3.4.1.

Two hours after the onset of snow drift total aerosol number densities $N_{0.4-12}$ started to gradually increase at 2 and 29 m to reach peak values first at 29 m after an initial spike, and with a delay of 2 hr also at 2 m coinciding with a decrease in snow particle concentrations (Fig. 10b-c). Despite $RH_{ice}>100\,\%$ within 2 m of the sea ice surface during the blowing snow event on 15 July (Fig. 9a) sub-saturation cannot be ruled out because of the large error in RH_{ice} near 0 °C. Thus, the observed anti-correlation between aerosol and snow particle number densities at both measurement heights is consistent with (a) increased aerosol production from snow particle sublimation near the top or above the blowing snow layer, where undersaturated conditions are more likely, and (b) reduced aerosol scavenging by snow particles.

Na^+ concentrations in aerosol followed the observed total $N_{0.4-12}$ showing first a maximum at 29 m and then near the surface at 2 m albeit of smaller magnitude (Fig. 10d) suggesting that much of the observed increase of aerosol particles consists of sea salt aerosol. Non-zero $DF_{SO_4^{2-}}$ in aerosol suggest that the sea salt particles originate from a fractionated sea ice source.

In order to further constrain the origin of the aerosol Na^+ and $DF_{SO_4^{2-}}$ of the snowpack were measured. Blowing snow was collected during the storm every two hours over a 12 hr period and snow pit profiles were sampled at various ice floe locations from 11 to 14 July prior to the storm. During the storm blowing snow Na^+ concentrations on average more than doubled from 4.5 to 12 $\mu g\,g^{-1}$ and salinities S_p increased from 0.02 to 0.04 psu, whereas $DF_{SO_4^{2-}}$ remained fairly constant at a median of ~0.54 (Fig. 10e-f). The large spatial variability in Na^+ concentrations and S_p of the snowpack masked any temporal trend, yet the snowpack profiles could be grouped into two types, one showing a very steep S_p (Na^+) decline with snow layer height from 1–10 psu ($10^2\,\mu g\,g^{-1}$) near the bottom to 10^{-3} psu ($10^{-1}\,\mu g\,g^{-1}$) near the surface, and the other showing a less steep decline from 30 psu ($10^3\,\mu g\,g^{-1}$) to 10^{-2} psu ($10^1\,\mu g\,g^{-1}$) (Fig. 11a-b). $DF_{SO_4^{2-}}$ ~~showed large scatter, with the more saline snow being more depleted in sulphate~~ profiles exhibited large scatter: except at one location surface-near snow showed no or small depletion, whereas most profiles showed significant depletion in deeper layers within 5-10 cm of the sea ice surface (Fig. 11c). Negative $DF_{SO_4^{2-}}$ was found at the snow-ice interface and in some snow layers ~~indicating~~ suggesting the presence of mirabilite (Fig. 11c).

Comparison shows that the range of Na^+ concentrations and S_p values observed in blowing snow can be explained by mixing between the two snowpack types (Fig. 11a-b). An increase over time of salinity or Na^+ concentration in airborne snow is also consistent with snowpack erosion during the storm and exposure to uplift of deeper and more saline snow layers. ~~The~~ However, the $DF_{SO_4^{2-}}$ values of blowing snow were at the top end of the range observed ~~in the more saline~~ only in the deeper and more saline local snowpack (Fig. 11c). A plausible explanation for this observation during the storm on 15 July is that blowing snow integrates snow contributions from a wider area. And given the spatial heterogeneity of local snowpack thickness and composition blowing snow contributions must have dominated from areas where fractionated snow was at or near the surface such as seen in one of the profiles sampled on 12 July (Fig. 11c). Taking the median $DF_{SO_4^{2-}}$ values in aerosol (=0.48-0.61) and blowing snow (=0.54) it can be concluded that 89-100 % of the observed aerosol comes from the local fractionated snow source.

In summary, observations show that blowing or drifting snow leads to increases in aerosol number densities during and after a storm. ~~Spectral $N_{0.4-12}$~~ Aerosol size spectra show that number densities of particles with size $d_p<2\,\mu m$ increased during individual storms by 2-3 orders of magnitude above background levels~~for particle sizes $d_p<2$~~. Concurrent increases in aerosol Na^+ concentration ~~show~~ suggest that the observed new particles consist mainly of sea salt aerosol. Observed aerosol gradients suggest that net production of SSA takes place near the top of the blowing or drifting snow layer. Furthermore, similar ~~sulphate~~ sulfate depletion in aerosol, blowing snow and the local snowpack is strong evidence that the bulk of the observed SSA originated from snow on sea ice and not the open ocean, which is consistent with the independent model results of ~~?~~Yang et al. (2019). Advection of SSA from the open ocean cannot be ruled out during storms with warm and moist air, but plays only a minor role due to the large distance to the nearest open water, in particular at ice stations S1-S6 (Table 1). The scale-length for SSA removal over an ice shelf had been estimated previously to be ∼30 % per 100 km, thus the reduction of the SSA burden during advection over 600 to 1000 km would be larger than a factor 6 to 20 (Wagenbach et al., 1998, and refs. therein). Distance to the open ocean together with a temporally very close association of snow particle and aerosol number density dynamics (Fig. 10) further support the above finding that a local SSA sea ice source dominates over advection. Open leads, which may have been present in areas of reduced sea ice concentration e.g. near ice stations S2-3 and S7-9 (Fig. 1) are another potential wind-dependent source of SSA from open water as observed in the Arctic (Nilsson et al., 2001; May et al., 2016), albeit with a much smaller flux contribution per surface area compared to the open ocean due to reduced fetch and low fraction of surface coverage (<15 %). Observations show also that snow drift is conceptually not different from a blowing snow event with the same physical processes leading to SSA production.

3.4 Evaluation of SSA production scheme from blowing snow

It has been proposed that the production or mass flux of SSA from blowing snow, Q_{SSA}, is proportional to the bulk sublimation flux of suspended snow particles, Q_s in units of kg m^{-2}s^{-1}, and snow salinity, S_p in psu ~~(Yang et al., 2008; ?)~~(Yang et al., 2008, 2019). The model scheme however relies on blowing snow measurements above ice sheets (Budd, 1966; Mann et al., 2000; Nishimura and Nemoto, 2005), and parameterisations developed for in-land regions in the high Arctic (Déry and Yau, 2001, and ref. therein). Below we briefly summarise the model mechanism and then evaluate its applicability to snow on sea ice based on the Weddell Sea observations.

The mass flux of SSA from blowing snow Q_{SSA} in units of kg m^{-2}s^{-1} is computed as

$$Q_{SSA} = \frac{Q_s}{1000} \int_0^\infty \int_0^\infty f(d_p)\, S_p\, \psi(S_p)\, d(d_p)\, d(S_p) \qquad (1)$$

where d_p is the snow particle diameter (m), $f(d_p)$ is the particle size distribution of blowing snow and $\psi(S_p)$ the snow salinity probability distribution. The quantities $f(d_p)$ and $\psi(S_p)$ are compared to direct observations from this study, whereas the blowing snow bulk sublimation flux Q_s was not amenable to direct measurement under field conditions. However, the model parameterisation used for Q_s (Déry and Yau, 2001) depends on observable quantities, which are validated below against measurements from this study.

3.4.1 Blowing snow bulk sublimation flux $\boldsymbol{Q_s}$

The blowing snow bulk sublimation flux Q_s is the local bulk sublimation rate integrated over the entire blowing snow column. Q_s is parameterised after Déry and Yau (1999, 2001),

$$Q_s = K\,A'\,Q'_s\,\frac{q_{bsalt}}{q_{b0}} \tag{2}$$

where K (= 1.1574×10^{-5}) is a factor to convert Q'_s into units of $\mathrm{kg\,m^{-2}\,s^{-1}}$, A' is an empirical snow age factor, Q'_s is a normalised column-integrated sublimation rate ($\mathrm{mm\,day^{-1}}$, snow water equivalent), q_{bsalt} is the saltation layer blowing snow mixing ratio ($\mathrm{kg\,kg^{-1}}$) under ambient conditions, and q_{b0} the value it would have when the 10-m threshold wind speed U_t, below which no snow drift occurs, has its minimum value U_{t0} (= $6.975\,\mathrm{m\,s^{-1}}$) based on the empirical model of Li and Pomeroy (1997). The saltation layer is a layer just above the snow surface usually several centimetres thick (e.g. Déry and Yau, 1999). The ratio q_{bsalt}/q_{b0} comes from the required introduction of a lower boundary condition for particle number densities in the saltation layer and scales the normalised Q'_s accordingly. Values for q_{bsalt} are computed with

$$q_{bsalt} = 0.385\,(1-\frac{U_t}{U_{10m}})^{2.59}u_*^{-1} \tag{3}$$

where U_{10m} is the 10-m wind speed ($\mathrm{m\,s^{-1}}$) and u_* is the friction velocity (Eq.24 in Déry and Yau, 1999). For the 10-m threshold wind speed U_t an empirical model for dry snow was previously derived based on observations in the prairies of Western Canada, which applies to dry snow conditions and is a function of ambient temperature T_a (Li and Pomeroy, 1997)

$$U_t = U_{t0} + 0.0033\,(T_a + 27.27)^2 \tag{4}$$

This expression is compared to observations above sea ice from this study as follows. The onset of drifting or blowing snow is defined similar to Mann et al. (2000) as the moment when snow drift density μ right above the snow surface exceeds a ~~threshold value of~~ critical value μ_c (= 0.005~~(0.001)~~ $\mathrm{kg\,m^{-3}}$). For comparison a lower value of μ_c (= 0.001 $\mathrm{kg\,m^{-3}}$) is also considered. The snow drift density is calculated as $\mu = \frac{4}{3}\pi\,\rho_{ice}\int_0^\infty N_s(d_p)(\frac{d_p}{2})^3\,d\,d_p$ with the density of ice ρ_{ice} (= $917\,\mathrm{kg\,m^{-3}}$) and the measured spectral number density N_s. U_{10m} is extrapolated from the sonic anemometer measurements at 2 m assuming a logarithmic wind profile and T_a comes from the uppermost sensor on the sea ice at ∼2 m. The observed threshold wind speed U_t and friction velocity u_{*t} are the respective measurements at the onset of drifting or blowing snow. Using the lower ~~μ threshold~~ threshold μ_c (= 0.001 $\mathrm{kg\,m^{-3}}$) most observed U_t values ~~are~~ fall still within the model range of uncertainty (Fig. 12) and show a mean U_t of 7.1 (range 2.2-9.8) $\mathrm{m\,s^{-1}}$ corresponding to u_{*t} of 0.37 (range 0.08 - 0.58) $\mathrm{m\,s^{-1}}$. For comparison, u_{*t} for blowing snow above an Antarctic ice shelf during winter was observed to range between 0.18 and 0.38 $\mathrm{m\,s^{-1}}$ (Dover, 1993; Mann et al., 2000). Earlier work on land based snowpacks found u_{*t} to range from 0.15 $\mathrm{m\,s^{-1}}$ for loose, fresh, dry snow to 0.4 $\mathrm{m\,s^{-1}}$ for old, wind-hardened snow (Dover, 1993, and references therein). Thus, u_{*t} observed for snow on sea ice are on average at the upper end of previous observations for snow on land or ice shelves. It is concluded that Eq. 4 provides robust estimates of U_t above sea ice for the snowpack conditions encountered during this study exhibiting in general very low salinities (Table 5). However, temperature alone may not be a good predictor of U_t if surface snow on sea ice exposed to wind is very saline with a relatively larger liquid fraction at a given temperature due to freezing point depression leading to increased snow crystal cohesion.

In a next step blowing snow mixing ratios in the saltation layer q_{bsalt} were computed by dividing observed drift density μ by the density of air and then compared to q_{bsalt} predicted by the empirical parameterisation after Déry and Yau (1999) (Eq. 3). Considered were only observations when μ>0.001 $\mathrm{kg\,m^{-3}}$ and when the SPC was mounted below reported values of the saltation layer depth (=0.1 m). It is found that the model overpredicts observed q_{bsalt} on average by at least a factor ∼10 (Fig. 13) suggesting that the conditions during this study were likely different to those in the Canadian Prairie for which Eq. 3 was developed. One model uncertainty is the assumption that the saltation layer is saturated with respect to ice, which has not been confirmed yet for the dry and cold polar boundary layer due to the lack of sufficiently accurate humidity measurements.

However, relative changes of q_{bsalt} are well captured by the model, in general showing an increase with wind speed (Fig. 13a,c). Except during the blowing snow event on 14-15 July (ice station S6) q_{bsalt} decreased even though wind speed remained constant at ∼12 $\mathrm{m\,s^{-1}}$ (Fig. 13b), as noted above for total N_{46-478} near the snow surface (Fig. 10b). Strong warming during the storm of ∼20 K increased snow particle cohesion and therefore the drift threshold wind speed U_t as predicted by the model, thereby reducing the uplift of snow particles (Fig. 13b). A similar case occurred during 26-27 June, when warming increased the theoretical drift threshold and wind speed dropped at the same time below U_t consistent with the absence of blowing snow particles at 29 m (Fig. 8b).

The model bias in q_{bsalt} ~~has only a minor impact on~~ is expected to cancel out in estimates of bulk sublimation rate Q_s (Eq. 2) and therefore also of SSA production Q_{SSA} (Eq. 1) because the calculation uses not absolute values but ratios of actual q_{bsalt} and its maximum q_{b0}.

3.4.2 Snow particle size distribution $f(d_p)$ above sea ice

Previous studies concluded that a 2-parameter gamma probability density function gives a reasonable fit to observed distributions of snow particle diameter $f(d_p)$ (Budd, 1966; Schmidt, 1982; Dover, 1993):

$$f(d_p) = \frac{e^{-\frac{d_p}{\beta}}\, d_p^{\alpha-1}}{\beta^{\alpha}\,\Gamma(\alpha)} \tag{5}$$

with shape and scale parameter α and β, and mean particle diameter $\overline{d_p} = \alpha\,\beta$. Particle size distributions of blowing snow have been found to vary with wind speed and height: at a given height, $\overline{d_p}$ increases with wind speed, whereas at a given wind speed, preferential removal of large snow particles due to gravitational settling leads to a decrease in $\overline{d_p}$ (e.g. Dover, 1993; Mann et al., 2000) and an increase in α with height (Nishimura and Nemoto, 2005). Increasing α is equivalent to a shift from skewed to more symmetrical size distributions. Model predictions of the mass flux of SSA from blowing snow Q_{SSA} depend critically on $f(d_p)$ (Eq. 1) and therefore on α and β (Eq. 5).

In this study we derived $\overline{d_p}$ and α by fitting a 2-parameter gamma distribution to observed particle size spectra. Confidence in retrieved values of α and β is affected by two limitations of the SPC measurements. Firstly, SPC size spectra are clipped due to instrument configuration and exclude very small snow particles (d_p<46 µm). And secondly, SPC data include noise in the particle number count due to natural variability. A Monte Carlo model, which generates multiple noisy gamma distributions of known α and β shows that retrieving these parameters is robust, even when the data are limited to $d_p > \overline{d_p}$, that is capture only the tail of the data. Furthermore, the uncertainty from under-sampling and data noise in α and β can be retrieved from the relative scale of the smallest size bin and the residual noise.

During blowing snow episodes when U_{10m} was above the mean observed 10-m drift threshold wind speed U_t of 7.1 m s^{-1} $\overline{d_p}$ decreased with height, whereas α increased with height as shown by the respective median values (Table 6) consistent with previous observations. Increase of α with height during blowing snow was found previously at Mizuho station on the Antarctic Plateau where α was ∼3 near the surface and increased to values >10 further aloft (Nishimura and Nemoto, 2005). Another study at Halley in coastal Antarctica found no gradient in α within the lower 4 m (Dover, 1993), which was set to 2 following the analysis of King et al. (1996).

However, the observed decrease in mean particle size $\overline{d_p}$ with height was much smaller than that inferred from previous studies. For example, median $\overline{d_p}$ at 29 m was 43 % larger than d_p observed between 1.0 and 9.6 m (=80 µm regardless of wind speed) at Mizuho station (Nishimura and Nemoto, 2005) and ∼4 times the d_p predicted by a parameterisation based on the Halley vertical d_p profiles between 0.1 and 4.0 m (King et al., 2001). Further examination of the snow particle size distributions at 29 m reveals in general an unexpected long tail indicating significant relative contributions from large particles. For example, during the blowing snow event on 14 July $\overline{d_p}$ and α near the surface were 105 µm and 5.2, respectively (Fig. 14b). At 29 m total N_{46-478} was as expected about two orders of magnitude smaller than near the surface. Yet compared to the near-surface values average $\overline{d_p}$ was larger (131 µm) and the size distribution more skewed (α= 3.2) with a long tail showing significant contributions from particles with d_p>200 µm (Fig. 14a).

It is suggested that small or no decrease of $\overline{d_p}$ with height and the long tail in $f(d_p)$ at 29 m can be explained by contributions from falling snow particles since blowing snow frequently coincided with precipitation. In order to analyse $f(d_p)$ of snow precipitation only, a calm 17 h period (3 July 14:30 to 4 July 7:00) ~~period)~~ was chosen during which light snowfall (N_{46-478}<800 m^{-3} at both levels) but no snow drift ~~(~~occurred with U_{10m} (=2.7 m s^{-1}) ~~occurred.~~ $<U_t$. For the early morning of 4 July 2013 webcam images from the crow's nest confirmed the presence of large airborne snow crystals visible during darkness in the beam of the ship's search lights, whereas the ship's 3-hourly weather report noted the presence of airborne ice needles. It is found that the size distribution ($\overline{d_p}$, α)

of precipitation at 29 m (Fig. 14c) was very similar to that during a blowing snow event (Fig. 14a)~~, and~~ . The size spectrum of falling snow also showed no preferential large size mode as observed previously at Mizuho station (Nishimura and Nemoto, 2005)~~preventing~~ , which prevents a correction of blowing snow particle spectra for snow precipitation based on particle size. The spectral shift to smaller particles near the surface during the snowfall event (Fig. 14d) was likely due to a combination of two processes: sublimation of larger snow particles supported by a mean RH_{ice} of 98.0 % between 0.2 and 2.0 m. And fragmentation of snow particles by more vigorous and smaller eddies near the surface during calm conditions, either through direct break-up of the dentrites or through separation of snow flakes that have ~~have~~ loosely adhered on the decent. Similar size distributions ($\overline{d_p}$, α) near the snow surface and at 29 m during blowing snow imply that at 29 m particle sizes lost from the blowing snow size spectrum due to gravitational settling were being replenished by falling snow. ~~Due to the increase in the fraction of precipitating snow with height snow particle size distributions measured at 29 have additional uncertainty, whereas those observed near the surface are representative of blowing snow.~~

~~Plotting~~ Plotting the fitted parameters $\overline{d_p}$ and α against wind speed allows to evaluate the parameter range characteristic for blowing snow: $\overline{d_p}$ shows the expected increase near the surface but large scatter and little change at 29 m (Fig. 15a-b). Values of α show at both heights some dependence on wind speed (Fig. 15c-d) and cluster between 3 and 6 when $U_{10m} > U_t$. Median, lower and upper quartiles of $\overline{d_p}$ and α for blowing snow, i.e. when windspeed U_{10m} is above the observed mean ~~threshold~~ drift threshold wind speed U_t (=7.1 m s^{-1}), are summarised in Table 6 as guidance for model sensitivity studies. Due to the increase in the fraction of precipitating snow with height snow particle size distributions measured at 29 m have additional uncertainty, whereas those observed near the surface are representative of blowing snow.

3.4.3 Salinity probability distribution $\psi(S_p)$ of snow on sea ice

Correct modelling of SSA production from blowing snow (Eq. 1) requires choosing a snow salinity probability distribution $\psi(S_p)$ representative of the region and season under consideration (Massom et al., 2001). High salinities near the snow-sea ice interface originate from incorporation of frost flowers or upwards migration of brine due to capillary action. Brine is found at the top of sea ice as a result of ion exclusion during the freezing of seawater or of flooding due to negative freeboard. Top snow layers in deeper snowpacks not affected by brine migration receive sea salt aerosol through dry or wet deposition of background aerosol or sea spray.

Vertical profiles of snow salinity S_p measured during this study (Frey, 2017) showed a marked decrease with height above the sea ice surface (Fig. 16a) in agreement with previous sea ice surveys in Antarctica (Massom et al., 2001). High salinities S_p (1–43 psu) were found in basal snow, the sea ice surface and frost flowers, whereas very low salinities (<0.2 psu) were observed in snow layers >20 cm above the snow-ice interface and in blowing snow (range 0.01–0.12 psu) (Fig. 16a). The inferred mean migration distance of ∼20 cm above sea ice that brine can affect the snowpack falls within the range of those reported by previous studies, up to 17 cm in the Arctic (Domine et al., 2004), and 30 cm in the Weddell sea (Massom et al., 2001).

From the above follows that to a first order the distance of individual snow layers to the sea ice surface determines their salinity, and therefore snowpack depth determines to a first order mean volume-integrated salinity and salinity probability distributions $\psi(S_p)$ in snow on sea ice. Average $(\pm\sigma)$ snowpack depth based on snow pits from this study was 21 (± 8) cm above first-year sea ice (FYI) and 50 (± 32) cm above multi-year sea ice (MYI) (Table 5), in the range of previous observations in the Weddell sea sector, e.g. mean snowpack depth during winter 1992 was 14 cm (Massom et al., 2001, and references therein). As expected the ~~mean~~ median salinity of the shallow FYI snowpack (~~=1.4~~0.11 psu) was significantly larger than that of the deep MYI snowpack (~~0.82~~0.02 psu) (Table 5) based on the Wilcoxon rank-sum test ($p<0.01$), and corresponding salinity probability distributions $\psi(S_p)$ for snow on FYI are shifted to higher salinities when compared to $\psi(S_p)$ above MYI (Fig. 16b). Secondary factors identified previously (e.g. Massom et al., 2001), which contribute to higher salinities of snow on FYI in comparison to snow on MYI are more frequent flooding of thin FYI with sea water due to negative freeboard and brine rejection and drainage, which decreases MYI salinity over time.

Previous modelling of SSA production from blowing snow based $\psi(S_p)$ on much higher mean snow salinities S_p than observed during this study: 8.5 psu from observations in the Indian ocean sector in August 1995 (Yang et al., 2008) and half that value in a later study (Levine et al., 2014). Bearing in mind that only surface snow, which often has lower density and crystal cohesion, is likely to get airborne, it is sensible to include only the top snow layers in the calculation of average snow salinity. For example, in this study the mean S_p of snow layers within the top 10 cm of the snow surface was 0.31 psu (Table 5), a factor 28 smaller than that used for $\psi(S_p)$ by Yang et al. (2008). More recent studies updated the model scheme accordingly using the very low salinities found here in surface and blowing snow ~~(Rhodes et al., 2017; ?)~~(Rhodes et al., 2017; Yang et al., 2019). It should be noted that snow on sea ice even at the lower end of the S_p spectrum contains amounts of sea salt large enough to produce significant SSA especially in the sub-micron range ~~(e.g. ?)~~(e.g. Yang et al., 2019), and is on average significantly saltier than snow in inner Antarctica. For example, mean ice core Cl^- or Na^+ concentrations on the West Antarctic ice sheet are $\sim$100 ng g^{-1} or less (Frey et al., 2006), equivalent to S_p of $\sim 10^{-3}$ psu, thus up to 4 orders of magnitude smaller than in snow on sea ice (Fig. 16a).

In summary, model parameterisations for SSA production from blowing snow require a snow salinity probability distribution $\psi(S_p)$, which takes into account regional and seasonal variabilities. Snow depth on sea ice, retrievable from satellite measurements, may be a good predictor of mean snow salinity as more field measurements become available.

3.5 The sea ~~ice source of sea~~ salt ~~aerosol~~ atmosphere-snow mass budget

~~Below we discuss chemical fractionation in snow and aerosol, aerosol spectra and the air-snow sea salt budget characteristic for sea ice.~~

3.5.1 ~~Chemical fractionation of~~

~~In non-summer months when biogenic non-ss is at a minimum Antarctic aerosol was observed to be depleted in (with respect to) and in (with respect to) (Wagenbach et al., 1998; Legrand et al., 2017). Similar fractionation in brine and frost flowers in the sea ice nearby attributed to precipitation of the mineral mirabilite () suggested that the observed SSA must originate from the sea ice and not from the open ocean (Wagenbach et al., 1998; Rankin et al., 2000).~~

~~Here we show for the first time that snow on sea ice is depleted in sulphate (Fig. 4a). DF of most snow samples was positive, showing large scatter and no particular dependence on snowpack depth or sea ice age (Fig. 4a). Negative DF suggests presence of mirabilite precipitated during freezing. The median volume-integrated DF in snow ranged between 0.24 and 0.35 (Table 5) matching very well the sulphate depletion found in aerosol during the period the snow was sampled (ANT6) with median DF ranging between 0.29 and 0.48 (Table 4). The similarity of sulphate depletion in both snow and aerosol strongly suggests that snow sea ice in the Weddell Sea is the dominant source of regional sea salt aerosol.~~

~~The sulphate depletion observed in aerosol and snow (Figs. 2f, 4a) is consistent with mirabilite precipitation. Mean temperatures during all ice stations except S3 were below the -6.4°C threshold of mirabilite precipitation(Table 1). And a recent lab study found that mirabilite precipitation results in DF of 0.93 in sea water brine cooled down to -20.6 (Butler et al., 2016). Conversely, $DF<0$ in snow or aerosol suggests contributions from non-sea salt or crystallized mirabilite, which has a DF of -7.3. The latter is supported by the observation that most $DF<0$ occur in or near the sea ice surface, where most of the partitioning between brine and mineral is expected to have occurred during freezing (Fig. 4a).~~

~~If the partitioning of crystallised between brine and the snow-ice matrix is the dominating fractionation process then should be depleted as well in the brine. Following the analysis of Wagenbach et al. (1998) we take as the reference species for bulk sea water and find from a mass balance calculation that the to mass ratio would then be linearly related to the to ratio with a slope of -0.98 and an intercept of 2.04. From that a theoretical relationship between $DF_{\mathrm{Na^+}}$ (with respect to) and $DF_{\mathrm{SO_4^{2-}}}$ (with respect to) is derived and compared to observations (Fig. 5). The observed fractionation is largely in agreement with the model prediction. Snow on sea ice follows closely the theoretical mirabilite fractionation line, whereas aerosol shows large scatter and a tendency to apparent enrichment (Fig. 5). The latter was observed previously and attributed to acid-induced chloride loss, which had occurred from aerosol in the atmosphere or as a sampling artefact from sea salt already accumulated on the filter surface (Wagenbach et al., 1998; Legrand et al., 2017). It is noted that if all sulphate is removed by mirabilite precipitation ($DF_{SO_4^{2-}}=1$) then sodium depletion reaches a theoretical maximum of ~12 % ($DF_{Na^+}=1.1204$) (Fig. 5).~~

~~The median DF values of bulk aerosol observed during this study were smaller than previous winter observations at coastal Antarctic sites, where the sea-ice surface was shown to be the dominant source of sea-salt aerosol. Wagenbach et al. (1998) reported sulphate depletion in aerosol corresponding to $DF_{\mathrm{SO_4^{2-}}}$ of 0.72 at Halley (75S, 26W), of 0.76 at Neumayer (70S, 85W), and of 0.62 at Dumont d'Urville (66S, 140E). The main cause of smaller DF observed in aerosol above the Weddell Sea in winter 2013 appears to be the snow source being less depleted~~

~~in sulphate during that particular year. Thus, caution is warranted when sea ice SSA fractions of the total aerosol burden at a specific location are estimated based on sulphate depletion (e.g. Legrand et al., 2017), since $DF$of pure sea ice emissions vary temporally and spatially thereby introducing additional uncertainty if not accounted for.~~

3.5.1 ~~Chemical fractionation of~~

~~The importance of sea salt as a source of atmospheric bromine species in the mid to high southern latitudes is now well established, and SSA from blowing snow is expected to release bromine (Yang et al., 2008, 2010) driving ozone depletion events observed during or after snow storms (Jones et al., 2009). One of a number of processes identified to cause halogen release from aerosol or ice surfaces involves the reaction of with halides (and) on acidic ice surfaces forming and that are subsequently photolyzed to form reactive halogen atoms (Abbatt et al., 2012, and references therein). This is a multiphase process which, depending upon the substrate, may or may not proceed faster under acidic conditions (Abbatt et al., 2012), and associated uncertainties are currently still significantly limiting the modelling of impacts on tropospheric halogen chemistry (Sander et al., 2003; Long et al., 2014). Multi-phase bromine chemistry models use observed sea salt aerosol depletion of bromide relative to sodium (or chloride) with respect to seawater composition, i.e. bromide depletion factors DF, to estimate the bromine flux from sea-salt aerosol (e.g. Yang et al., 2008; Long et al., 2014) . However, to date observations of bromide aerosol depletion are only available from north of 55S (Sander et al., 2003, and references therein), with the exception of two recent pioneering studies in Antarctica (Legrand et al., 2016; Hara et al., 2018). Below we discuss bromine chemistry observations above the Weddell Sea during this study.~~

~~Bulk aerosol concentrations of bromide ranged between $<$1 and 19 (Fig. 6a), showing occasional large increases to levels seen elsewhere in coastal Antarctica only during summer (Legrand et al., 2016). However, median bulk aerosol concentrations of (Table 4) were similar to coastal observations at Dumont d'Urville during winter (Legrand et al., 2016). It should be borne in mind that the bromide aerosol concentrations were often below the estimated LOD due to the short filter exposure times employed (Fig. 6a). Median bromide concentrations in snow ranged between 70 and 180 (Table 5).~~

~~It is found that aerosol at 29 was on average strongly depleted in bromide relative to sodium with respect to seawater, whereas aerosol near the sea ice surface at 2 showed mostly strong enrichment (Table 4, Fig. 6b). Median $DF_{\mathrm{Br^-}}$ in the snowpack was 0.00–0.06 suggesting overall no or small depletion in bromide (Table 5). However, examination of individual snow layers as well as blowing snow samples shows large scatter with both positive and negative $DF_{\mathrm{Br^-}}$, suggesting both bromide depletion and enrichment (Fig. 4b). The sea ice surface below the snow was with the exception of one sample always enriched in bromide (Fig. 4b). During the storm on 14-15 July (see section 3.3.2) it is found that the median $DF_{\mathrm{Br^-}}$ in blowing snow collected on 15 July at $<$1 was close to zero but 0.39 in aerosol at 29 sampled over the same time interval.~~

~~These observations are in agreement with previous studies in coastal Antarctica: Legrand et al. (2016) were the first to report bromide depletion in aerosol at Dumont D'Urville. And Hara et al. (2018) observed at Syowa Station bromide depletion in aerosol but not in blowing snow, which was enriched, and concluded that heterogeneous chemistry driving bromine activation occurs on sea salt aerosol and not on blowing snow. Lieb-Lappen and Obbard (2015) observed bromide depletion in blowing snow but only at $>$5 above the surface.~~

~~From this study it is concluded that air-ice recycling of bromine occurs on surface snow, airborne snow and aerosol particles. However, the vertical gradient in $DF_{\mathrm{Br^-(Na^+)}}$ observed in aerosol suggests that the bulk of the net bromine release must take place in the aerosol phase between 2 and 29 above the sea ice surface. The bromine net release from large snow particles is expected to be reduced compared to aerosol due a combination of shorter atmospheric lifetime and smaller specific surface area limiting diffusional outgassing. The bromine release from SSA produced by blowing snow may be more efficient because it has a large fraction of sub-micron sized particles (see section 3.2.3), resides at the well ventilated top of the blowing snow layer, and may also be more acidic. Thus sea salt aerosol from blowing snow provides an additional bromine reservoir, which is readily depleted.~~

~~Models assume a dependence of $DF_{\mathrm{Br^-}}$ on season and aerosol diameter (Yang et al., 2008; Sander et al., 2003). $DF_{\mathrm{Br^-}}$ of aerosol showed a weak positive trend from winter into spring largely due to less frequent negative values during August and September (Fig. 6b, Table 4). Increasing $DF_{\mathrm{Br^-}}$ is consistent with enhanced bromine loss from aerosol as incident radiation increases concurrent with activation of the reactive bromine () cycle (Fig. 6b). This becomes more evident considering monthly median $DF_{\mathrm{Br^-}}$ values of aerosol at 29 , which increased from June (0.25), July (0.44), August (0.54) into September (0.59). Lower values but a similar trend had been observed at Dumont d'Urville, where $DF_{\mathrm{Br^-}}$ in bulk aerosol increased gradually from a minimum in June (0.04), intermediate values in July to Sep (0.22-0.39) to a maximum in October (0.42) (Legrand et al., 2016). $DF_{\mathrm{Br^-}}$ values from this study would be even higher had they been referenced to a sea water ratio adjusted for the maximum possible removal of sodium due to precipitation of mirabilite as done by Legrand et al. (2016). Assuming that observed $DF_{\mathrm{Br^-}}$ is representative of SSA with a median particle diameters d_p of ~0.60-0.66 , it is found that observed bromide depletion is larger than that reported by Sander et al. (2003) with a maximum of 0.4 for a d_p of 1.3 , dropping to 0.1 at 10 .~~

3.5.1 ~~Aerosol size distribution~~

~~Average aerosol number and volume distributions observed in the Weddell sea show that during calm conditions (U_{10m} 3±1) concentrations across most of the size spectrum were smaller above sea ice than above the open ocean (Fig. 7). The wind speed chosen for calm conditions is well below the mean snowdrift threshold U_t of 7.1 observed during this study and at the lower end of the range when breaking of waves commences (O'Dowd et al., 1997). A low sea salt aerosol background above compact sea ice during calm conditions is consistent with the absence of any active local sources and the long distance to the nearest open ocean. The average aerosol volume distribution shows~~

~~two modes, one at 1-2 and the other at >7 (Fig. 7b), indicating that most of the aerosol particle mass resides in the super-micron range as expected for sea salt aerosol.~~

~~During stormy conditions (U_{10m} 10±1) average aerosol number and volume concentrations above the sea ice increased significantly for all particle diameters d_p below 10 , and slightly more so at smaller particle sizes (d_p<2), albeit remained below those above the open ocean observed over two days during this study (Fig. 7). However, the relative increase of aerosol number and volume concentrations during storms above background levels over the sea ice was equal or larger than above the open ocean. This implies that corresponding aerosol number and mass fluxes during storms were also equal or larger above sea ice than above the open ocean consistent with Yang et al. (2008) and underlining the importance of a sea ice source for atmospheric sea salt aerosol in winter and early spring (Fig. 7).~~

~~The main observational constraint for the origin of the observed sea salt aerosol comes from its chemical source signature as discussed above. In addition, the relatively larger increase of small particle number densities provides further support for the blowing snow SSA source based on physical arguments: snow particles of low salinity as observed during this study will generate very small sea salt particles after complete loss of water ice by sublimation. Taking the dry particle diameter $d_{dry} = d_p(S_p/1000\,\rho_{ice}/\rho_{\mathrm{NaCl}})^{1/3}$, where ρ_{ice} and ρ_{NaCl} are densities of ice and , respectively, we would expect based on observed snow salinity and snow particle size (Table 5, 6) potential d_{dry} on the order of 10^{-3}, or larger if not all water is lost. Instruments with a lower size detection limit than available in this study are needed to further investigate very small particle formation from blowing snow.~~

~~It is important to note that the use of sea salt measured in ice cores as a proxy of past sea ice conditions requires that average emissions above sea ice exceed those above an equivalent area of open ocean and consequently lead to a comparatively larger burden of atmospheric SSA. Observations from this study support the former requirement, but not the latter. The low SSA background concentrations observed above sea ice may have been due to a combination of low storm frequency and low snow salinities in the area. Indeed, model calculations suggest that size distribution and associated flux of SSA originating from blowing snow are very sensitive to snow salinity S_p, e.g. decreasing S_p from 0.92 to 0.06 causes SSA spectral number densities to decrease by about one order of magnitude (?). Further atmospheric modelling is needed to address this issue and will be subject of future research.~~

3.5.1 ~~The sea salt atmosphere-snow mass budget~~

Assessing the sea salt mass distribution between atmosphere and snow during calm and blowing snow conditions provides further evidence for the importance of snow on sea ice as a SSA source (Fig. 17). To do this atmospheric sea salt concentrations were estimated in two ways for the time period when *RV Polarstern* was well within the FYI zone (18 June to 21 July 2013; Fig. 1)~~: one by~~. One by converting spectral particle number densities $N_{0.4-12}$ at 29 m into total particle mass concentration assuming spherical particles with the density of NaCl (= 2160 kg m^{-3}). And the other by multiplying the Na$^+$ concentration measured on aerosol filters at 29 m by 3.262 based on the Na$^+$ mass fraction in reference seawater (Millero et al., 2008). ~~And the other by converting the observed spectral particle~~

~~number densities $N_{0.4-12}$ into total particle mass concentration assuming spherical particles with the density of (= 2160~~Note that as shown in section 3.2.1 depletion of SO_4^{2-} due to the precipitation of mirabilite decreases Na^+ by up to 12~~). Comparison shows that the ~~%. Reduction in both ions decreases the mass fraction of Na^+ in the depleted sea salt aerosol by a maximum of ∼0.7 % compared to reference seawater. Thus, by not considering the depletion effect conversion factor and calculated SSA mass are underestimated by up to ∼0.7 %, which is negligible given all other uncertainties. The sea salt mass estimates show that most filter-based values have a low bias compared to median sea salt concentrations derived from $N_{0.4-12}$ during filter sampling intervals ~~are on average ~~(Fig. S3), on average of ∼~~40~~26 %~~larger than filter-based values (data not shown) .~~. The bias also shows a weak but significant positive correlation with wind speed (R=0.40, $p<0.01$) (Fig. S3). A low bias of the filter samples especially during high wind speeds is expected because the smaller cut-off diameter (<6 µm) compared to the optical particle counter (>11 µm) limits capture of coarse sea salt aerosol, where much of the particle mass is located (Fig. 7b).

During storms median atmospheric sea salt concentrations from both estimates showed ~~a significant increase~~ increases above background values (Fig. 17a) that were statistically significant based on the Wilcoxon rank-sum test ($p<0.01$). For example, median sea salt concentration based on $N_{0.4-12}$ increased by a factor ∼~~3, from 390 to 1215~~4, from 0.37 to 1.48 µg m^{-3} when comparing calm (~~3±1~~≤4 m s^{-1}) with windy (~~10±1~~≥9 m s^{-1}) conditions (Fig. 17a).

A potential atmospheric sea salt concentration if surface snow released its sea salt content by blowing snow sublimation is estimated as follows: taking a typical column total blowing snow sublimation rate of 0.1 mm day^{-1} observed at Halley during winter (King et al., 2001) and assuming a mean storm duration of 1 day on average the sea salt within the top 0.1 mm of snow can be released. Total sea salt mass observed in the top 0.1 mm of surface snow was converted into atmospheric concentration assuming a snow density ρ_{snow} of 300 kg m^{-3} and complete mixing into a winter atmospheric boundary layer with an estimated mean depth of 100 m (Fig. 17a). Further assuming that the atmospheric concentration measured at 29 m is constant throughout the 100 m atmospheric column it is found that the potential snow reservoir is more than a factor 10 larger in comparison to the total atmospheric burden and therefore easily accounts for the sea salt aerosol increase observed during blowing snow (Fig. 17a).

~~Sulphate depletion in ~~Sulfate depletion in winter aerosol and snow in Antarctica provides a means to estimate source contributions from the open ocean and the blowing snow source above sea ice ~~.~~as discussed in section 3.2.1. The overlap in $DF_{SO_4^{2-}}$ (relative to Na^+) in aerosol and snow suggests that most of the aerosol observed during storms (U_{10m}≥9 m s^{-1}) had its origin in the regional snow on sea ice (Fig. 17b). During the 8 June and 12 August 2013 (ANT6) median $DF_{SO_4^{-2}}$ of aerosol observed at 29 m was 0.29 and that of the top 10 cm of snowpack was 0.27 ~~and that of aerosol observed at 29 was 0.29 (Table 5,4~~(Tables 4,5). Assuming linear mixing between two end members, i.e. the open ocean and the snow source, and assuming they are constant in space and time, one finds ~~that on average ∼93~~based on the median values that >90 % of the aerosol observed originates from snow on sea ice. ~~Similarly for the the time period of the sea salt mass budget estimate the overlap in the ranges of $DF_{SO_4^{2-}}$ (with respect to) observed in aerosol and snow show that most of the aerosol observed during storms had its origin in the regional snow on sea ice (Fig. 17b).~~

4 Conclusions

Two consecutive sea ice cruises in the Weddell sea, Antarctica, during winter/spring 2013 provided the first direct observations of sea salt aerosol production from blowing snow above sea ice, thereby validating a model hypothesis to account for winter time sea salt maxima in ~~polar regions not explained otherwise~~the Antarctic. Blowing or drifting snow ~~always~~ often lead to increases in aerosol during and after storms consisting mostly of sea salt inferred from the concurrent increase in atmospheric sodium concentrations. Observed aerosol gradients suggest that net production of SSA takes place near the top of the atmospheric layer containing suspended snow particles at RH_{ice}<100 %. Within the blowing snow layer SSA net production is suppressed due to saturated conditions and scavenging by snow particles which is efficient at the warmer temperatures encountered during storms.

~~During storms average number and volume spectra of SSA over the sea ice increased significantly above background concentrations but remained below those over the open ocean. However, the observed relative increase of SSA concentrations with wind speed suggests that on average the corresponding aerosol mass flux during storms was equal or larger above sea ice than above the open ocean, demonstrating the importance of the blowing snow source for atmospheric sea salt aerosol in winter and early spring. Lower SSA concentrations above sea ice relative to the open ocean may have been due to a combination of low storm frequency and low snow salinities in the area sampled. Upscaling of the SSA source flux of Weddell sea ice and atmospheric modelling similar to the study of Levine et al. (2014) are needed to address this issue as well as implications for the sea ice proxy interpretation.~~

The main evidence for the sea ice origin of the sea salt aerosol observed comes from its chemical fractionation: for the first time we show that snow on sea ice is depleted in ~~sulphate~~ sulfate relative to sodium with respect to sea water. Similar depletion observed in the aerosol above the sea ice observed in the ~0.3-6 µm range suggests that most sea salt originated from snow on sea ice with possibly minor contributions from frost flowers, and not the open ocean or leads, e.g. ~~on average ~93~~based on median values >90 % during the 8 June and 12 August 2013 period. A temporally very close association of snow particle and aerosol number density dynamics together with the far distance to the open ocean further support that the local blowing snow source of SSA dominates over advection. A mass budget calculation shows that even snow with low salinity (<1 psu) can account for observed increases of sea salt from blowing snow. Significant increases of sub-micron aerosol are also consistent with sublimation of snow particles of low salinity (<1 psu) generating very small aerosol particles, potentially down to nm size if all water ice is lost. The degree of water ice loss from particles has implications for particle surface area and heterogeneous chemistry, which future experiments will need to address.

It is found that SSA ~~originating from~~ further aloft produced by blowing snow is ~~an important~~ depleted in bromide suggesting it is a source of reactive bromine to the atmosphere even in winter, which then can contribute to ozone depletion events. On average snow on sea ice and blowing snow showed no or small depletion of bromide relative to sodium with respect to sea water, whereas aerosol at ~~29~~2 m was enriched ~~suggesting that~~ and at 29 m depleted suggesting that significant bromine loss takes place ~~preferentially~~ in the aerosol phase between 2 and 29 m above the sea ice surface.

During storms average size spectra of SSA number densities over the sea ice show a significant increase above background concentrations for particle diameters <2 µm, with sub-micron particles reaching levels similar to those observed above the open ocean. The relative increase of SSA concentrations with wind speed suggests that on average the corresponding aerosol mass flux during storms was equal or larger above sea ice than above the open ocean, demonstrating the importance of the blowing snow source for atmospheric sea salt aerosol in winter and early spring. Lower SSA concentrations above sea ice relative to the open ocean may have been due to a combination of low storm frequency and low snow salinities in the area sampled. Upscaling of the SSA source flux of Weddell sea ice and atmospheric modelling similar to the study of Levine et al. (2014) are needed to address this issue as well as implications for the sea ice proxy interpretation.

Evaluation of the current model mechanism for sea salt aerosol production from blowing snow ~~(Yang et al., 2008; ?)~~ (Yang et al., 2008, 2019) showed that the model parameterisations used can generally be applied to snow on sea ice:

- estimates of snow drift threshold wind speed based on the empirical model of (Li and Pomeroy, 1997) that depends on temperature only agreed well with observations above the low-salinity snow encountered during this study. However, temperature alone may not be a good predictor if the surface snow is very saline, implying a relatively larger liquid fraction at a given temperature and therefore increased snow crystal cohesion and drift threshold wind speed. Further measurements above a variety of sea ice surfaces will be needed to address this issue.

- modelled saltation layer snow mixing ratios exceed absolute values by a factor of 10, but the relative changes match the observations, and so the impact on calculating the SSA mass flux from blowing snow Q_{SSA} is minor

- retrieval of mean particle diameter $\overline{d_p}$ and shape parameter α from fitting a 2-parameter gamma distribution to observed snow particle size spectra is robust, even when data exclude very small snow particles (d_p<46 µm); a recommend range of $\overline{d_p}$ and α values is given for blowing snow episodes. Relative contributions from precipitating snow to total suspended snow particles become more important a few tens of meters above the sea ice surface and need to be accounted for when interpreting snow particle size spectra. Future work needs to fill the observational gap (d_p 12-46 µm)between very small snow particles and aerosol due to the importance for the formation of sub-micron aerosol and associated climate impacts.

- ~~to a first order it is the distance to~~ at a given salt migration distance from the sea ice surface ~~, i.e.~~ it is total snowpack depth, that determines the salinity probability distribution of snow on sea ice consistent with previous studies (Domine et al., 2004; Massom et al., 2001). FYI can therefore be distinguished from MYI based on snow salinity, because snow on FYI is in general more shallow than on MYI. Secondary factors potentially increasing the difference in salinity between FYI and MYI and identified previously (e.g. Massom et al., 2001) are more frequent flooding of FYI with seawater due to negative freeboard and MYI desalination due to brine drainage. Snow depth retrieved from satellites may allow estimating snow salinity in the absence of ground-based measurements.

Snow salinity was shown to be a sensitive model parameter ~~(?)~~(Yang et al., 2019), which implies that SSA production above FYI should be larger than above MYI. Therefore, shifts in the ratio of FYI and MYI over time are expected to contribute to the variability of SSA in ice cores, which both represents an opportunity and a challenge for the quantitative interpretation of the sea salt sea ice proxy. ~~It is expected that similar processes take place in the Arctic regions~~Similar in situ measurements are needed to corroborate the importance of sea salt aerosol production from blowing snow also in the Arctic to validate atmospheric and ice core models (e.g. Rhodes et al., 2017; Huang and Jaeglé, 2017).

Data availability. All data are stored in the UK Polar Data Centre, Natural Environment Research Council, UK Research and Innovation (https://doi.org/10.5285/853dd176-bc7a-48d4-a6be-33bcc0f17eeb, Frey et al., 2019).

Author contributions. MF, EW, AJ and PA designed the field experiments. MF, DJ and MNM carried out the field measurements. SN and IB contributed to CLASP, KN and PA to SPC instruments and data interpretation. MF prepared the manuscript and led the data interpretation with contributions from all co-authors.

Competing interests. The authors declare that they have no conflict of interest.

Acknowledgements. We are grateful to the Alfred Wegener Institute for Polar and Marine Research to enable our participation in expedition ANT-XXIX/6 and ANT-XXIX/7, cruise leader P. Lemke, captain and crew of *RV Polarstern*, and participating scientists for providing scientific and logistical support. We gratefully acknowledge financial support from the Natural Environment Research Council (UK) through the BLOWSEA project (NE/J023051/1 and NE/J020303/1). We thank E. Ludlow and R. Tuckwell for support of the IC analysis at BAS, J. Klepacki, A. Webb (BAS) and S. Rodwell (SAMS) for invaluable engineering support, K.C. Leonard for helpful discussions and lending the rocket traps, T. Phillips for generating the Antarctic sea ice map, and LL & MM for continued inspiration.

References

Abbatt, J. P. D., Thomas, J. L., Abrahamsson, K., Boxe, C., Granfors, A., Jones, A. E., King, M. D., Saiz-Lopez, A., Shepson, P. B., Sodeau, J., Toohey, D. W., Toubin, C., von Glasow, R., Wren, S. N., and Yang, X.: Halogen activation via interactions with environmental ice and snow in the polar lower troposphere and other regions, Atmos. Chem. Phys., 12, 6237–6271, doi:10.5194/acp-12-6237-2012, 2012.

Abrahamsson, K., Granfors, A., Ahnoff, M., Cuevas, C. A., and Saiz-Lopez, A.: Organic bromine compounds produced in sea ice in Antarctic winter, Nature Communications, 9, 5291, doi:10.1038/s41467-018-07062-8, 2018.

Abram, N. J., Wolff, E. W., and Curran, M. A.: A review of sea ice proxy information from polar ice cores, Quaternary Science Reviews, 79, 168–183, doi:10.1016/j.quascirev.2013.01.011, 2013.

Anderson, P. S.: A Method for Rescaling Humidity Sensors at Temperatures Well below Freezing, J. Atmos. Ocean Tech., 11, 1388–1391, doi:10.1175/1520-0426(1994)011<1388:AMFRHS>2.0.CO;2, 1994.

Arndt, S. and Paul, S.: Variability of winter snow properties on different spatial scales in the Weddell Sea, J. Geophys. Res., doi:10.1029/2018JC014447, 2018.

Boucher, O., et al., IPCC, 5^{th} Assess. Rep. - WG1, Ch.7, 571—658 (2013).

Budd, W.: The drifting of non-uniform snow particles, in: Studies in Antarctic Meteorology, edited by Rubin, M. J., vol. 9 of Antarct. Res. Ser., pp. 59–70, American Geophysical Union, 1966.

Butler, B. M., Papadimitriou, S., Santoro, A., and Kennedy, H.: Mirabilite solubility in equilibrium sea ice brines, Geochimica et Cosmochimica Acta, 182, 40 – 54, doi:10.1016/j.gca.2016.03.008, 2016.

Choi, S., Theys, N., Salawitch, R. J., Wales, P. A., Joiner, J., Canty, T. P., Chance, K., Suleiman, R. M., Palm, S. P., Cullather, R. I., Darmenov, A. S., Silva, A., Kurosu, T. P., Hendrick, F., and Van Roozendael, M.: Link Between Arctic Tropospheric BrO Explosion Observed From Space and Sea-Salt Aerosols From Blowing Snow Investigated Using Ozone Monitoring Instrument BrO Data and GEOS-5 Data Assimilation System, J. Geophys. Res., 123, 6954–6983, doi:10.1029/2017JD026889, 2018.

Comiso, J. C. 2017. Bootstrap Sea Ice Concentrations from Nimbus-7 SMMR and DMSP SSM/I-SSMIS, Version 3, Boulder, Colorado USA. NASA National Snow and Ice Data Center Distributed Active Archive Center, doi:10.5067/7Q8HCCWS4I0R, accessed on 22 February 2018.

de Leeuw, G., Andreas, E. L., Anguelova, M. D., Fairall, C. W., Lewis, E. R., O'Dowd, C., Schulz, M., and Schwartz, S. E.: Production flux of sea spray aerosol, Rev. Geophys., 49, doi:10.1029/2010RG000349, 2011.

DeMott, P. J., Hill, T. C. J., McCluskey, C. S., Prather, K. A., Collins, D. B., Sullivan, R. C., Ruppel, M. J., Mason, R. H., Irish, V. E., Lee, T., Hwang, C. Y., Rhee, T. S., Snider, J. R., McMeeking, G. R., Dhaniyala, S., Lewis, E. R., Wentzell, J. J. B., Abbatt, J., Lee, C., Sultana, C. M., Ault, A. P., Axson, J. L., Diaz Martinez, M., Venero, I., Santos-Figueroa, G., Stokes, M. D., Deane, G. B., Mayol-Bracero, O. L., Grassian, V. H., Bertram, T. H., Bertram, A. K., Moffett, B. F., and Franc, G. D.: Sea spray aerosol as a unique source of ice nucleating particles, Proc. Natl. Acad. Sci., 113, 5797–5803, doi:10.1073/pnas.1514034112, 2016.

Déry, S. and Yau, M. K.: Simulation Of Blowing Snow In The Canadian Arctic Using A Double-Moment Model, 99, 297–316, doi:10.1023/A:1018965008049, 2001.

Déry, S. J. and Yau, M.: A Bulk Blowing Snow Model, Bound.-Lay. Meteorol., 93, 237–251, doi:10.1023/A:1002065615856,1999.

Dominé, F., Sparapani, R., Ianniello, A., and Beine, H. J.: The origin of sea salt in snow on Arctic sea ice and in coastal regions, Atmos. Chem. Phys., 4, 2259–2271, doi:10.5194/acp-4-2259-2004, 2004.

Dover, S. E.: Numerical Modelling of Blowing Snow, Ph.D. thesis, 233 pages, University of Leeds, Leeds, 1993.

Flato, G., et al., IPCC, 5^{th} Assess. Rep. - WG1, Ch.9, 741—866, 2013.

Frey, M.: Salinity profiles of snow on sea ice in the Weddell Sea (Antarctica) during austral winter 2013, Tech. rep., NERC - Polar Data Centre, Cambridge, UK, http://doi.org/b9c6, 2017.

Frey, M. M., Bales, R. C., and McConnell, J. R.: Climate sensitivity of the century-scale hydrogen peroxide (H_2O_2) record preserved in 23 ice cores from West Antarctica, J. Geophys. Res., 111, doi:10.1029/2005JD006816, 2006.

Giordano, M. R., Kalnajs, L. E., Goetz, J. D., Avery, A. M., Katz, E., May, N. W., Leemon, A., Mattson, C., Pratt, K. A., and DeCarlo, P. F.: The importance of blowing snow to halogen-containing aerosol in coastal Antarctica: influence of source region versus wind speed, Atmos. Chem. Phys., 18, 16 689–16 711, doi:10.5194/acp-18-16689-2018, 2018.

Hara, K., Osada, K., Yabuki, M., Takashima, H., Theys, N., and Yamanouchi, T.: Important contributions of sea-salt aerosols to atmospheric bromine cycle in the Antarctic coasts, Scientific Reports, 8, 13 852, doi:10.1038/s41598-018-32287-4, 2018.

Hill, M. K., Brooks, B. J., Norris, S. J., Smith, M. H., Brooks, I. M., and de Leeuw, G.: A Compact Lightweight Aerosol Spectrometer Probe (CLASP), J. Atmos. Ocean Tech., 25, 1996–2006, doi:10.1175/2008JTECHA1051.1, 2008.

Hill, K. D., T. M. D. and Woods, D. J.: The extension of the Practical Salinity Scale 1978 to low salinities,, IEEE J. Oceanic Eng., 11, 109–112, 1986.

Huang, J. and Jaeglé, L.: Wintertime enhancements of sea salt aerosol in polar regions consistent with a sea ice source from blowing snow, Atmos. Chem. Phys., 17, 3699–3712, doi:10.5194/acp-17-3699-2017, 2017.

Jacobson, M. Z.: Fundamentals of Atmospheric Modeling, Cambridge University Press, Cambridge, United Kingdom, 2005.

Jones, A. E., Wolff, E. W., Ames, D., Bauguitte, S. J.-B., Clemitshaw, K. C., Fleming, Z., Mills, G. P., Saiz-Lopez, A., Salmon, R. A., Sturges, W. T., and Worton, D. R.: The multi-seasonal NO_y budget in coastal Antarctica and its link with surface snow and ice core nitrate: results from the CHABLIS campaign, Atmos. Chem. Phys., 11(17), 9271–9285, doi:10.5194/acp-11-9271-2011, 2011.

Jones, A. E., Anderson, P. S., Begoin, M., Brough, N., Hutterli, M. A., Marshall, G. J., Richter, A., Roscoe, H. K., and Wolff, E. W.: BrO, blizzards, and drivers of polar tropospheric ozone depletion events, Atmos. Chem. Phys., 9, 4639–4652, 2009.

Jourdain, B., Preunkert, S., Cerri, O., Castebrunet, H., Udisti, R., and Legrand, M.: Year-round record of sizesegregated aerosol composition in central Antarctica (Concordia station): Implications for the degree of fractionation of sea-salt particles, J. Geophys. Res., 113, doi:10.1029/2007JD009584, 2008.

Kaimal, J. and Finnigan, J. J.: Atmospheric Boundary Layer Flows, Oxford University Press, Oxford, United Kingdom, 1994.

Kalnajs, L. E., Avallone, L. M., and Toohey, D. W.: Correlated measurements of ozone and particulates in the Ross Island region, Antarctica, Geophys. Res. Lett., 40, 6319–6323, doi:10.1002/2013GL058422, 2013.

King, J. C., Anderson, P. S., and Mann, G. W.: The seasonal cycle of sublimation at Halley, Antarctica, J. Glaciol., 47, 1–8, 2001.

King, J. C., Anderson, P. S., Smith, M. C., and Mobbs, S. D.: The surface energy and mass balance at Halley, Antarctica during winter, J. Geophys. Res., 101, 19 119, 1996.

King, J. C. and Anderson, P. S.: Heat and water vapor fluxes and scalar roughness lengths over an Antarctic ice shelf, Bound.-Lay. Meteorol., 69, 101–121, 1994.

Legrand, M., Yang, X., Preunkert, S., and Theys, N.: Year-round records of sea salt, gaseous, and particulate inorganic bromine in the atmospheric boundary layer at coastal (Dumont d'Urville) and central (Concordia) East Antarctic sites, J. Geophys. Res., doi:10.1002/2015JD024066, 2016.

Legrand, M., Preunkert, S., Wolff, E., Weller, R., Jourdain, B., and Wagenbach, D.: Year-round records of bulk and size-segregated aerosol composition in central Antarctica (Concordia site) – Part 1: Fractionation of sea-salt particles, Atmos. Chem. Phys., 17, 14 039–14 054, doi:10.5194/acp-17-14039-2017, 2017.

Lemke, P.: The Expedition of the Research Vessel Polarstern to the Antarctic in 2013 (ANT-XXIX/6), Reports on Polar and Marine Research, 679, 154 pp., doi:10.2312/BzPM-0679-2014, 2014.

Levine, J. G., Yang, X., Jones, A. E., and Wolff, E. W.: Sea salt as an ice core proxy for past sea ice extent: A process-based model study, J. Geophys. Res., 119, doi:10.1002/2013JD020925, 2014.

Li, L. and Pomeroy, J. W.: Estimates of Threshold Wind Speeds for Snow Transport Using Meteorological Data, J. Appl. Meteorol., 36, 205–213, doi:10.1175/1520-0450(1997)036<0205:EOTWSF>2.0.CO;2, 1997.

Lieb-Lappen, R. M. and Obbard, R. W.: The role of blowing snow in the activation of bromine over first-year Antarctic sea ice, Atmos. Chem. Phys., 15, 7537–7545, doi:10.5194/acp-15-7537-2015, 2015.

Long, M. S., Keene, W. C., Easter, R. C., Sander, R., Liu, X., Kerkweg, A., and Erickson, D.: Sensitivity of tropospheric chemical composition to halogen-radical chemistry using a fully coupled size-resolved multiphase-chemistry global climate system: halogen distributions, aerosol composition, and sensitivity of climate-relevant gases, Atmos. Chem. Phys., 14, 3397–3425, doi:10.5194/acp-14-3397-2014, 2014.

Mann, G. W., Carslaw, K. S., Reddington, C. L., Pringle, K. J., Schulz, M., Asmi, A., Spracklen, D. V., Ridley, D. A., Woodhouse, M. T., Lee, L. A., Zhang, K., Ghan, S. J., Easter, R. C., Liu, X., Stier, P., Lee, Y. H., Adams, P. J., Tost, H., Lelieveld, J., Bauer, S. E., Tsigaridis, K., van Noije, T. P. C., Strunk, A., Vignati, E., Bellouin, N., Dalvi, M., Johnson, C. E., Bergman, T., Kokkola, H., von Salzen, K., Yu, F., Luo, G., Petzold, A., Heintzenberg, J., Clarke, A., Ogren, J. A., Gras, J., Baltensperger, U., Kaminski, U., Jennings, S. G., O'Dowd, C. D., Harrison, R. M., Beddows, D. C. S., Kulmala, M., Viisanen, Y., Ulevicius, V., Mihalopoulos, N., Zdimal, V., Fiebig, M., Hansson, H.-C., Swietlicki, E., and Henzing, J. S.: Intercomparison and evaluation of global aerosol microphysical properties among AeroCom models of a range of complexity, Atmos. Chem. Phys., 14, 4679–4713, doi:10.5194/acp-14-4679-2014, 2014.

Mann, G., Anderson, P., and Mobbs, S.: Profile measurements of blowing snow at Halley, Antarctica, J. Geophys. Res., 105, 24 491–24 508, doi:10.1029/2000JD900247, 2000.

Massom, R. A., Eicken, H., Hass, C., Jeffries, M. O., Drinkwater, M. R., Sturm, M., Worby, A. P., Wu, X., Lytle, V. I., Ushio, S., Morris, K., Reid, P. A., Warren, S. G., and Allison, I.: Snow on Antarctic Sea Ice, Rev. Geophys., 39, 413–445, doi:10.1029/2000RG000085, 2001.

May, N. W., Quinn, P. K., McNamara, S. M., and Pratt, K. A.: Multiyear study of the dependence of sea salt aerosol on wind speed and sea ice conditions in the coastal Arctic, J. Geophys. Res., 121, 9208–9219, doi:10.1002/2016JD025273, 2016JD025273, 2016.

McDougall, T. and Barker, P.: Getting started with TEOS-10 and the Gibbs Seawater (GSW) Oceanographic Toolbox, Tech. Rep. ISBN 978-0-646-55621-5, SCOR/IAPSO WG127, http://www.teos-10.org, 2011.

Meyer, B.: The Expedition of the Research Vessel Polarstern to the Antarctic in 2013 (ANT-XXIX/7), Reports on Polar and Marine Research, 674, 130 pp., doi:10.2312/BzPM-0674-2014, 2014.

Millero, F. J., Feistel, R., Wright, D. G., and McDougall, T. J.: The composition of standard seawater and the definition of the reference-composition salinity scale, Deep-Sea Res. Part I-Oceanographic Research Papers, 55, 50–72, 2008.

Nilsson, E. D., Rannik, Ü., Swietlicki, E., Leck, C., Aalto, P. P., Zhou, J., and Norman, M.: Turbulent aerosol fluxes over the Arctic Ocean: 2. Wind-driven sources from the sea, J. Geophys. Res., 106, 32 139–32 154, doi:10.1029/2000JD900747, 2001.

Nishimura, K., Yokoyama, C., Ito, Y., Nemoto, M., Naaim-Bouvet, F., Bellot, H. and Fujita, K. (2014), Snow particle speeds in drifting snow, J. Geophys. Res. Atmos., 119, doi:10.1002/2014JD021686.

Nishimura, K. and Nemoto, M.: Blowing snow at Mizuho station, Antarctica, Phil. Trans. R. Soc. A, 363, 1647–1662, doi:10.1098/rsta.2005.1599, 2005.

Norris, S. J., Brooks, I. M., Hill, M. K., Brooks, B. J., Smith, M. H., and Sproson, D. A. J.: Eddy covariance measurements of the sea spray aerosol flux over the open ocean, J. Geophys. Res., 117, doi:10.1029/2011JD016549, 2012.

Norris, S. J., Brooks, I. M., de Leeuw, G., Smith, M. H., Moerman, M., and Lingard, J. J. N.: Eddy covariance measurements of sea spray particles over the Atlantic Ocean, Atmos. Chem. Phys., 8, 555–563, doi:10.5194/acp-8-555-2008, 2008.

O'Dowd, C. D., Smith, M. H., Consterdine, I. E., and Lowe, J. A.: Marine aerosol, sea-salt, and the marine sulphur cycle: a short review, Atmos. Environ., 31, 73 – 80, doi:10.1016/S1352-2310(96)00106-9, 1997.

Oum, K. W., Lakin, M. J., and Finlayson-Pitts, B. J.: Bromine activation in the troposphere by the dark reaction of O_3 with seawater ice, Geophys. Res. Lett., 25, 3923–3926, doi:10.1029/1998GL900078, 1998.

Pratt, K. A., Custard, K. D., Shepson, P. B., Douglas, T. A., Pohler, D., General, S., Zielcke, J., Simpson, W. R., Platt, U., Tanner, D. J., Huey, G., Carlsen, M., and Stirm, B. H.: Photochemical production of molecular bromine in Arctic surface snowpacks, Nature Geosci, doi:10.1038/ngeo1779, 2013.

M. Rankin, A. and W. Wolff, E.: A year-long record of size-segregated aerosol composition at Halley, Antartica, J. Geophys. Res., 108, doi:10.1029/2003JD003993, 2003.

Rankin, A. M., Auld, V., and Wolff, E. W.: Frost flowers as a source of fractionated sea salt aerosol in the polar regions, Geophys. Res. Lett., 27, 3469–3472, doi:10.1029/2000GL011771, 2000.

Rhodes, R. H., Yang, X., Wolff, E. W., McConnell, J. R., and Frey, M. M.: Sea ice as a source of sea salt aerosol to Greenland ice cores: a model-based study, Atmos. Chem. Phys., 17, 9417–9433, doi:10.5194/acp-17-9417-2017, 2017.

Roscoe, H. K., Brooks, B., Jackson, A. V., Smith, M. H., Walker, S. J., Obbard, R. W., and Wolff, E. W.: Frost flowers in the laboratory: Growth, characteristics, aerosol, and the underlying sea ice, J. Geophys. Res., 116, doi:10.1029/2010JD015144, 2011.

Sander, R., Keene, W. C., Pszenny, A. A. P., Arimoto, R., Ayers, G. P., Baboukas, E., Cainey, J. M., Crutzen, P. J., Duce, R. A., Hönninger, G., Huebert, B. J., Maenhaut, W., Mihalopoulos, N., Turekian, V. C., and Van Dingenen, R.: Inorganic bromine in the marine boundary layer: a critical review, Atmos. Chem. Phys., 3, 1301–1336, doi:10.5194/acp-3-1301-2003, 2003.

Schmidt, R. A.: Vertical profiles of wind speed, snow concentration, and humidity in blowing snow, Boundary-Layer Meteorology, 23, 223–246, doi:10.1007/BF00123299, 1982.

Schmidt, R., Meister, R., and Gubler, H.: Comparison of snow drifting measurements at an alpine ridge crest, Cold Regions Science and Technology, 9, 131 – 141, doi:10.1016/0165-232X(84)90005-3, 1984.

Simpson, W. R., Alvarez-Aviles, L., Douglas, T. A., Sturm, M., and Domine, F.: Halogens in the coastal snow pack near Barrow, Alaska: Evidence for active bromine air-snow chemistry during springtime, Geophys. Res. Lett., 32, L04 811, l04811, 2005.

Soo, J.-C., Monaghan, K., Lee, T., Kashon, M., and Harper, M.: Air sampling filtration media: Collection efficiency for respirable size-selective sampling, Aerosol Sci. Technol., 50, 76–87, 2016.

Spolaor, A., Vallelonga, P., Plane, J. M. C., Kehrwald, N., Gabrieli, J., Varin, C., Turetta, C., Cozzi, G., Kumar, R., Boutron, C., and Barbante, C.: Halogen species record Antarctic sea ice extent over glacial-interglacial periods, Atmos. Chem. Phys., 13, 6623–6635, doi:10.5194/acp-13-6623-2013, 2013.

Unesco: Algorithms for computation of fundamental properties of seawater., Unesco technical papers in marine science 44, 53 pp., 1983.

Unesco: The Practical Salinity Scale 1978 and the International Equation of State of Seawater 1980, Unesco technical papers in marine science 36, 25pp, 1981.

Van Dijk, A., Moen, A., and De Bruin, H.: The principles of surface flux physics: theory, practice and description of the ECPACK library, Internal Report 2004/1, Meteorology and Air Quality Group, Wageningen University, Wageningen, The Netherlands, 2006.

Wagenbach, D., Ducroz, F., Mulvaney, R., Keck, L., Minikin, A., Legrand, M., Hall, J. S., and Wolff, E. W.: Sea-salt aerosol in coastal Antarctic regions, J. Geophys. Res., 103, 10 961–10 974, doi:10.1029/97JD01804, 1998.

Weller, R., Wagenbach, D., Legrand, M., Elsässer, C., Tian-Kunze, X., and König-Langlo, G.: Continuous 25-yr aerosol records at coastal Antarctica – I: inter-annual variability of ionic compounds and links to climate indices, Tellus B, 63, 901–919, doi:10.1111/j.1600-0889.2011.00542.x, 2011.

Wolff, E. W., Rankin, A. M., and Rothlisberger, R.: An ice core indicator of Antarctic sea ice production?, Geophys. Res. Lett., 30, 2158, 2003.

Wolff, E. W., Legrand, M. R., and Wagenbach, D.: Coastal Antarctic aerosol and snowfall chemistry, J. Geophys. Res., 103, 10 927–10 934, 1998.

Yang, X., Frey, M. M., Rhodes, R. H., Norris, S. J., Brooks, I. M., Anderson, P. S., Nishimura, K., Jones, A. E., and Wolff, E. W.: Sea salt aerosol production via sublimating wind-blown saline snow particles over ~~sea-ice~~sea ice: parameterizations and relevant ~~micro-physical~~ microphysical mechanisms, Atmos. Chem. Phys.~~Disc., 2018, 1–30~~, 19, 8407–8424, doi:10.5194/~~acp-2018-1080, 2018.~~ acp-19-8407-2019, 2019.

Yang, X., Neděla, V., Runštuk, J., Ondrušková, G., Krausko, J., Vetráková, Ä., and Heger, D.: Evaporating brine from frost flowers with electron microscopy and implications for atmospheric chemistry and sea-salt aerosol formation, Atmos. Chem. Phys., 17, 6291–6303, doi:10.5194/acp-17-6291-2017, 2017.

Yang, X., Pyle, J. A., Cox, R. A., Theys, N., and Van Roozendael, M.: Snow-sourced bromine and its implications for polar tropospheric ozone, Atmos. Chem. Phys., 10, 7763–7773, doi:10.5194/acp-10-7763-2010, 2010.

Yang, X., Pyle, J. A., and Cox, R. A.: Sea salt aerosol production and bromine release: Role of snow on sea ice,, Geophys. Res. Lett.,, 35, doi:10.1029/2008GL034536, 2008.

Table 1. Overview of duration Δt, mean position, distance to the nearest open water Δx and meteorology (ambient temperature T_a, wind speed U_{39m} and wind direction at 39 m) for ice stations S1-S9 during ANT-XXIX/6 (8 June to 12 August 2013).

Station ID[a]	begin – end (UTC)	Δt (hr)	lat / lon (°)	Δx[b] (km)	T_a (°C)	U_{39m} ($\mathrm{m\,s^{-1}}$)	wdir (°)
S1 (PS81/0493-2)	21.06.2013 14:23 – 22.06.2013 00:29	10	-66.445 / 0.116	607	-20.6	8.2	207
S2 (PS81/0496-1)	24.06.2013 08:23 – 24.06.2013 18:18	10	-67.470 / -0.033	721	-12.6	12.5	51
S3 (PS81/0497-1)	26.06.2013 11:20 – 26.06.2013 14:20	3	-68.049 / -0.340	786	-3.4	13.2	19
S4 (PS81/0500-5)	03.07.2013 08:32 – 05.07.2013 20:52	60	-67.909 / -6.762	993	-23.2	5.2	200
S5 (PS81/0503-2)	08.07.2013 11:50 – 08.07.2013 23:39	12	-67.192 / -13.225	913	-14.0	3.8	251
S6 (PS81/0506-1)	11.07.2013 09:38 – 15.07.2013 12:41	99	-67.203 / -23.165	803	-16.8	6.3	167
S7 (PS81/0515-1)	26.07.2013 11:30 – 27.07.2013 00:00	13	-63.415 / -51.246	381	-19.6	13.9	246
S8 (PS81/0517-2)	29.07.2013 12:35 – 02.08.2013 20:24	104	-63.400 / -51.170	379	-25.2	6.8	208
S9 (PS81/0518-3)	04.08.2013 13:44 – 05.08.2013 20:18	31	-62.918 / -53.265	214	-7.8	9.1	273

[a] station ID used in this paper (Figs. 1,2); in brackets *RV Polarstern* nomenclature

[b] horizontal distance to the nearest open water on the ice station longitude based on sea ice extent on 15-June for S1-S3, on 15-July for S4-S7, and 15-Aug for ~~S8~~ S8-S9 (Fig. 1).

Table 2. Overview of observed parameters, instruments used and reported data resolution Δt during ANT-XXIX/6 (ANT6) from 8 June to 12 August 2013, and ANT-XXIX/7 (ANT7) from 14 August to 16 October 2013.

Parameter	Instrument	Δt	ANT6	ANT7
1. Crow's nest (height 29 m)	continuous			
snow particle number density, N_{46-478} (d_p 46-478 µm)	Snow Particle Counter[a]	1 min	✓	✓
aerosol number density, $N_{0.4-12}$ (d_p 0.36-11.62 µm)	~~Compact Light-Weight~~ CLASP[b] ~~Aerosol Spectrometer[b]~~	1 min	✓	
bulk aerosol chemistry ($Na^+, Cl^-, SO_4^{2-}, Br^-$)	Low-Volume Filter Samples	3–48 h	✓	✓
meteorology ($T, p, RH, U, wdir$)	*RV Polarstern* Observatory[c]	1 min	✓	✓
2. Sea ice (height 0.07-2.0 m)	during ice stations			
snow particle number density, N_{46-478} (d_p 46-478 µm)	Snow Particle Counter[a]	1 min	✓	
aerosol number density, $N_{0.4-12}$ (d_p 0.36-11.62 µm)	~~Compact Light-Weight~~ CLASP[b] ~~Aerosol Spectrometer[b]~~	1 min	✓	
bulk aerosol chemistry ($Na^+, Cl^-, SO_4^{2-}, Br^-$)	Low-Volume Filter Samples	3–48 h	✓	
snow chemistry ($Na^+, Cl^-, SO_4^{2-}, Br^-, S_p$)	Ion Chromatography, Salinometer[d]	hr–days	✓	
3-D wind field (u, v, w)	Sonic Anemometer[e]	1 min	✓	
T, RH	Temperature/ Humidity Probe[f]	1 min	✓	

[a] SPC-95, Niigata Electric Co., Ltd. (Nishimura et al., 2014) [b] ~~CLASP~~ Compact Light-Weight Aerosol Spectrometer Probe (CLASP) (Hill et al., 2008; Norris et al., 2008) [c] details at https://spaces.awi.de/confluence/display/PSdevices/Bordwetterwarte [d] SensIon 5, Hach [e] METEK USA-1 [f] VAISALA HMP45

Table 3. Overview of mean aerosol filter procedure blanks and resulting limit of detection (LOD): 1. ultra-high purity (UHP) water, 2. filter extraction, 3. cleaned and unused filter and 4. field blank (see text). Field blank values are used to correct the raw filter ion concentration.

Parameter	Na^+	Cl^-	SO_4^{2-}	Br^-	N[a]
A) Aerosol filter procedure blank					
1. UHP (electric resistivity 18.2 MΩcm) (ng g^{-1})	0.4	4.0	4.5	0.0	85
2. extraction (ng g^{-1})	3.6	4.8	8.6	3.4	14
3. filter (ng g^{-1})	2.3	9.5	8.5	0.0	8
4. field (ng g^{-1})	6.0	16.8	9.1	0.5	10
ratio field blank : sample mean (%)	3.1	4.9	20.3	34.3	183
B) Limit of detection (LOD)					
LOD (ng g^{-1})[b]	13.4	27.9	17.1	1.0	10
LOD (ng m^{-3})[c]	22.6	47.2	29.0	1.7	141
~~LOD ()[d] 35.4 73.9 45.4 2.6 43~~height					

[a]sample size [b]defined as 2×1-σ of the field blank [c]based on crow's nest mean ~~air sample~~ sample air STP-volume (6.4 m^3)~~and interval (12) [d]based on sea ice mean air sample~~ ; mean sample air STP-volume ~~(~~for filters deployed on the sea ice was 3.3 m^3 ~~) and interval (5.6)~~ increasing respective LODs by a factor 1.6

Table 4. Descriptive statistics of the aerosol chemistry during ANT-XXIX/6 (ANT6) and ANT-XXIX/7 (ANT7) with mean and median values weighted by the filter sampling interval. Ion and sea salt concentrations are in units of ng m^{-3}. See section ~~2.4~~ 2.3 for definition of depletion factors DF.

Parameter	ANT6						ANT7		
	at 2 m			at 29 m			at 29 m		
	mean $\pm\sigma$	median	N^a	mean $\pm\sigma$	median	N^a	mean $\pm\sigma$	median	N
sea-salt[b]	707 ±1500	336	43	1253 ±2319	639	106	559 ±486	425	28
Na^+	217 ±460	103	43	384 ±711	196	106	171 ±149	130	28
Cl^-	379 ±765	179	43	656 ±1225	302	106	311 ±282	232	27
SO_4^{2-}	28[c] ±61	19[c]	38	75 ±152	45	84	33 ±30	23[c]	28
Br^-	2.0 ±1.0	1.9	42	1.5[c] ±3.0	0.7[c]	98	0.5[c] ±0.6	0.5[c]	23
$DF_{SO_4^{2-}}$	0.29 ±0.57	0.48	38	0.07 ±0.94	0.29	74	0.12 ±0.60	0.21	27
DF_{Na^+}	-0.08 ±0.29	-0.03	43	~~-0.09~~ -0.46 ±2.29	~~-0.03~~ -0.04	~~99~~ 97	-0.02 ±0.19	-0.01	27
DF_{Br^-}	~~-0.50~~ -1.66 ±1.86	~~-0.41~~ -1.86	~~25~~ 36	~~0.08~~ 0.04 ±0.96	0.37	~~88~~ 89	~~0.27~~ 0.05 ±1.26	~~0.51~~ 0.49	~~22~~

[a] sample size [b] sea salt concentration is derived by multiplying the Na^+ concentration by 3.262 based on the Na^+ mass fraction in reference seawater after Millero et al. (2008)

[c] below the estimated LOD (Table 3)

Table 5. Descriptive statistics of the volume-integrated snow chemistry during ANT-XXIX/6 on first-year sea ice (FYI) at ice stations S1-S6, on multi-year sea ice (MYI) at ice stations S7-9, and for snow layers within 10 cm of the snow surface (TOP10). Ion and sea salt concentrations are in units of µg g^{-1}. See section 2.4 for definition of depletion factors DF.

Parameter	FYI			MYI			TOP10	
	mean $\pm\sigma$	median	N^a	mean $\pm\sigma$	median	N^a	mean $\pm\sigma$	median
snow depth (cm)	20.9 ±8.3	19.0	17	50.0 ±32.2	33.0	7	-	-
S_p (psu)	1.40 ±3.99	0.11	110	0.82 ±4.31	0.02	104	0.31 ±0.90	0.06
sea salt[b]	~~1163~~ 1176 ±3518	~~82~~ 83	~~87~~ 86	~~584~~ 590 ±3157	~~21~~ 22	~~96~~ 95	~~246~~ 249 ±729	~~57~~ 58
Na^+	~~357~~ 361 ±1079	~~25~~ 26	~~87~~ 86	~~179~~ 181 ±968	~~6~~ 7	~~96~~ 95	76 ±223	~~17~~ 18
Cl^-	~~676~~ 680 ±2035	48	~~88~~ 87	~~302~~ 305 ±1842	13	~~99~~ 98	~~143~~ 141 ±415	~~35~~ 34
SO_4^{2-}	61 ±182	~~5.89~~ 6	~~88~~ 87	30 ±166	~~0.87~~ 1	~~99~~ 98	17 ±62	~~2.68~~ 3
Br^-	~~4.25~~ 4.28 ±12.23	0.18	~~86~~ 85	~~1.74~~ 1.76 ±10.92	0.07	~~91~~ 90	1.01 ±3.72	0.12
$DF_{SO_4^{2-}}$	0.19 ±0.41	0.24	86	0.33 ±0.44	0.35	94	0.27 ±0.39	0.27
DF_{Na^+}	~~0.02~~ 0.01 ±0.38	0.06	~~87~~ 86	~~0.04~~ -1.09 ±8.88	~~0.08~~ 0.07	~~91~~ 94	~~0.00~~ -0.11 ±0.99	0.06
DF_{Br^-}	~~-0.12~~ -0.25 ±0.98	0.05	~~81~~ 83	~~0.01~~ -0.28 ±1.16	~~0.00~~ -0.01	~~80~~ 86	~~-0.01~~ -0.21 ±0.99	~~0.05~~ 0.04

[a] sample size [b] sea salt concentration is derived by multiplying the Na^+ concentration by 3.262 based on the Na^+ mass fraction in reference seawater after Millero et al. (2008)

Table 6. Summary of snow particle size distribution properties during blowing snow, i.e. when $U_{10m}>U_t$ (=7.1 m s^{-1} as observed during this study): median, lower ($Q_{0.25}$) and upper quartile ($Q_{0.75}$) of particle mean diameter $\overline{d_p}$ ($=\alpha\,\beta$) in µm and shape parameter α, both derived from fitting a 2-parameter gamma probability density function (Eq. 5) to observations; Δt is total sampling time. Note that the parameter range based on near-surface measurements is representative of blowing snow, whereas that based on measurements at 29 m has additional uncertainties due to precipitating snow (see text).

parameter	median	$Q_{0.25}$	$Q_{0.75}$	Δt (hr)
$\overline{d_p}$ at <0.2 m	129	117	152	47
$\overline{d_p}$ at 29 m[a]	115	95	139	47
$\overline{d_p}$ at 29 m	115	93	147	867
α at <0.2 m	4.8	4.0	11.2	47
α at 29 m[a]	8.0	4.1	11.8	47
α at 29 m	6.4	4.2	11.0	867

[a] including only data when also measurements at <0.2 m are available during blowing snow ($U_{10m}>U_t$).

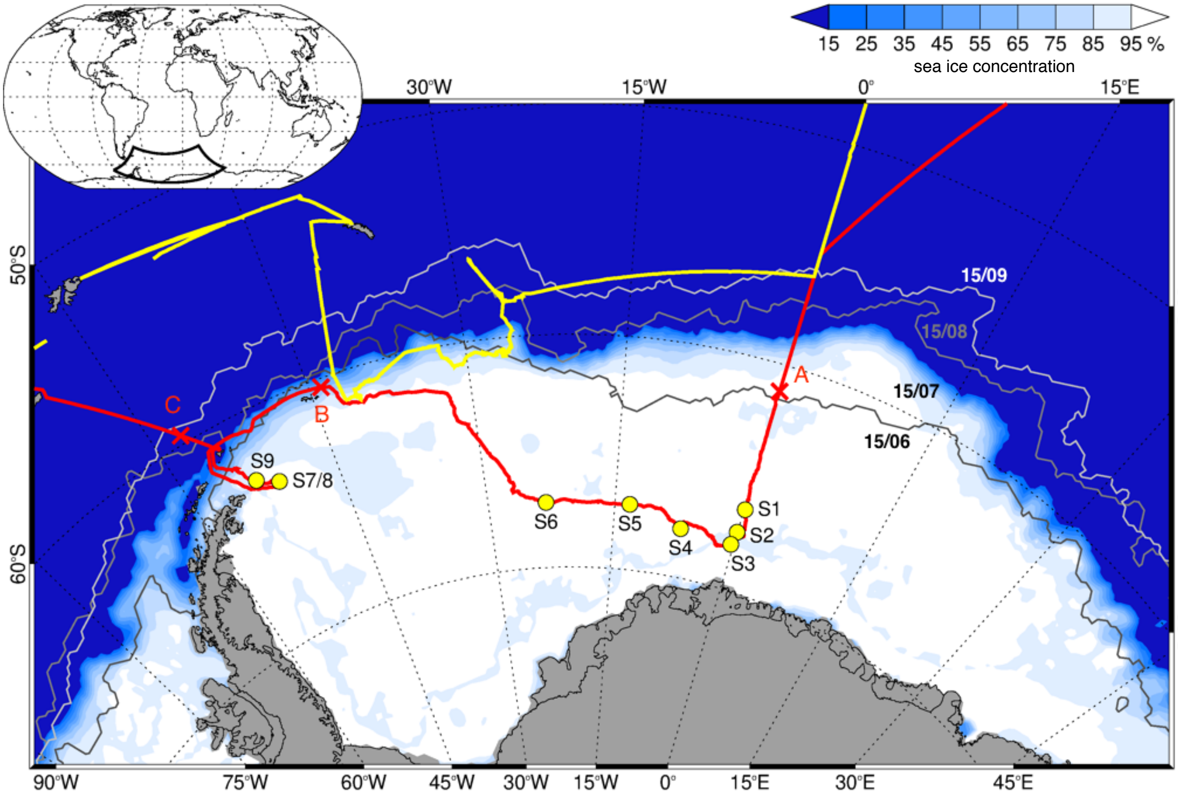

Figure 1. Cruise tracks of *RV Polarstern* in the Weddell Sea for the winter expedition ANT-XXIX/6 from 8 June to 12 August 2013 (red line) and the spring expedition ANT-XXIX/7 from 14 August to 16 October 2013 (yellow line). ~~Symbols~~ Circles indicate the location of ice stations S1–9 (Table 1). Crosses show ship positions when entering the sea ice on 17 June (A), reaching the marginal sea ice zone MIZ on 22 July (B) and returning to the open ocean on 9 August (C). Sea ice concentrations on 15 July 2013 are shown as areas shaded ~~area~~in white to blue, and sea ice extent on 15 June, 15 August and 15 September 2013, respectively, as grey solid lines, all based on Nimbus-7 satellite microwave radiometer measurements (Comiso, 2018).

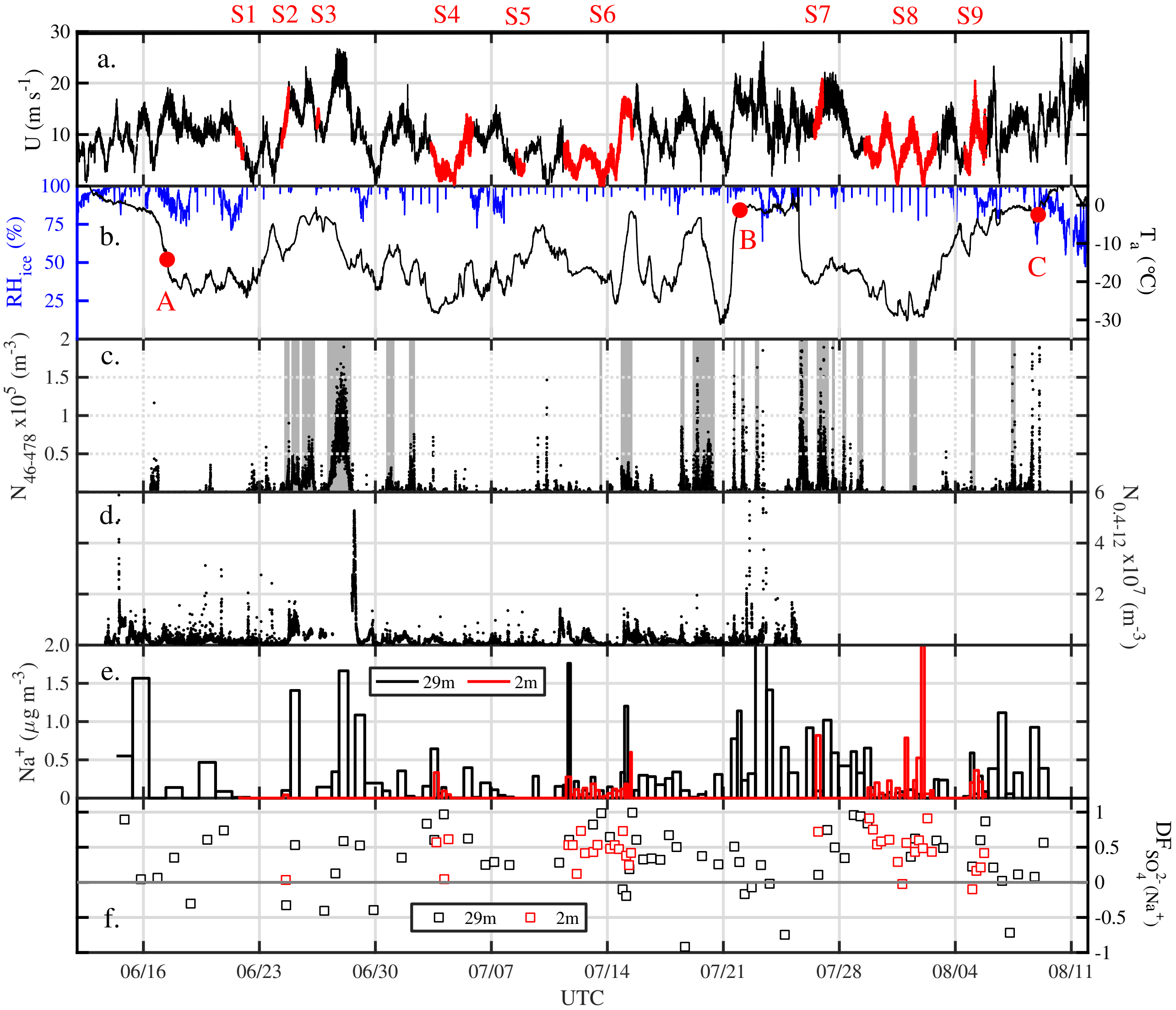

Figure 2. Overview of atmospheric observations in the Weddell Sea from 8 June to 12 August 2013 (ANT-XXIX/6): (a) horizontal wind speed U at 39 m; time periods at ice stations S1-9 (Table 1) are highlighted in red. (b) ambient temperature T_a and relative humidity with respect to ice RH_{ice} at 29 m; red symbols refer to *RV Polarstern* positions shown in Fig. 1, indicating when the ship entered the sea ice on 17 June (A), reached the marginal sea ice zone (MIZ) on 22 July (B) and returned to the open ocean on 9 August (C). (c) total number densities N_{46-478} of airborne snow particles at 29 m with grey shaded areas indicating periods with observed drifting or blowing snow. (d) total number densities $N_{0.4-12}$ of aerosol at 29 m, (e) aerosol Na$^+$ concentrations and (f) ~~sulphate~~ sulfate depletion factor $DF_{\mathrm{SO}_4^{2-}}$, both at 29 m and 2 m, respectively.

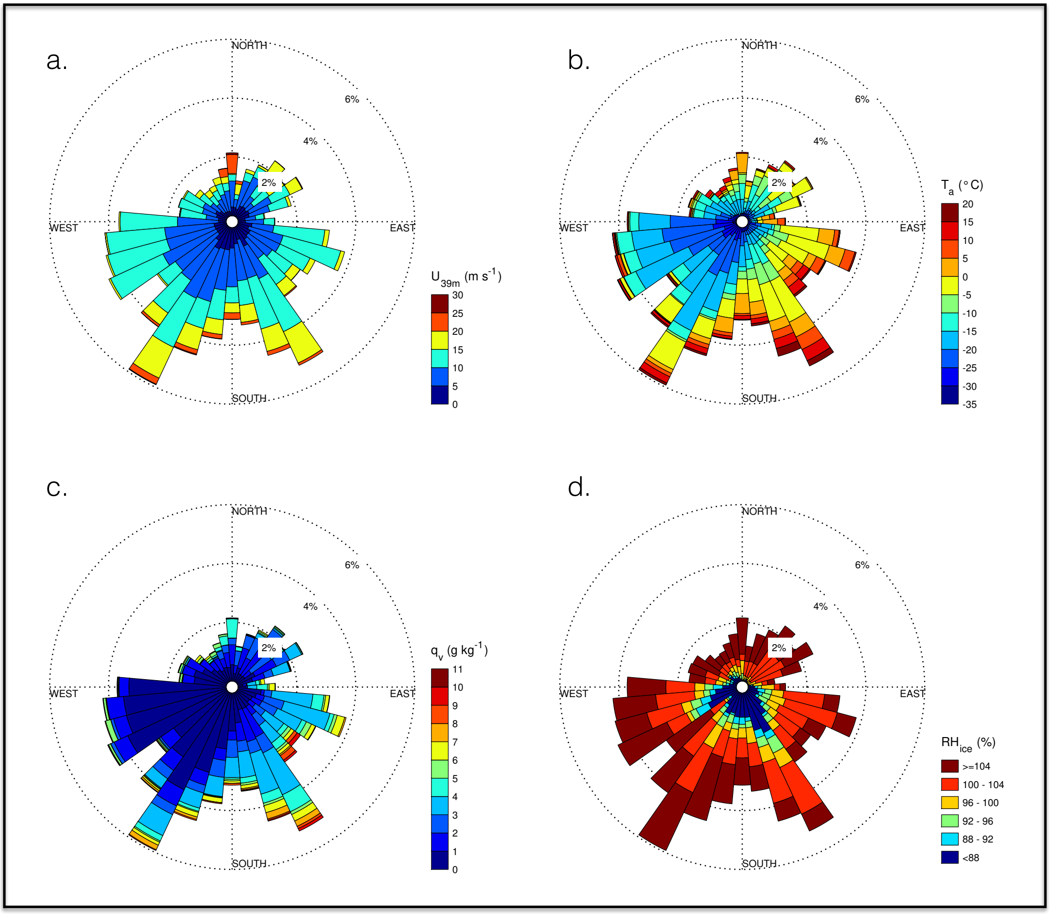

Figure 3. Wind rose plots for the position of *RV Polarstern* during ANT-XXIX/6 (8 June–12 August 2013): (a) horizontal wind speed U at 39 m, (b) ambient temperature T_a, (c) specific humidity of air q_v, and (d) relative humidity with respect to ice RH_{ice} (b–d at 29 m).

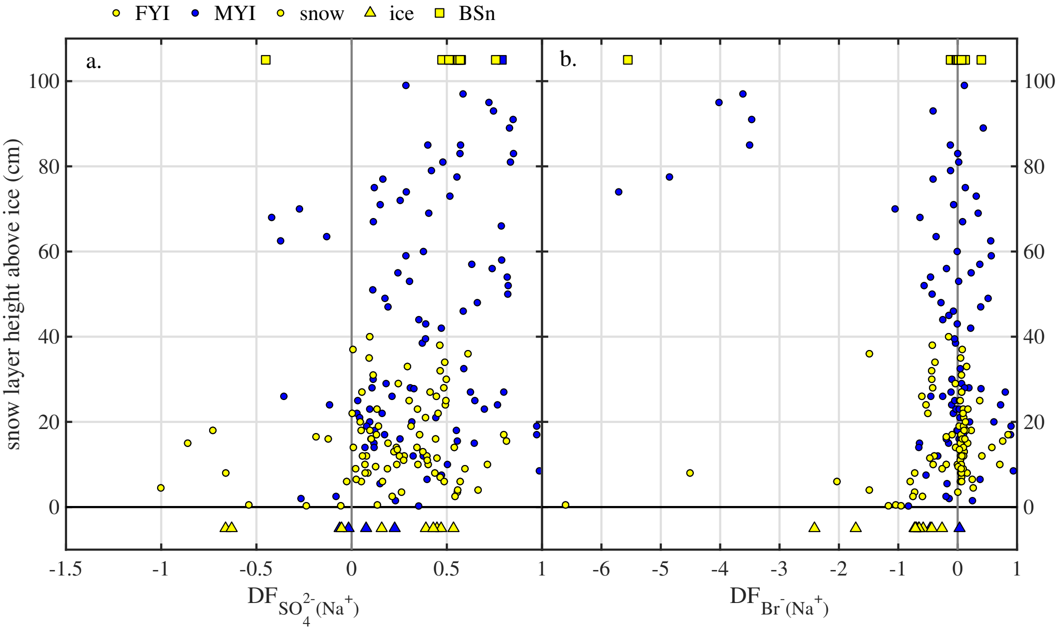

Figure 4. Chemical fractionation of snow on sea ice in the Weddell Sea during austral winter 2013. Panel (a) shows sulfate depletion factors $DF_{SO_4^{2-}}$ (relative to Na^+) of snow on first-year sea ice (FYI, yellow symbols) at ice stations S1-6 and multi-year sea ice (MYI, blue symbols) at ice stations S7-9 in the Weddell Sea as a function of snow layer height above the sea ice surface. For comparison $DF_{SO_4^{2-}}$ of the sea ice surface (triangles) and blowing snow at 1-17 cm above the snowpack (squares) are shown as well. Panel (b) shows the same but for bromide depletion factors DF_{Br^-} (relative to Na^+). The sample statistics are summarised in Table 5.

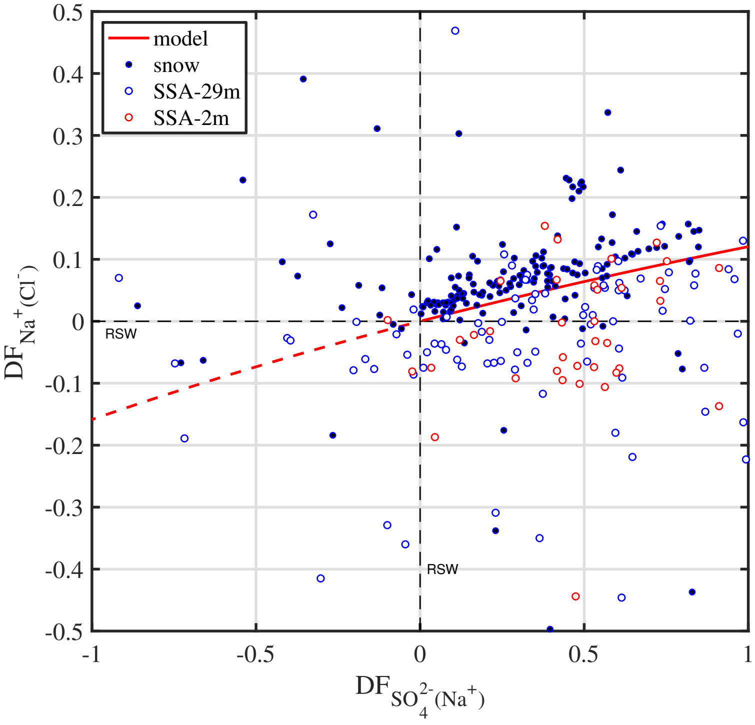

Figure 5. Theoretical relationship between depletion factors of sodium DF_{Na^+} (relative to Cl^-) and of sulfate $DF_{SO_4^{2-}}$ (relative to Na^+) in freezing seawater if mirabilite ($Na_2SO_4 \cdot 10\,H_2O$) is progressively precipitated and instantaneously removed (red line). When all sulfate is removed ($DF_{SO_4^{2-}} = 1$) sodium depletion reaches its theoretical maximum ($DF_{Na^+} = 1.1204$). See section 2.4 for definition of depletion factors DF, which are zero in reference seawater (RSW) (black dashed lines). Data refer to all observations from this study in snow (solid symbols), and aerosol at 2 m and 29 m above the sea ice surface (open symbols).

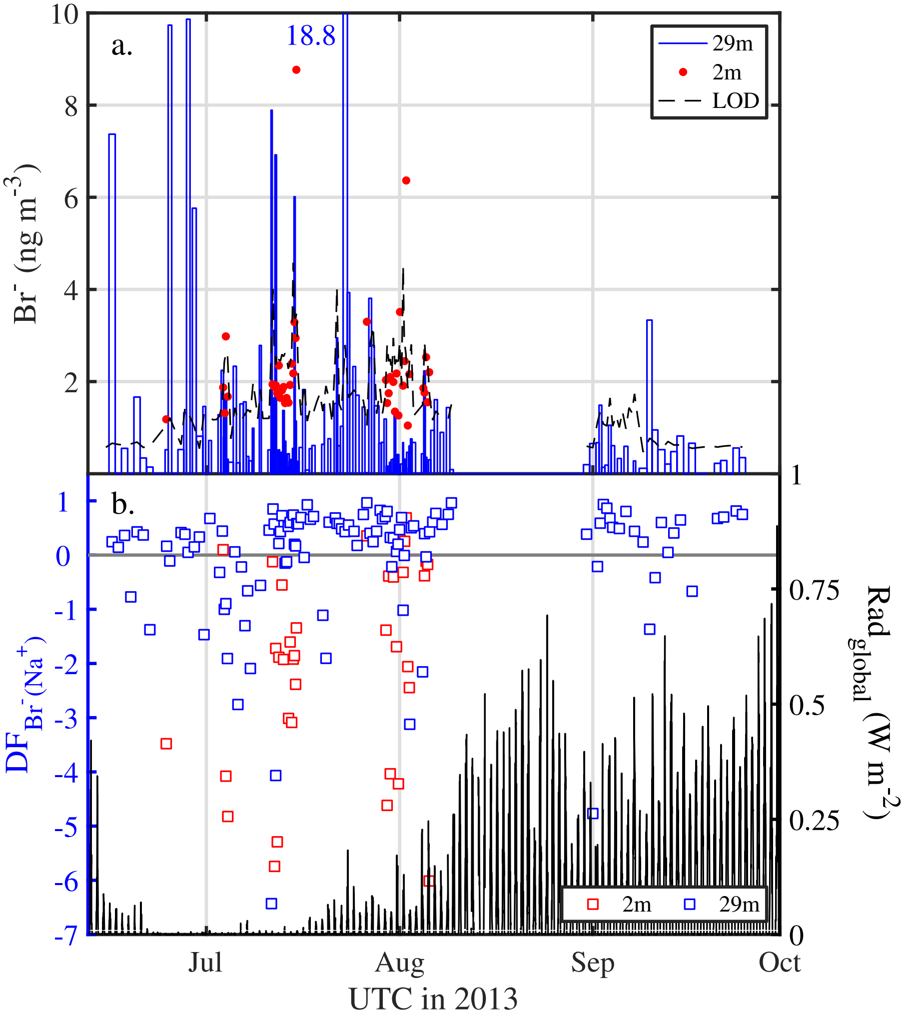

Figure 6. Aerosol bromine chemistry above sea ice observed in the Weddell Sea during austral winter/spring 2013. (a) aerosol Br^- concentrations at 29 and 2 m with the dashed line indicating the theoretical LOD (Table 3); (b) depletion factors of bromide DF_{Br^-} (relative to Na^+) in aerosol at 29 and 2 m and global radiation to indicate light conditions.

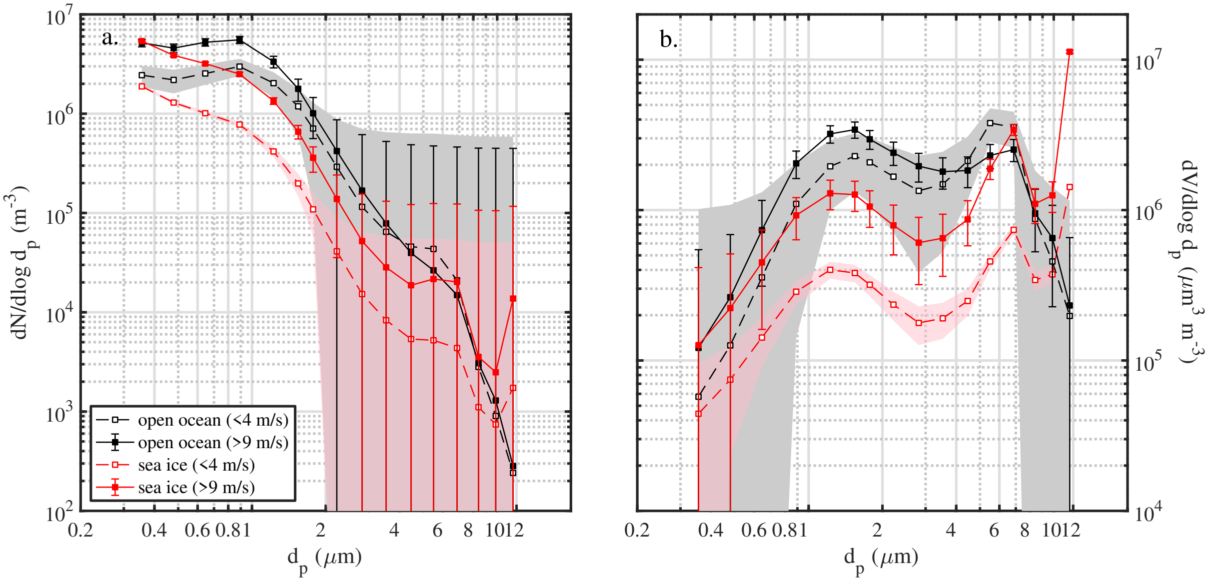

Figure 7. Comparison of mean number distributions (a.) and volume distributions (b.) of aerosol above the open ocean (13 to 16 June 2013) and sea ice in the Weddell Sea (18 June to 21 July 2013) during calm (U_{10m}<4 $\mathrm{m\,s^{-1}}$) and windy (U_{10m}>9 $\mathrm{m\,s^{-1}}$) conditions. Shaded areas and error bars show the standard deviation of the mean during calm and windy conditions, respectively. Data included are observations from 29 m above the sea surface at ambient *RH*.

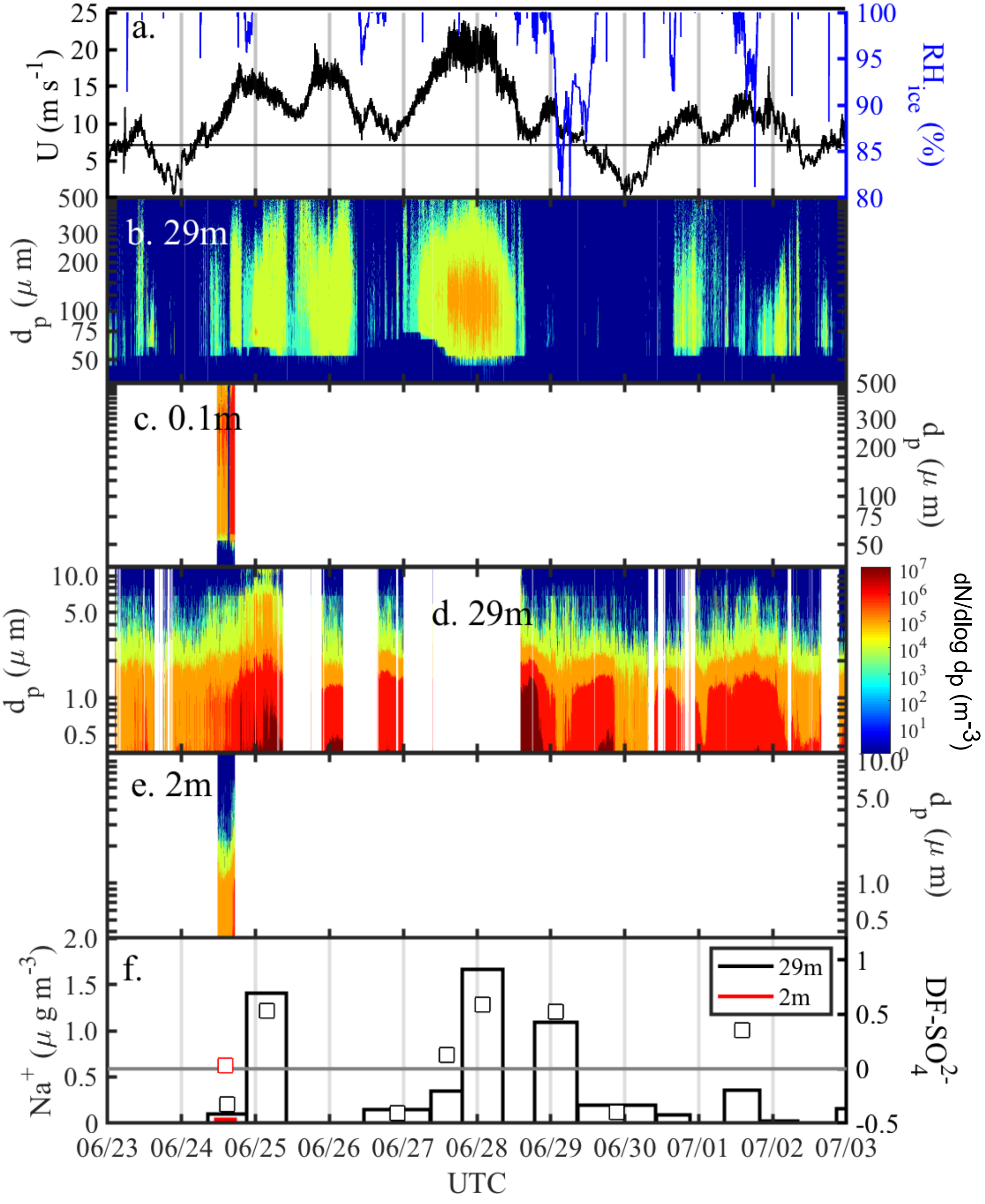

Figure 8. Blowing snow events during the 23 June – ~~2~~ 3 July 2013 period: (a) wind speed U ~~at 39~~extrapolated to 10 m with the horizontal black line showing the snow drift threshold wind speed U_t (section 3.4.1) and ~~and~~ RH_{ice} at 29 m, (b) snow particle size distribution $\mathrm{d}N/\log d_p$ (46 µm< d_p < 478 µm) at 29 m and (c) at 0.1 m; (d) aerosol size distribution $\mathrm{d}N/\log d_p$ (0.36 µm < d_p < 11.62 µm) at 29 m and (e) at 2 m; dark blue shading indicates zero particle counts and white background that no data are available. (f) aerosol Na$^+$ concentrations (vertical bars) and ~~sulphate~~ sulfate depletion factor $DF_{\mathrm{SO}_4^{2-}}$ (open symbols) at 29 m and 2 m, respectively.

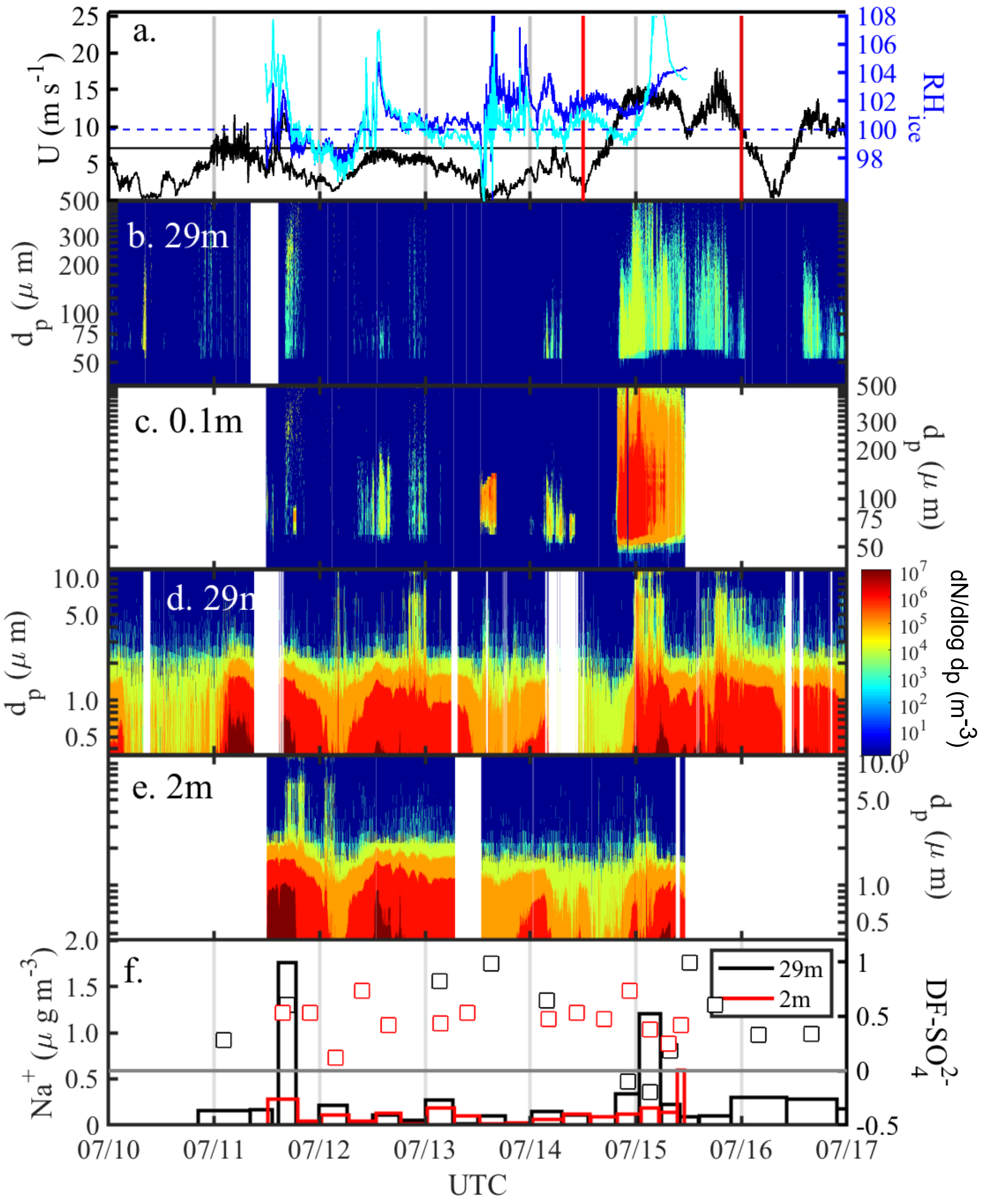

Figure 9. Blowing snow events during the 10–16 July 2013 period: (a) wind speed U ~~at 39~~extrapolated to 10 m with the horizontal black line showing the snow drift threshold wind speed U_t (section 3.4.1) and RH_{ice} at 1.2 and 2.0 m (blue and cyan solid lines, repectively); vertical red lines delimit the period shown in more detail in Fig. 10. (b) snow particle size distribution d$N/\log d_p$ (46 µm $<$ d_p $<$ 478 µm) at 29 m and (c) at 0.1 m; (d) aerosol size distribution d$N/\log d_p$ (0.36 µm $<$ d_p $<$ 11.62 µm) at 29 m and (e) at 2 m; dark blue shading indicates zero particle counts and white background that no data are available; (f) aerosol Na$^+$ concentrations (vertical bars) and ~~sulphate~~ sulfate depletion factor $DF_{\mathrm{SO}_4^{2-}}$ (open symbols) at 29 m and 2 m, respectively.

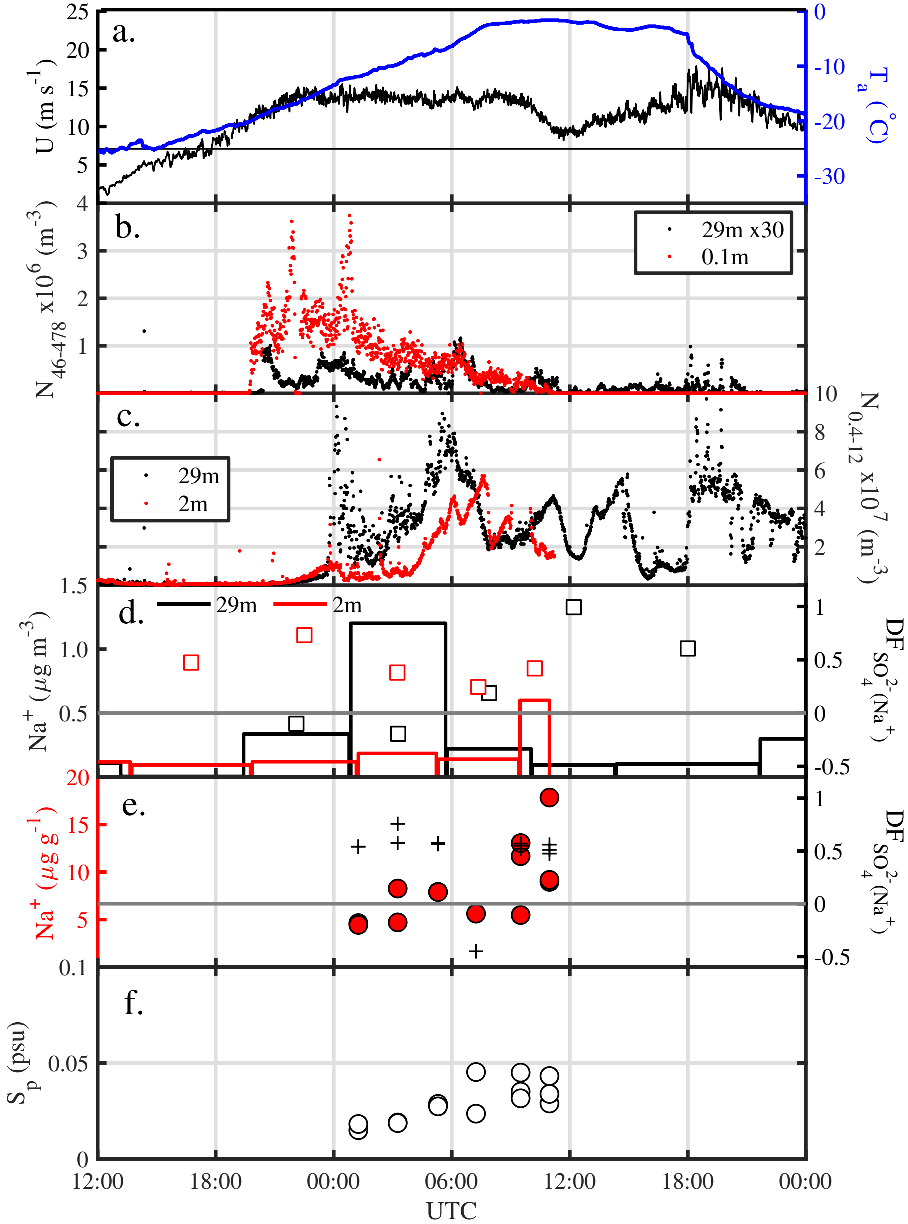

Figure 10. Details of the blowing snow event from 14 to 15 July 2013 (period marked by vertical red lines in Fig. 9a): (a) ambient temperature T_a at 29 m and wind speed U ~~at 39~~extrapolated to 10 m with the horizontal black line showing the snow drift threshold wind speed U_t (see section 3.4.1), (b) total number densities N_{46-478} of airborne snow particles at 29 and 0.1 m, (c) total number densities $N_{0.4-12}$ of aerosol at 29 and 2 m, (d) aerosol Na$^+$ concentrations (vertical bars) and $DF_{\mathrm{SO}_4^{2-}}$ (open symbols) at 29 m and 2 m, respectively; (e) Na$^+$ concentrations, ~~sulphate~~ sulfate depletion factor $DF_{\mathrm{SO}_4^{2-}}$ and (f) salinity S_p in blowing snow collected 1-17 cm above the surface.

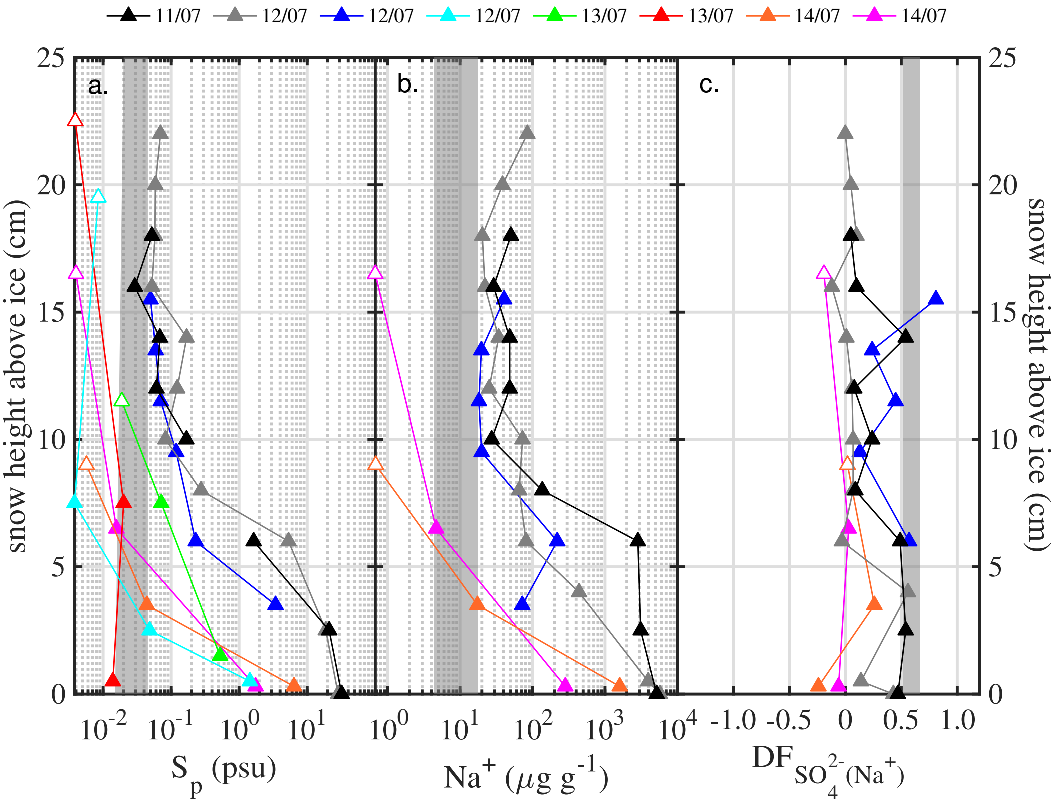

Figure 11. Vertical snowpack profiles sampled at various locations on the ice floe of ice station S6 during the 11–14 July 2013 period (color indicates day of sampling): (a) salinity S_p, (b) Na$^+$ concentrations and (c) ~~sulphate~~ sulfate depletion factor $DF_{\mathrm{SO}_4^{2-}}$ with respect to Na$^+$ as a function of snow height above the sea ice surface. Symbols illustrate averages for snow layers of 2 cm thickness, except those with white face color indicating 0.5-1.0 cm layer thickness. Data points at the top of each profile represent the surface snow layer, thus adding half the snow layer thickness to snow height yields total snowpack depth. Shaded areas illustrate the range of the respective parameter measured in blowing snow on 15 July 2013 (Fig. 10e-f).

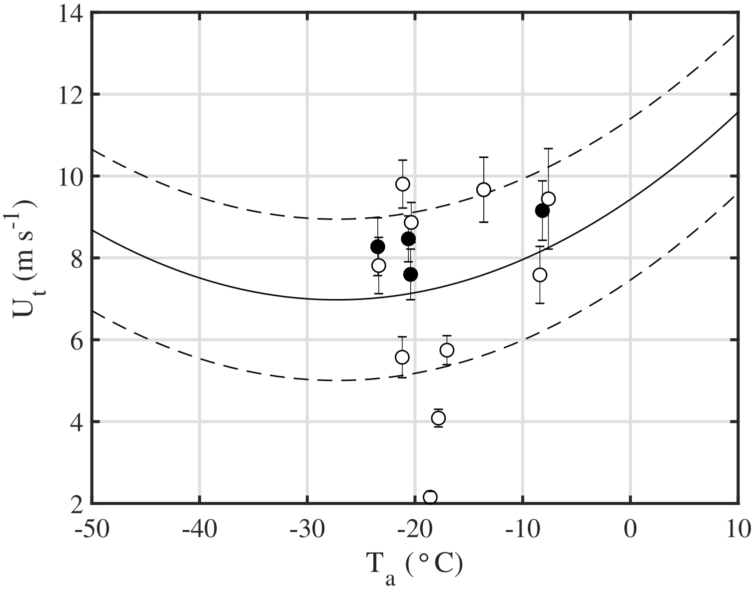

Figure 12. The threshold wind speed of blowing snow U_t at 10 m as a function of ambient temperature T_a at 2 m, above the sea ice in the Weddell Sea. Plotted are 10-minute means of observations centred on the time, when the snow drift density μ right above the snow surface exceeds a threshold of 0.005 $\mathrm{kg\,m^{-3}}$ (closed symbols) and 0.001 $\mathrm{kg\,m^{-3}}$ (open symbols), respectively; errobars indicate $\pm 1\sigma$. Shown for comparison are predictions by the parameterisation of Li and Pomeroy (1997) (Eq. 4) and their stated uncertainties as solid and dashed lines, respectively.

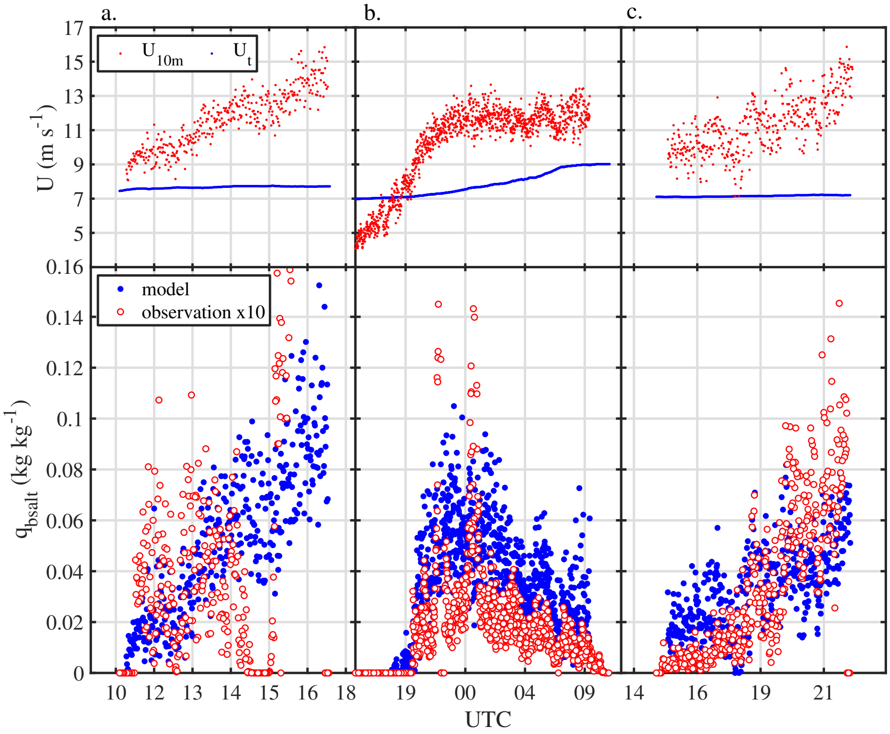

Figure 13. Snow mixing ratios in the saltation layer, q_{bsalt}, during (a) 24 June (ice station S2), (b) 14-15 July (ice station S6) and (c) 26 July (ice station S7), where the snow particle counter was mounted below the reported value of the saltation layer depth (=0.1 m). Observations multiplied by ten are compared to predictions by the parameterisation of Déry and Yau (1999) (Eq. 3). The top panels show observed wind speed U_{10m} and the 10-m drift threshold wind speed U_t computed with the empirical model of Li and Pomeroy (1997) (Eq. 4), both at 10 m.

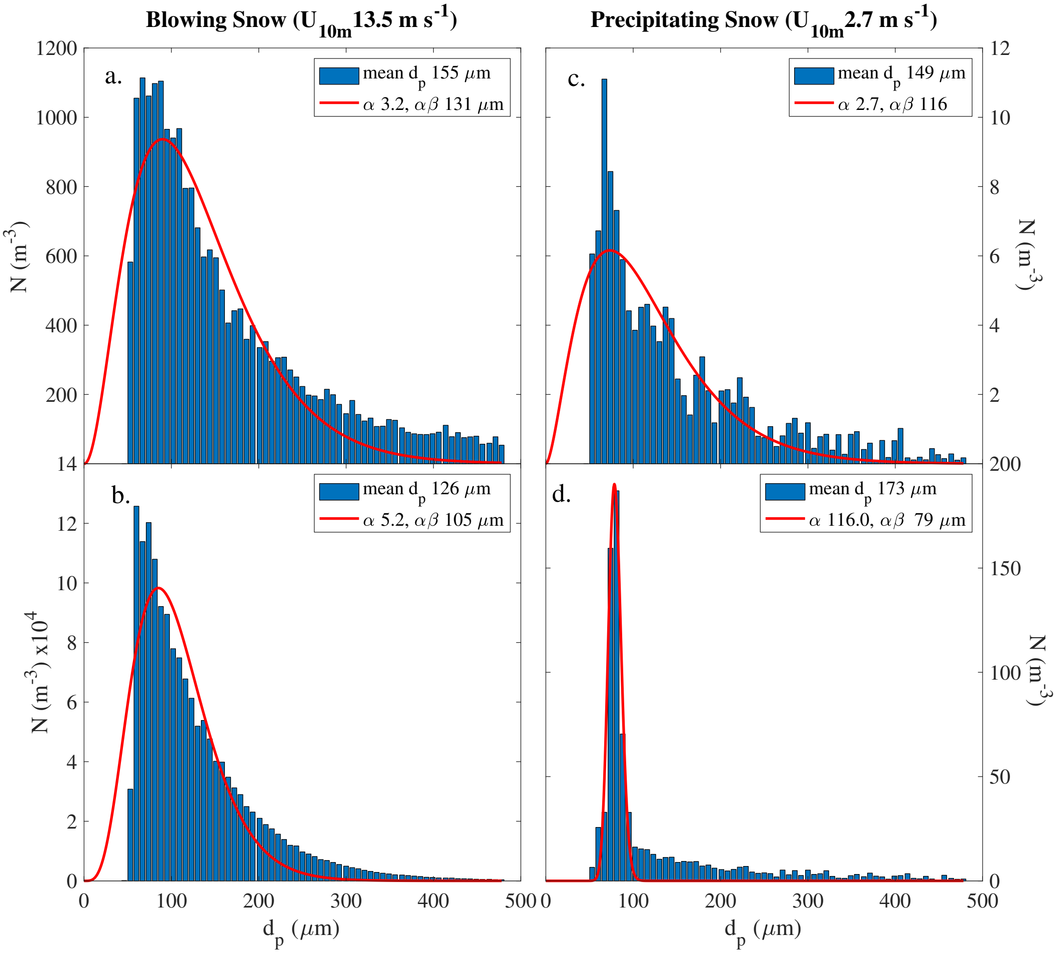

Figure 14. Average snow particle size spectra $f(d_p)$ measured at 29 m and <0.2 m during blowing snow on 14 July 23:15-23:25 (a,b) and during light snowfall coinciding with very low winds on 3 July 14:30 - 4 July 7:00 (c,d). Solid lines indicate the fit obtained with a 2-parameter gamma probability density function (Eq. 5). Note that ~~mean particle diameters d_p~~ $\overline{d_p}$ computed from observations show a positive bias compared to ~~d_p~~ $\overline{d_p}$ (=$\alpha\beta$) retrieved from the fitting procedure, since the SPC instrument does not detect small particles (d_p<46 µm).

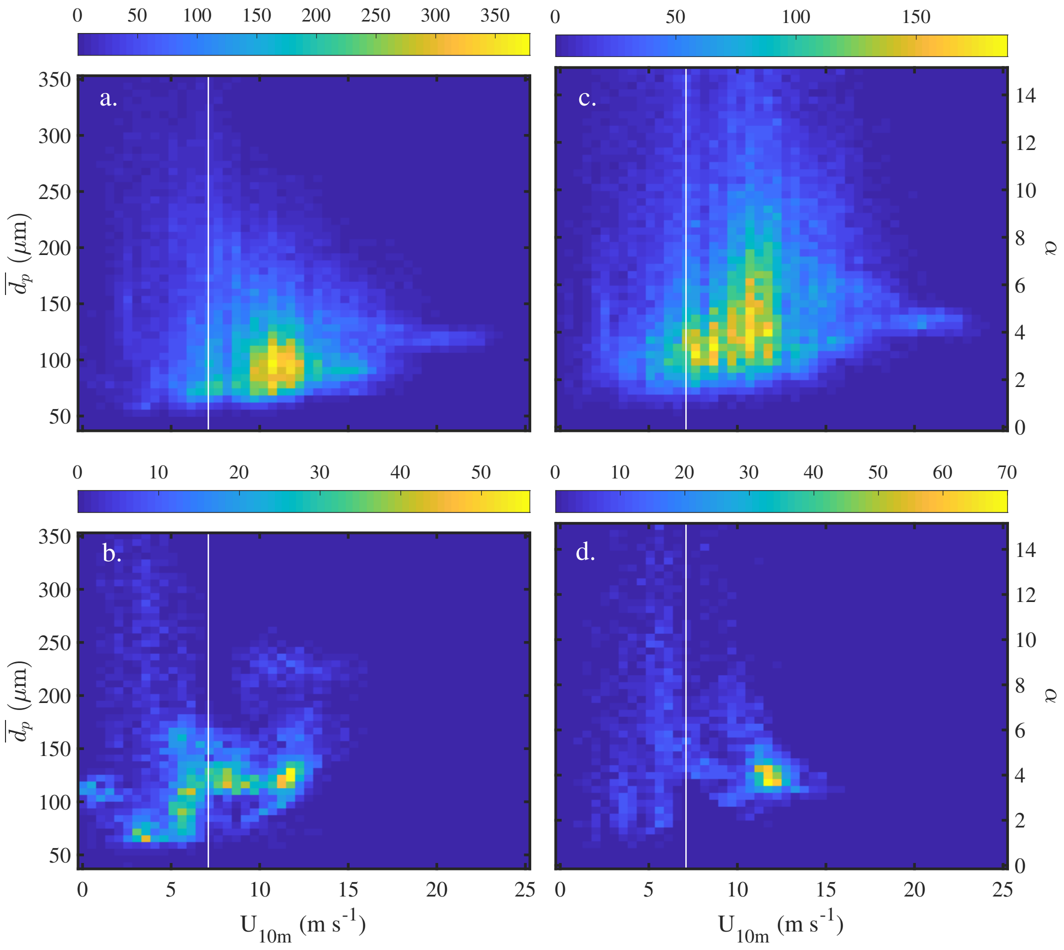

Figure 15. Properties of blowing snow particle size distributions above sea ice as a function of the 10-m wind speed U_{10m} retrieved from fitting a 2-parameter gamma probability density function (Eq. 5) to observations. Mean snow particle diameters $\overline{d_p}$ ($=\alpha\beta$) (a) at 29 m during ANT-XXIX/6 and 7, and (b) at <0.2 m during ANT-XXIX/6. The shape parameter α (c) at 29 m and (d) at <0.2 m. The vertical line represents the observed mean snowdrift threshold wind speed U_t of 7.1 m s^{-1} corresponding to u_{*t} of 0.37 m s^{-1}. Data were binned into 50 bins in x and y direction, with the colour indicating the sample density in each bin.

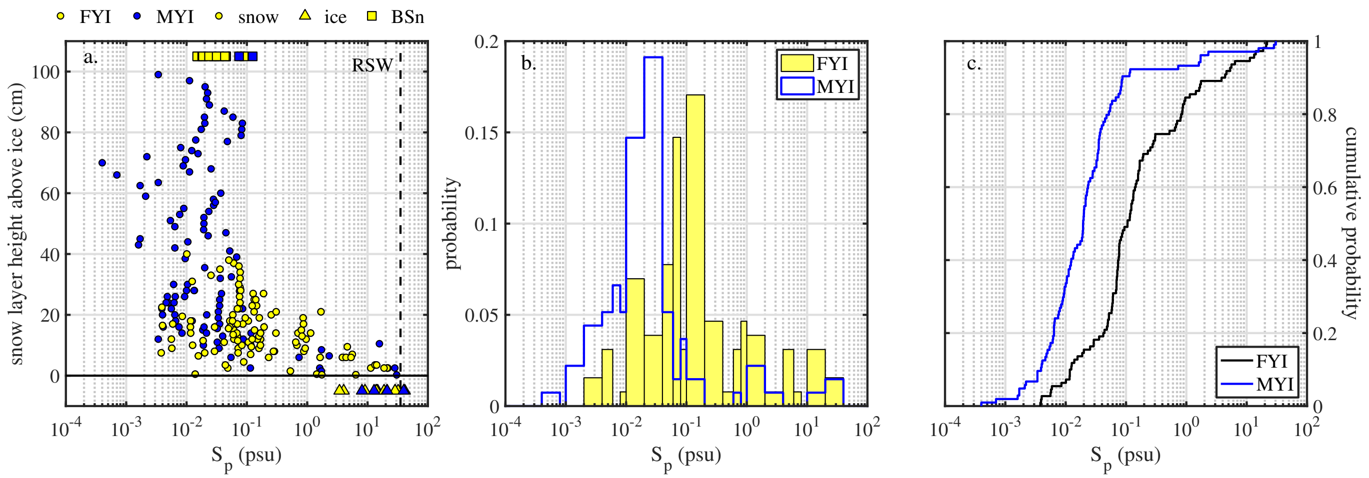

Figure 16. Panel (a) shows salinity S_p of snow on first-year sea ice (FYI, yellow symbols) at ice stations S1-6 and multi-year sea ice (MYI, blue symbols) at ice stations S7-9 in the Weddell Sea during austral winter 2013 as a function of snow layer height above the sea ice surface. For comparison S_p of the sea ice surface (triangles) and blowing snow at 1-17 cm above the snowpack (squares) are shown as well. The vertical dashed line indicates S_p (=35.165 psu) of reference sea water (RSW). Panel (b) shows salinity S_p probability distributions for shallow snowpacks (mean depth 21 cm) above first-year sea ice (FYI) at ice stations S1-6 and for deep snowpacks (mean depth 50 cm) above multi-year sea ice (MYI) at ice stations S7-S9 in the Weddell Sea during austral winter 2013. Panel (c) shows respective cumulative probabilities of S_p. The distribution statistics are summarised in Table 5.

~~Chemical fractionation of snow on sea ice in the Weddell Sea during austral winter 2013. Panel (a) shows sulphate depletion factors $DF_{SO_4^{2-}}$ (with respect to) of snow on first-year sea ice (FYI, yellow symbols) at ice stations S1-6 and multi-year sea ice (MYI, blue symbols) at ice stations S7-9 in the Weddell Sea as a function of snow layer height above the sea ice surface. For comparison $DF_{SO_4^{2-}}$ of the sea ice surface (triangles) and blowing snow at 1-17 above the snowpack (squares) are shown as well. Panel (b) shows the same but for bromide depletion factors DF_{Br^-} (with respect to). The sample statistics are summarised in Table 5.~~

~~Theoretical relationship between depletion factors of sodium DF_{Na^+} (with respect to) and of sulphate $DF_{SO_4^{2-}}$ (with respect to) in freezing seawater if mirabilite () is progressively precipitated and instantaneously removed (red line). When all sulphate is removed ($DF_{SO_4^{2-}} = 1$) sodium depletion reaches its theoretical maximum ($DF_{Na^+} = 1.1204$). See section 2.4 for definition of depletion factors DF, which are zero in reference seawater (RSW) (black dashed lines). Data refer to all observations from this study in snow (solid symbols), and aerosol at 2 and 29 above the sea ice surface (open symbols).~~

~~Aerosol bromine chemistry above sea ice observed in the Weddell Sea during austral winter/spring 2013. (a) aerosol concentrations at 29 and 2 m with the dashed line indicating the theoretical LOD (section 2.3); (b) depletion factors of bromide DF_{Br^-} (with respect to) in aerosol at 29 and 2 m and global radiation to indicate light conditions.~~

~~Average number distributions (panel a) and volume distributions (panel b) of aerosol above the open ocean (13 to 16 June 2013) and sea ice in the Weddell Sea (18 June to 21 July 2013) during calm and windy conditions. Data used are observations from 29 above the sea surface at ambient RH; numbers in brackets indicate the wind speed U_{10m} ±1 . Note that standard deviations of the mean values are always smaller than half the symbol size.~~

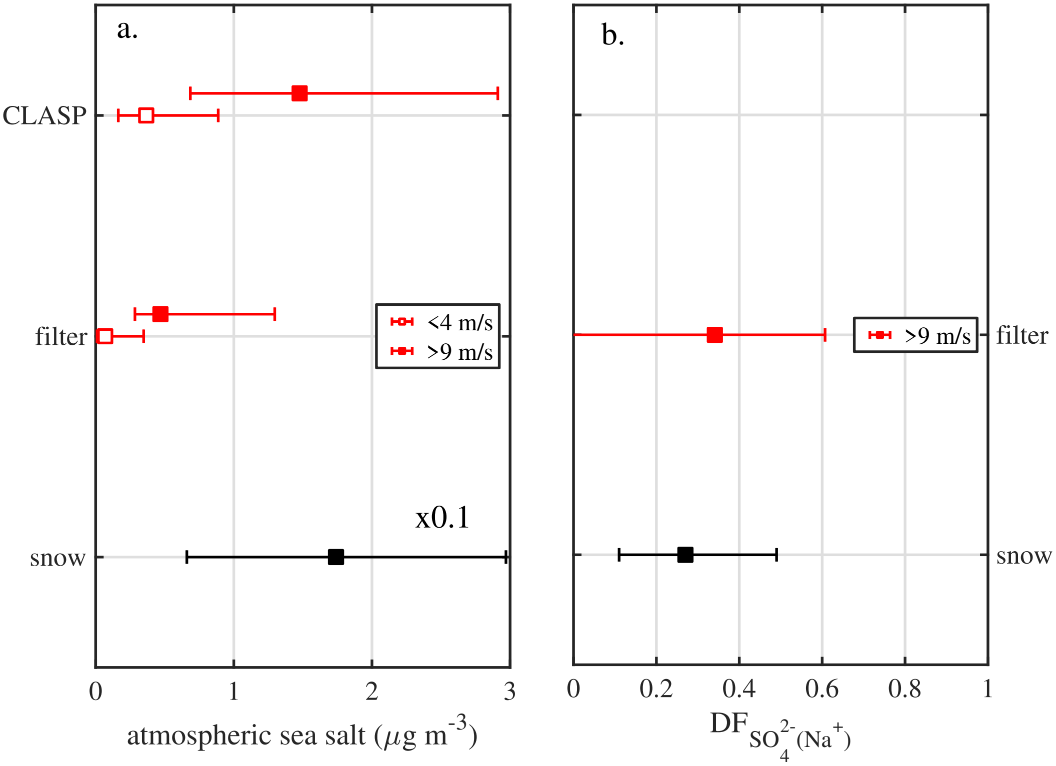

Figure 17. The partitioning of sea salt ~~mass budget~~ between atmosphere and ~~sulphate depletion in~~ snow, and ~~atmosphere~~ sulfate depletion above first year sea ice ~~(~~from 18 June to 21 July ~~2013):~~ 2013. Panel (a) shows median atmospheric sea salt concentrations ~~derived from particle number densities $N_{0.4-12}$ and filter concentrations at 29~~ during calm (~~3±1~~U_{10m}<4 m s^{-1}) and windy (~~10±1~~U_{10m}>9 m s^{-1}) conditions derived from aerosol filter measurements (filter) and spectral particle number densities $N_{0.4-12}$ (CLASP) (see text). For comparison, ~~total~~ a potential atmospheric concentration is calculated assuming that all sea salt ~~mass~~ observed in the top 0.1 mm of ~~surface~~ snow on sea ice was ~~converted into atmospheric concentration assuming a snow density ρ_{snow} of 300~~ released by sublimation and ~~mixing~~ mixed into a 100 m ~~deep atmospheric~~ thick boundary layer (for better comparison ~~with atmospheric observations~~ multiplied here by 0.1). Panel (b) shows for the same time period median ~~sulphate~~ sulfate depletion ~~factor~~ factors $DF_{SO_4^{2-}}$ (with respect to Na$^+$) in ~~aerosol and~~ in surface snow and in aerosol during windy (U_{10m}>9 m s^{-1}) conditions. Symbols and errorbars represent median and lower and upper quartiles, respectively.